https://ntrs.nasa.gov/search.jsp?R=19940008958 2020-06-16T21:52:14+00:00Z

NASA Contractor Report 189687

HIGH TEMPERATURE ELECTROMAGNETIC CHARACTERIZATION OF THERMAL PROTECTION SYSTEM TILE MATERIALS

(NASA-CR-189687) HIGH TEMPERATURE ELECTROMAGNETIC CHARACTERIZATION OF THERMAL PROTECTION SYSTEM TILE MATERIALS Final Report (McDonnell-Douglas Corp.) 138 p

N94-13431

Unclas

G3/27 0186493

G. G. HEIL

MCDONNELL DOUGLAS AEROSPACE
Saint Louis, Missouri

Contract NAS1-18763
September 1993

National Aeronautics and
Space Administration

Langley Research Center
Hampton, Virginia 23681-0001

ABSTRACT

This study investigated the impact of elevated temperatures on the electromagnetic performance of the LI-2200 thermal protection system. A 15 kilowatt CO_2 laser was used to heat a LI-2200 specimen to 3000°F while electromagnetic measurements were performed. The electromagnetic measurement system consisted of two Dual Lens Spot Focusing (DLSF) Antennas, a sample support structure and a HP-8510B vector network analyzer. Calibration of the electromagnetic system was accomplished with a Transmission-Reflection-Line (TRL) procedure and was verified with measurements on a two layer specimen of known properties. The results of testing indicated that the LI-2200 system's electromagnetic performance is only slightly temperature dependent at temperatures up to 3000°F.

TABLE OF CONTENTS

PRECEDING PAGE BLANK NOT FILMED

LIST OF FIGURES

LIST OF TABLES

LIST OF ABBREVIATIONS

CO2	-	CARBON DIOXIDE
CW	-	CONTINUOUS WAVE
dB	-	DECIBLE
DLSF	-	DUAL LENS SPOT FOCUSING
EDC	-	ELECTRIC DISCHARGE CONVECTION
ETEC	-	ELEVATED TEMPERATURE ELECTROMAGNETIC CHARACTERIZATION
GHz	-	GIGAHERTZ
kW	-	KILOWATT
LRM	-	LINE-REFLECTION-MATCH
MAS	-	MICROWAVE AUTOMATED SCANNING
MRIS	-	MICROWAVE REFLECTION IONIZATION SENSOR
NASA	-	NATIONAL AERONAUTICS AND SPACE ADMINISTRATION
NIST	-	NATIONAL INSTITUTE OF STANDARDS AND TECHNOLOGY
RCG	-	REACTION CURED GLASS
S-Parameter	-	SCATTERING PARAMETER
S11	-	SCATTERING PARAMETER MATRIX ELEMENT (1,1)
S12	-	SCATTERING PARAMETER MATRIX ELEMENT (1,2)
S21	-	SCATTERING PARAMETER MATRIX ELEMENT (2,1)
S22	-	SCATTERING PARAMETER MATRIX ELEMENT (2,2)
SEM	-	SCANNING ELECTRON MICROSCOPE
TPS	-	THERMAL PROTECTION SYSTEM
TRL	-	TRANSMISSION-REFLECTION-LINE
μm	-	MICROMETER
°F	-	DEGREE FAHRENHEIT

LIST OF EQUIPMENT

EQUIPMENT AND INSTRUMENTS USED IN THIS TEST ARE LISTED BELOW. ADDITIONAL DESCRIPTIONS ARE LOCATED IN APPENDIX A.

ITEM	MANUFACTURER AND MODEL NUMBER	SERIAL OR LABORATORY NUMBER
15 KW CO_2 CW LASER	MCAIR	075529
NON-CONTACT THERMOMETER	E^2T TECHNOLOGY CORP. PULSAR II MODEL 7000FF-HR	689049
NON-CONTACT THERMOMETER	IRCON 7000 SERIES, MODEL MODLINE PLUS	128690
DATA ACQUISITION	FLUKE 2280 DATALOGGER	108109
DATA ACQUISITION	HEWLETT-PACKARD 7132A STRIP RECORDER	089507
DATA ACQUISITION	HEWLETT-PACKARD 8510B VECTOR NETWORK ANALYZER	134757
DATA ACQUISITION	HEWLETT-PACKARD 360 WORKSTATION	139722

1.0 INTRODUCTION

1.1 TASK OBJECTIVE. An effort is underway to develop the necessary technology for the design of practical aeroassisted reentry vehicles. As part of this effort, flowfield simulations used to calculate the aerodynamic forces on these vehicles need to be improved. A Microwave Reflectometer Ionization Sensor (MRIS) is being developed to make nonintrusive measurement of the flowfield characteristics.

Due to the extreme thermal environments experienced by transatmospheric vehicles, thermal protection systems (TPS) have been developed for them. TPS materials of the type used in the space transportation system orbiters will be used to protect the MRIS system. The insulating characteristics of these systems are well understood; however, other characteristics of the TPS materials are not. The MRIS will sense the flowfield through the TPS, and therefore, it is necessary to fully understand the microwave characteristics of the TPS.

The objective of this task was to measure the complex reflection and transmission characteristics of LI-2200 TPS materials over the frequency range 19 to 21 GHz at temperatures as high as 3000°F.

1.2 TECHNICAL APPROACH. This study was designed to determine the dependence of the electromagnetic characteristics of LI-2200 TPS materials on the thermal environment. Previous attempts to characterize the electromagnetic properties of LI-2200 at elevated temperatures were unable to determine the performance of the system above 2400°F. These attempts allowed the TPS specimen to soak at the measurement temperature and, at temperatures above 2400°F, to soften and deform.

This test program utilized a high power carbon dioxide laser to heat the surface of the TPS tile. This technique provided a more realistic simulation of aerodynamic heating and eliminated the possibility of sample deformation due to softening.

Laser power density calculations were used to determine the maximum diameter of the laser beam that would provide sufficient energy density to raise the temperature of the specimen to 3000°F. These calculations indicated that a focusing microwave antenna system would be required to confine the microwave energy to the region of the specimen heated by the laser.

A dual lens antenna was proposed for focusing the microwave radiation into the specimen and a thermal analysis was performed to determine if candidate lens materials would withstand the heat flux re-radiated by the specimen. This analysis indicated that the preferred material candidate, Rexolite 1422, would be damaged by the heat flux, therefore optical quality fused quartz was used.

Dual lens antenna systems were designed at NASA Langley Research Center and the components were fabricated at Langley and by subcontract. The components were then assembled and optically aligned at McDonnell Aircraft. After assembly and alignment the two antenna systems were adjusted to produce the smallest spot and flattest wave front at the focal plane. This optimization was performed using an automated scanning system in which a WR-34 waveguide probe was raster scanned in the focal plane of the antenna.

A Transmission-Reflection-Line (TRL) calibration procedure was used to error correct the S-parameter data from the assembled measurement system. This procedure was then verified with S-parameter measurements on a two layer system with known characteristics. Predictions and dielectric constant

calculations on well characterized materials were also used to verify overall system performance.

The laser heating process was qualified prior to electromagnetic measurements to insure that the laser and data acquisition subsystems were operating properly and to determine whether the LI-2200 system could withstand the sudden thermal shock imparted by the laser beam. These tests were run on 23 October 1991.

Measurement of the elevated temperature characteristics of the LI-2200 system were performed on 18-20 November 1991. A total of thirteen laser exposures were made on twelve LI-2200 tile specimens. The measurement system was calibrated prior to each laser test and ambient temperature S-parameter measurements were made for each specimen. A detailed comparison of ambient and elevated temperature characteristics will be made later in this report.

2.0 TECHNICAL DETAILS

2.1 POWER DENSITY AND SPOT SIZE DETERMINATION. Approximate calculations of the energy radiated by the TPS specimen at 3000°F were used to determine the largest laser illumination area possible. These calculations assumed that the LI-2200 materials were perfect thermal insulators and that the Reaction Cured Glass (RCG) coating would perform as a perfect black body. The equations used took the form :

$$q = \epsilon\sigma(T_s^4 - T_0^4) \quad \text{Watts/m}^2 \qquad \text{Eq. 1}$$

where

q = radiated power density
ϵ = emissivity = 1.0
σ = Stefan-Boltzmann Constant = 5.67×10^{-8}
T_s = Tile temperature
T_0 = Ambient Temperature

The maximum laser output power was limited to 12.5 kilowatts to reduce the risk of damaging the laser output coupling device and a safety factor of 2 was introduced into equation 1 to account for the assumptions made in using this simple approach.

$$A = (q_{max}/2q) \quad \text{m}^2 \qquad \text{Eq. 2}$$

where

A = illuminated area
q_{max} = Maximum Laser Power = 12,500 watts

The maximum radius of the laser spot was determined to be approximately 2 inches based on the assumption that the spot would be a perfect circle. In the actual measurement set up the laser beam was introduced to the sample 40° from normal which resulted in an slightly elliptical illumination area.

2.2 THERMAL ANALYSIS OF LENS/SPECIMEN INTERACTION. The requirement of focusing the microwave radiation into the region heated by the laser beam resulted in the need for a sophisticated focusing antenna system. Experts at NASA Langley Research Center suggested a dual lens system with lenses

manufactured from Rexolite 1422, a cross-linked styrene copolymer. Rexolite was chosen for its low dielectric constant and for its exceptional machinability.

As design of the dual lens system progressed, it became evident that close proximity of the forward lens and the test specimen would be required and that significant radiated heat flux would be captured by the lens. It was determined that a thermal analysis of the lens-specimen interaction would be prudent.

2.2.1 Thermal Model. An analysis was performed using a finite difference thermal modeling software package that was developed within McDonnell Douglas Corporation. The thermal model configuration is shown in Figure 1. The modeling was performed as follows:

a. The transient analysis was performed with 1 second time intervals for the time necessary for any lens node to reach the distortion temperature of 210°F.

b. The heated region was modeled as a square with side length equal to 3.0 inches. The heat input quantity to the region yields an approximately linear nodal heat up rate to 3000°F in 45 seconds. The heat input maintains the heated surface at 3000°F for 25 seconds then was set to zero. The heated surface of the tile was assumed to be isothermal.

c. The lens was modeled as a flat 3.0 inch square with three layers. The first layer was defined as .002 inches thick, the second .088 inches and the third .91 inches. This configuration adequately accounted for the depth-wise temperature distribution in the lens.

d. Heat input to the lens consisted only of radiation gain from the tile. Radiation exchange from the unheated areas of the tile are assumed

negligible because of the low conductivity of the tile material and because of the small view factor from that portion of the tile to the lens.

e. Table 1 contains a list of the material properties used in the analysis.

f. Convection losses from the RCG coated surface and from the lens surface were assumed negligible. However, forced convection losses were added to the lens surface in three cases for comparison purposes.

2.2.2 Modeling Results. The thermal analyses were performed for lens to tile distances of 3.0 through 12.0 inches at increments of 1.0 inch. A graph of the lens surface temperature versus time for the various separations without convection loss is given in Figure 2. The analysis was also performed including convection losses for lens to tile distances of 8.0, 9.0 and 10.0 inches. A graph of lens surface temperature versus time for these separation distances with and without convection is given in Figure 3. Convection losses were modeled as a heat loss to air at ambient temperature with a convection coefficient of 20 Btu/hr-ft^2-°F.

In addition, the model was modified to analyze the transient effects of instantly exposing the lens to the 3000°F tile for a short duration. This models the lens/tile configuration as having an opaque shutter between the two which is opened at T=0. The results for a 1.5 second lens exposure at a lens/tile distance of 8.0 inches are presented in Figure 4.

Examination of the results presented in Figure 2 suggests that Rexolite could have been used but that there was a clear danger of exceeding the design limits for the material. Because the results were marginal it was decided to more accurately determine the emissivity of the Rexolite material and to

re-examine the thermal model.

A sample of Rexolite 1422 was requested from the manufacturer and Hemispheric Reflectance and Transmittance were measured at facilities within McDonnell Aircraft. The results of these measurements were integrated to yield a average emissivity over the wavelength region of interest and the thermal model was re-run. All parameter values given in Table 1 were used to re-run the model with the exception of the emissivity of the Rexolite 1422. The value used for this parameter was ϵ=.38. A graph of the modified transient analysis is shown in Figure 5.

2.2.3 Thermal Analysis Conclusions. The results of this analysis show a large variation between the modeling results and the test plan requirements. Figure 5 clearly demonstrates that the Rexolite lens would exceed 210°F within 2 seconds of exposure to the heated tile. Further, these results suggest that the Rexolite 1422 temperature limitations would be exceeded before the tile could be brought to the test temperature. For these reasons, optical quality fused quartz was recommended and utilized as the lens material.

2.3 ANTENNA ASSEMBLY AND ALIGNMENT. The system designed for measuring the electromagnetic performance of the TPS specimens consisted of two Dual Lens Spot Focusing (DLSF) antennas, a sample holder and a support structure that allowed one of the antennas to move parallel to the optical axis of the system. This configuration is shown in Figure 6.

The DLSF antenna system was designed to operate over a frequency range of 19 to 21 GHz and to illuminate a 2 inch diameter spot at the focal plane. The power level at the edge of the 2 inch spot was designed to be at least 3 dB below the power level at the center. Each DLSF antenna consisted of a thick lens, a thin lens, a dual mode feed horn and the hardware required to assemble

and align the microwave components. The origins of the various components used to assemble the DLSF antennas are shown in Table 2.

The most significant requirement in the assembly of the DLSF antenna systems was careful alignment of components. Because of the relatively long wavelength of the microwave radiation and the high cost associated with optical alignment procedures, a retro-reflection technique was used.

The retro-reflect technique involved directing a laser beam through the optical axis of the antenna and adjusting the lenses and feed horns such that reflections from the various surfaces coincide with the laser beam. The estimated axial and angular errors for this technique are .02 inches and 12 arc-minutes respectively.

The support structure for the measurement system was designed such that the two antenna systems would automatically align when installed. Proper alignment of the two antenna systems with the sample holder was verified prior to calibration and prior to elevated temperature testing.

2.4 ANTENNA OPTIMIZATION. A DLSF antenna, shown in Figure 7, consists of two lenses and a dual mode feed horn. A sensitivity analysis of this design indicated that the critical dimension was the distance between the phase center of the feed horn and the center of the rear lens. This distance is identified as L1 in Figure 7 and is subject to uncertainty because of the difficulty in calculating the phase center of the feed antenna. For this reason it was determined that an optimization procedure would be required to guarantee optimal performance of the measurement system.

2.4.1 Antenna Optimization Procedure. The Microwave Automated Scanning (MAS) system is a laboratory instrument developed by McDonnell Aircraft to evaluate the electromagnetic performance of materials as a function of

position. The MAS system consists of a two dimensional scanning system, a microwave source, a network analyzer, microwave probes and a computer. In traditional MAS system measurements, a sample of material is raster scanned between two waveguide probes such that the performance of the material is mapped out as a function of position. This data can then be presented as surface contour maps, gray scale plots or as linear cuts through the 2 dimensional data.

The MAS system was modified so that a WR-34 waveguide probe could be raster scanned in the focal plane of the DLSF antenna. The DLSF antenna, the waveguide and the bed of the scanning system were carefully aligned using a retro-reflect technique similar to that discussed above. Figure 8 shows this system schematically.

It is understood that this technique can not provide an absolute measurement of the performance of the DLSF antenna. Significant error is introduced by the interaction of the near fields of the test and probe antennas and by multiple reflections between scanning bed structure and the test antenna. It was felt, however, that this technique would provide an excellent means for qualitatively optimizing the antennas.

The following procedure was used to optimize the antennas:

a. Align waveguide probe, scanning test bed and DLSF antenna using laser retro-reflect technique.

b. Move waveguide probe so that the radiation axis coincides with the radiation axis of the DLSF antenna then collect a normalization value.

c. Raster scan the waveguide probe in the focal plane of the DLSF antenna so that a 10 inch by 10 inch area is completely characterized. Note that 10,000 data points were collected over this area yielding a spacial resolution of .1 inches.

d. Examine the 3dB amplitude spot and the 20° phase spot of the DLSF antenna.

e. Move the feed horn relative to the rear lens and repeat step c and d.

f. Note the effect of moving the feed horn and repeat step e until optimal performance is achieved.

2.4.2 Antenna Optimization Results. Calculations to determine the phase center of the dual mode feed horn indicated that the phase center would be located in the throat very near the mouth of the horn. The DLSF antenna mounting hardware was designed so that the feed antenna position could be adjusted by ±.25 inches around the design value.

Initial MAS system measurements were made at 20 GHz with the feed horn positioned at the design value. Subsequent measurements were made with the feed horn both closer and farther from the rear lens. It was observed that although the 3dB spot size was effected only slightly by the shift, the wave front curvature was significantly effected. Further, the DLSF antenna performed better when the feed horn was closer to the rear lens. This implies that the phase center of the feed horn was further down the throat than indicated by calculations.

Both of the DLSF antennas were tested in a similar way and in both cases it was found that the optimal performance was achieved with the feed horn as far forward as the hardware would allow. MAS system data indicated that the DLSF antennas would easily meet the ETEC system's requirements although the optimal feed horn position may lay slightly beyond the designed positioning range. It should be noted that the change in performance with change in feed position indicates that the feed horn was very near its optimal location.

Figures 9 through 12 are examples of the MAS system output used to optimize the DLSF antennas. Figures 9 and 10 show gray maps of the 3dB spot for the DLSF antennas. In Figure 9, the DLSF antenna is optimally configured, and in Figure 10 it is in the worst case configuration. Note that there is only a slight change in the diameter of the spot. Figures 11 and 12 show line cuts of the phase through the center of the focal plane of the antenna system. Figure 11 corresponds to the optimal position and Figure 12 to the worse case feed position. Note that there is a significant flattening of the wave front when the feed antenna is in the optimal position.

In addition to the measurements already discussed, MAS system measurements were made for both antennas with the feeds adjusted for optimal performance but the frequency adjusted to 19 GHz. This was done to determine the frequency sensitivity of the antenna design. Figures 13 and 14 present data from one of these tests. Note that the 3dB spot remained largely unchanged but that the wave front curvature has increased. These results indicate that the DLSF antenna systems could introduce phase distortion outside a narrow window of frequencies around 20 GHz.

2.4.3 Antenna Optimization Conclusions. Figures 9 through 12 clearly demonstrate that the DLSF antennas performed as anticipated. The 3dB spot for these antennas had approximately a 1 inch radius. At a radius of 2 inches, the radius of the laser beam, the radiation is reduced by 12dB relative to the value at the center of the test zone. At 1 inch from the center of the test zone the phase for the DLSF antennas deviates less than 12° from the value at the center. The far field criteria of 22° wave front curvature was maintained over a region approximately 3.5 inches in diameter.

The results of testing at 19 GHz demonstrated that the amplitude

distribution of the DLSF antennas remains approximately constant over the frequency range 19 to 20 GHz but that the wave front curvature does not. It was found that at 20 GHz the phase taper at a radius of 1 inch was 12° and at 19 GHz the phase taper at 1 inch is approximately 18°. Further, the far field criteria was only maintained for a spot 2.5 inches in diameter at 19 GHz.

Equipment limitations prevented MAS system measurements above 20 GHz. The unavailability of this data forces us to assume that the performance of the antenna system above 20 GHz is adequate but we believe that this assumption is borne out by subsequent electromagnetic measurements.

2.5 FINAL TEST SYSTEM ASSEMBLY. After the DLSF antenna systems had been optimized the Elevated Temperature Electromagnetic Characterization (ETEC) system was assembled and mechanical measurements were made to determine the location of the antennas relative to each other and to the specimen support. A schematic of the ETEC system is presented in Figure 15. The dimensions labeled "Validation" were measured during the initial calibration and validation procedure. The second set of dimensions, labeled "Test", are the dimensions measured after the ETEC system had been moved to the laser test facility. Every effort was made to reproduce the exact dimensions used during the validation phase but some small deviations were expected.

Prior to actual electromagnetic measurements, the ETEC system was checked for optical alignment using the same retro-reflect technique described above. Several small adjustments were required to bring the system back to optimal alignment but the system had remained largely unaffected by disassembly and reassembly.

2.6 NETWORK ANALYZER CALIBRATION PROCEDURE. Two calibration techniques were considered for this testing, the Transmission-Reflection-Line (TRL) and

the Line-Reflect-Match (LRM). Both of these techniques share a common mathematics and error model, the difference being the standards used to determine the coefficients of the error terms.

2.6.1 The TRL Procedure. The TRL calibration technique requires three standards, a thru transmission measurement, a non-zero length transmission measurement and a reflection measurement from each port. The thru measurement was accomplished by measuring the ETEC system performance without a specimen in the sample holder. The line measurement, or non-zero length transmission measurement, was accomplished by moving one of the ETEC antennas to increase the path length of the ETEC system by ¼ wavelength at the calibration center frequency. The reflection standard was a .063 inch thick aluminum plate mounted in the sample holder with one surface placed at the location of the RCG plane.

2.6.2 LRM Procedure. The LRM calibration technique is similar to the TRL technique in that it requires three standards and relies on the same error model and mathematics. The standards required for the LRM technique are a thru transmission measurement, a reflection measurement from each port and a zero reflection, or match, measurement from each port. The first two standards for the LRM procedure were accomplished in exactly the same way as the transmission and reflection standards for the TRL procedure. The match was achieved by placing two sheets of carbon loaded foam absorber between the forward lens of the DLSF antennas and the specimen holder.

2.6.3 Calibration Procedure Results. These procedures were applied to the ETEC system over several frequency ranges and with several different definitions for the calibration standards. Initial measurements of the verification standard supplied by NASA indicated that the requested bandwidth

would be insufficient to allow useful time domain post processing. These measurements did, however, show that the results above and below the requested frequency range were in good agreement with the predicted performance of the validation standard. For these reasons, it was decided that calibration and testing would be performed from 16 to 26 GHz. This frequency range is broad enough to allow adequate time domain resolution for post processing.

After calibration, measurements of the transmission coefficient for the system without a specimen and the reflection coefficients of the system with a metal ground plane in the sample holder were made. Ideally the transmission coefficient would equal 1 (T=1+j0) and the reflection coefficients would equal -1 (R=-1+j0), but some deviation from this was expected. The transmission and reflection coefficients measured after a typical TRL calibration are presented in Figures 16 through 19.

There are several notable features to the data presented in these plots. The most obvious deviation from the ideal performance was that the transmission and reflection amplitudes are not exactly equal to 0dB. This, in fact, was expected and is consistent with a high directivity measurement apparatus. The noise is a result of reflections between the components of the DLSF antennas, most notably the forward lenses, and the metal ground plane used for the reflection coefficient measurements. Calculation of the mixing frequency, or beat frequency, for the reflection coefficient measurements indicated that the primary noise source is located approximately 10 inches from the metal reflector. This corresponds perfectly with the forward lens of the DLSF antenna.

Another notable deviation from the ideal performance of this system was the phase of the reflection and transmission coefficients not equaling the

expected values. We believe that this effect was a result of the placement of the reflection standards during calibration. However, modifications made to the TRL calibration procedure were unsuccessful in eliminating the effect. These phase aberrations did not, however, result in measurement error as they were present in all measurements made after calibration and were therefore eliminated with a simple normalization. The normalization procedure will be discussed in detail in section 4.4.1.

The most detrimental aberration detected in the reflection and transmission coefficient measurements manifested itself as non-repetitive spikes in the phase of the reflection and transmission coefficients. These spikes, or glitches, are attributed to a marginal detector in the network analyzer and became more prominent when the network analyzer was subjected to warm (above 75°F) room temperatures. Because these glitches are non-repetitive, time domain procedures are not effective for their removal. Time domain gating will be discussed in detail in section 4.4.3.

After a LRM calibration had been established, measurements similar to those made after the TRL calibration were made. A comparison of the data from the TRL and the LRM calibration procedures indicated that each of the three notable deviations from the ideal post calibration results identified for the TRL procedure were present to approximately the same degree for the LRM procedure. In fact, the results for the LRM procedure were very nearly identical to the results from the TRL procedure.

2.6.4 Calibration Procedure Conclusions. The electromagnetic testing performed for this contract involved the use of large and delicate antenna systems and would have benefitted from a calibration technique that does not require movement of the antennas. For this reason, all other things remaining

the same, the LRM technique has obvious advantages over the TRL technique. The LRM technique, however, requires that the match standards be as close to identical as possible. This requirement was not achievable at the time of testing. This fact coupled with our familiarity with the TRL procedure lead to our decision to use the TRL procedure for the high temperature testing.

3.0 LASER HEATING QUALIFICATION

Because of the uncertainties in the thermal characteristics of the LI-2200 materials and the difficulty in modeling the interactions between the heated tile and surrounding environment, it was decided that a preliminary laser test would be performed. Multiple non-contact thermometers were used to measure the temperature of the surface of the tile and several thermocouples were used to characterize the tile's radiated and conducted thermal energy.

A sketch of the optics and equipment layout used for this test is presented in Figure 20 and a photograph is presented in Figure 21. Initially only the E^2T non-contact thermometer was to be used to determine the temperature LI-2200 specimen, but reflected laser energy captured during the initial test slightly damaged the unit's lens. Subsequent tests used a second non-contact thermometer to verify the results of the first and placed the thermometers so that no reflected energy could be captured. Figures 20 and 21 represent the measurement system after these modifications were made.

In addition to the non-contact thermometers, several type K thermocouples were used to evaluate the impact of energy radiated from the heated LI-2200 specimen. These thermocouples were placed at the locations specified below :

1) The front surface of the simulated lens.

2) The rear surface of the simulated lens.

3) The front surface of the simulated lens mount.

4) The center of the rear surface of the LI-2200 specimen.

5) The edge of the rear surface of the LI-2200 specimen.

3.1 LASER HEATING QUALIFICATION PROCEDURE. After all laser optics and recording equipment were placed and adjusted, measurements were made to verify the laser illumination area and a test run was performed on a silicon fire

brick to verify operation of the laser. The power required to heat the TPS specimen to 3000°F was estimated and the laser gas flow and power supplies were adjusted.

The first laser test was configured to deliver 11,000 watts of laser power to the sample. Upon opening of the laser shutter it was immediately evident that the estimated power level was significantly higher than required. The sample immediately became white hot and the non-contact thermometer registered a temperature beyond its measurement range. Laser power was immediately removed. The actual power delivered during this test was calculated at 11,567 watts and the exposure time was less than 3 seconds.

Examination of the specimen after this exposure revealed that the surface of the tile had been damaged by the laser beam. The surface of the RCG coating had been fused and there appeared to be sagging or compression of the foam material below the RCG coating. The photograph presented in Figure 22 was taken of the specimen to record this damage.

The E^2T non-contact thermometer was slightly damaged by reflected laser energy during the first test. To verify that the thermometer was still in working order, it was removed and sent to the McDonnell Aircraft calibration laboratory for testing. Although it was determined that the thermometer's lens had been damaged, the thermometer did perform within specifications.

The second laser test was configured to deliver a significantly lower laser power level. The power was initially set at 6,000 watts and was slowly increased until the target temperature of 3000°F was achieved. The power level required to achieve and maintain 3000°F was 6,769 watts and the total duration of the exposure was approximately 60 seconds. Examination of the specimen after this exposure revealed no new damage.

3.2 LASER HEATING QUALIFICATION RESULTS. A plot of the TPS specimen's surface temperature versus time for the second laser test is presented in Figure 23. Note that the maximum temperature achieved in this test was approximately 2930°F and that this temperature was maintained for approximately 20 seconds. Figures 24 and 25 show corresponding temperature profiles for the front and rear surfaces of the simulated lens. The maximum temperatures recorded on the surfaces monitored by the thermocouples are summarized in Table 3.

The most significant data presented in Figures 23-25 is the data from the front surface of the simulated lens. Note that the maximum temperature achieved during this test was 180°F and that the derivative of the temperature profile during the laser exposure was approximately 3°F/second. This rate would have resulted in damage to a Rexolite 1422 lens within another 10 seconds of exposure.

After laser testing, the LI-2200 specimen was cross sectioned through a damaged region, polished and examined with a scanning electron microscope (SEM). Images of the RCG coating and RCG-substrate interface for damaged and undamaged areas of the specimen are presented in Figures 26-29. Note that the RCG surface appears to have undergone local melting but that the material immediately under the RCG shows no signs of deformation.

3.3 LASER HEATING QUALIFICATION CONCLUSIONS. This testing was of great benefit to the success of this project. It allowed the laser power levels to be established prior to electromagnetic testing and clearly demonstrated the ability of the LI-2200 system to withstand the thermal shock imparted by the high powered laser. Several conclusions can be made based on the data and experience gained from this testing.

A. The laser power required to achieve 3000°F was established at approximately 6,800 watts, and the time required stabilize at this temperature was established to be approximately 40 seconds. Note that at 6,800 watts the 500,000 joule limitation on the output of the laser would be exceeded after approximately 73 seconds.

B. The forward lens in the DLSF antenna will heat rapidly to approximately 200°F when the LI-2200 specimen is heated to 3000°F. This is well below the damage threshold for quartz.

C. The LI-2200 system will not be significantly effected by the sudden thermal shock imparted by the laser. No cracking or sagging was noted even when the specimen was subjected to 70% more power than required to raise the temperature to 3000°F. Unfortunately no temperature data is available for the first laser test but estimates based on laser power indicate that the RCG surface achieved between 3500 and 3600°F.

D. It is very important to note that all non-contact thermometers require the emissivity of the surface being studied to be fully characterized. Emissivity data for the RCG surface of the LI-2200 system was provided for temperatures up to 2300°F but this data was in the form of a photocopied plot and was deemed only marginally reliable. The value for emissivity was set to 0.83 based on the plotted data but it is very possible that this value is in error at temperatures above 2300°F. If, in the future, new emissivity data becomes available, it would be possible to re-scale the non-contact thermometer data to compensate for this error.

4.0 ELECTROMAGNETIC CHARACTERIZATION

Elevated temperature characterization of the electromagnetic performance of the LI-2200 system was performed on November 18-19. Tests were scheduled and performed for 1000, 1500, 2000, 2200, 2400, 2500, 2600, 2700, 2800, 2900 and 3000°F. In addition, tests were run at 3400 °F and at the maximum output power of the laser.

4.1 ELECTROMAGNETIC CHARACTERIZATION PROCEDURE. Prior to electromagnetic testing, the alignment and positioning of the components of the ETEC system were verified and photographs of the test system were taken. Figures 30 and 31 show the ETEC system and associated laser and data acquisition hardware. A sketch of the hardware layout is provided in Figure 32. Each of the laser tests was conducted following the procedure outlined in Appendix B.

4.2 THERMAL DATA REDUCTION RESULTS. Measurements of the surface temperature of the LI-2200 specimens were recorded starting prior to laser exposure and stopping after the surface temperature had returned to a temperature below the minimum measurable by the non-contact thermometer. This data was correlated with frequency data from the HP-8510B and plots were made of the temperature of the specimen as a function of the frequency at which electromagnetic data was collected. Plots of the complete temperature profile versus time and of the temperature profile versus frequency are included as Figures 33-42. Note that no thermal data was available for the 2500, 3400 or 3800°F tests. The 2500°F data was lost because of a failure in the datalogger tape drive and the 3400 and 3800°F data was subject to error because of uncertainties in the emissivity of the LI-2200 materials.

There are several aspects of this data that are significant and need some discussion. The first notable feature is the fact that, in most cases, the

temperature of the RCG coating remained stable (±20°F) during electromagnetic data acquisition. The only exception to this trend was the first test run, the 1500°F test. Also of significance is the fact that the temperatures measured on the RCG coating were systematically approximately 50°F below the target temperature. This deviation resulted from a misinterpretation of a 3 millivolt offset in the non-contact thermometer electronics. The 150°F deviation on the 1000°F test resulted from a erroneous set-point calculation during the testing.

Finally, the thermal data for the 3400 and 3800°F tests is considered unreliable because of obvious changes in the RCG coating's emissivity. Both of these tests were run on a single specimen and examination of that specimen after the initial test revealed changes in color of the RCG coating. This color change suggests that the emissivity in the infra-red band may have changed significantly from the baseline value.

4.3 THERMAL PROTECTION SYSTEM FAILURE ANALYSIS. Several types of damage were observed on the LI-2200 samples after heating. These damages are summarized below.

4.3.1 Surface Cracking. Small surface cracks were noted on a number of the specimens after exposure to the 15kW laser. This cracking usually took the form of a circle slightly larger than the incident laser beam which is consistent with the large thermal gradients experienced around the perimeter. The cracks, when measured with the scanning electron microscope, averaged between .5 and 1 mil wide. Figure 43 is a microphotograph of the surface of a specimen displaying a typical cracking pattern. Figure 44 is a SEM microphotograph taken looking down at the RCG surface of a specimen and Figure 45 was taken looking at the cross section of the specimen. Note that these

microphotographs are to scale therefore accurate thickness and crack width measurements can be made. Note also that the chipping visible at the top of Figure 45 was a result of the preparation required for the SEM.

4.3.2 Surface Glazing. This phenomena was also noted during the initial laser test performed in October. Figures 26 and 27 show microphotographs of a glazed and unglazed area on the test specimen. This phenomena appears to be a result of molten RCG material flowing into and filling the small pores that naturally exist in the surface layer.

4.3.3 Surface Sag or Compression. This effect was also noted during the initial laser test but failure analysis revealed little about the mechanism. Microphotographs taken of the specimen subjected to the full laser potential show this effect more clearly. These microphotographs are presented in Figures 46 through 48. Note that in Figure 47 the RCG appears to have flowed into the substrate material and that the fiber lengths immediately under the RCG coating, Figure 47, are much shorter than the fiber lengths of a specimen taken from further into the substrate, Figure 48. It appears that thermal stress in the substrate caused fiber breakage and compaction and that the RCG material flowed into the substrate possibly causing further compaction.

The effects described above are generally minor. The stress cracks observed in several specimens are believed to be a result of the very localized heating produced by the laser beam and would not occur in a system that more uniformly heats the material. Surface glazing was seen at temperatures above 2700°F only and, even at 3000°F, would not effect the performance of the tile as a heat shield. The third effect noted in this testing would be more detrimental to the proper functioning of the LI-2200 system but was seen only at temperatures significantly higher than

3000°F. The defects observed on each of the test specimens are summarized in Table 5.

4.4 ELECTROMAGNETIC DATA REDUCTION. Measurements were made on 12 specimens during the course of this testing. In each case the scattering matrix was completely characterized both before exposure and after the specimen had stabilized at the target temperature. In addition, predictions of the electromagnetic performance of the LI-2200 system have been made and normalization data for each of the 12 specimens exists. This wealth of data is too voluminous to report in this document but all data is available upon request.

4.4.1 Normalization. Due to the nature of the calibration standards used for these measurements it was necessary to correct the phase of the measured data by moving the calibration reference planes to correspond with the surfaces of the test specimen. This was accomplished using the four equations listed below. These equations remove the residual phase error from the measurements by normalizing to a known calibration standard. In addition, S22 is phase shifted to move the calibration reference plane to coincide with the surface of the tile specimen.

$$S11_{sample} = -\left(\frac{S11_{measured}}{S11_{metal}}\right)$$

$$S22_{sample} = -\left(\frac{S22_{measured}}{S22_{metal}}\right) * e^{\left(j * \left(2 * \pi * frequency * \frac{D}{c}\right)\right)}$$

$$S12_{sample} = \left(\frac{S12_{measured}}{S12_{thru}}\right)$$

$$S21_{sample} = \left(\frac{S21_{measured}}{S21_{thru}}\right)$$

where:

D = distance to shift reference plane
c = speed of light
frequency = test frequency

4.4.2 Non-repetitive Spike Removal. The non-repetitive spikes, glitches, noted in section 2.6.3 were also present in the electromagnetic data acquired during the elevated temperature testing. These anomalies are particularly troublesome because their non-repetitive nature causes severe distortion during the Chirp-Z transform used to convert from the frequency domain to the time domain.

Figures 49 and 50 are examples of the raw electromagnetic data acquired during this testing. Notice the phase anomalies at 25.65 and 25.85 GHz. Time domain transformation of these glitches results in broad spectrum distortion in much the same way as the Fourier transform of the Dirac Delta function. Convolution of this time domain response with a band pass gating filter would result in increased frequency domain distortion. This topic is covered in many advanced signal processing texts. For this reason a de-glitching procedure was used to remove these anomalies. This procedure is described below.

The test to determine whether a datum in the electromagnetic data is a glitch is described by the equations given below.

$$local_i = \frac{\left(\sum_{j=-a}^{a} Datum_{i+j}\right)}{N} \qquad \text{for } j \neq 0 \text{ and } N = 2a$$

$$l2_i = \frac{\left(\sum_{j=-a}^{a} Datum_{i+j}^2\right)}{N} \qquad std_i = \sqrt{l2_i - local_i^2}$$

$$averagestd = \frac{\left(\sum_{i=0}^{num} std_i\right)}{num}$$

where num = Number of data points

This value, averagestd, was then used to test each data point in the data set.

$$test_i = \left| \frac{(Datum_i - local_i)}{averagestd} \right|$$

If the value of test was determined to be larger than a specified number of standard deviations, the testing routine would report the datum as an anomaly. The operator was then given the choice of correcting or ignoring the data point in question. If the operator elected to correct the data point, the value of $Datum_i$ was replaced by the value of $local_i$. The results of processing the data shown in Figures 49 and 50 with this procedure are shown Figures 51 and 52.

4.4.3 Time Domain Gating. Time domain gating techniques were used to remove the effects of parasitic reflections in the measurement system. The procedure followed was identical for all data generated during these tests. The procedure is as follows :

a. Transform frequency domain data to the time domain.

b. Use the marker functions of the HP-8510B to locate the maximum response in the time domain.

c. Set the gate center to the marker value found in step b.

d. Set the gate span to 1 nanosecond.

e. Turn on the time domain gating function of the HP-8510B and then re-collect the data.

Time domain gating will result in distortion at the edges of the frequency domain. This distortion is a result of the convolution of the time domain limited band pass filter response with the measured data and will become more pronounced with narrower filter pass bands. Every effort has been made to minimize the effects of this error source and therefore the gating error can be considered insignificant over the requested frequency range of 19-21 GHz.

4.4.4 Electromagnetic Data Reduction Procedure. A computer algorithm was written to perform the electromagnetic data reduction functions described above. The functions were performed in the order they are described, first normalization then glitch removal and finally time domain gating. A printed report specifying the correction parameters and the action taken by the reduction routine was generated for each of the test measurements. An example of this report can be found in Figure 53. The results of processing the data shown in Figures 49-50 are presented in Figures 54-55.

4.5 ELECTROMAGNETIC PREDICTIONS. The permittivities of the two materials that make up the LI-2200 system are not well characterized, but enough data exists to model the system with a fair amount of accuracy. Baseline permittivities and thicknesses for one test specimen were used to model the system and the results were compared to actual measurements. The baseline values were modified to gain an understanding of the critical parameters of the LI-2200 system and to improve the results of the model. This iterative procedure was used to determine the best fit parameters for the specimen. Since our examination of the tiles revealed them to be only approximately modelable as two layers of uniform thickness, this prediction should be

considered approximate. A comparison of the model results with actual measurements is presented in Figures 56-59. The best fit parameters for the specimen studied are listed below.

RCG Layer : Thickness =.0115 inches
Permittivity =3.875-j.04

Substrate : Thickness =.7385 inches
Permittivity =1.335-j.003

Note, the thickness of the RCG layer for a different specimen was measured at .0115 inches during failure analysis and the thickness of the RCG layer was determined to be the critical parameter for this model.

4.6 ELECTROMAGNETIC CHARACTERIZATION RESULTS. The results of the testing at 3000°F are summarized in Figures 60-75. The first 8 Figures, 60-67, represent the performance of the specimen labeled 159849-003-1036 before exposure to the laser. The last 8, Figures 68-75, represent the performance of the specimen while it was being held at 3000°F. Notice that the performance is essentially unchanged. There was a slight decrease in the frequency of resonance in the S11 and S22 measurements and a corresponding decrease in the depth of the resonant notch. The S12 and S21 measurements also show a slight shift of the resonant peak and a slight decrease in the transmitted energy. No electromagnetic modeling was performed on the elevated temperature measurements but the experience gained in modeling the electromagnetic performance at room temperature suggests that the RCG coating is responsible for this shift. A very slight thickness change, such as that caused by thermal expansion, or a slight change in permittivity could cause the effects seen. Note that the data presented in Figures 60-75 is plotted from 16-26 GHz. This was done to show the resonant behavior of the LI-2200 system but, because of the limitations discussed in Section 2.4.2, the results

may be distorted outside the frequency range 19-21 GHz.

The graphs presented in Figures 76-77 summarize the shifts in performance detected during this testing. Figure 76 shows the shift in resonant frequencies for the S11 and S22 measurements as a function of target temperature. The resolution in the frequency variable was .05 GHz therefore it is difficult to determine a trend in this data. It appears, however, that the shift in resonant frequency is increasing with increasing temperature. Figure 77 is more easily interpreted. Clearly the depth of the resonant notch is decreasing with increasing temperature. The results above 3000°F suggest that a transition is occurring in one of the LI-2200 materials. This result may be due to permittivity changes in the materials or physical changes resulting in a non-planer sample. All electromagnetic data collected during this testing has been stored on magnetic media in the Hewlett-Packard logical interchange format. Appendix C details the storage format and lists the available data files.

5.0 CONCLUSIONS

The elevated temperature testing performed on the LI-2200 system of materials yielded extremely valuable information. Not only did we thoroughly characterize the electromagnetic performance of the LI-2200 system but we also demonstrated the feasibility of using a high powered laser to heat materials and determined the LI-2200 system's ability to withstand extremely high temperatures in localized areas.

To summarize the results, we learned that the LI-2200 system could withstand localized heating to a least 3000°F without significant degradation either mechanically or electrically. The electromagnetic data collected in this testing, when reduced for the dielectric constants of the LI-2200 system's constitutive materials, will allow accurate modeling of electromagnetic phenomena interacting with the LI-2200 thermal protection system. It will be possible to use the permittivities derived from this testing to model the heat shield protecting electromagnetic measurement equipment used during re-entry and to compensate the electromagnetic measurements for the heat shield's presence.

The goal of this testing was to characterize the heat shield that will be used to protect the MRIS system so that it's effects can be eliminated from 20 GHz measurements of the plasma surrounding a re-entry vehicle. This testing program gathered the data required to completely satisfy this goal.

PRECEDING PAGE BLANK NOT FILMED

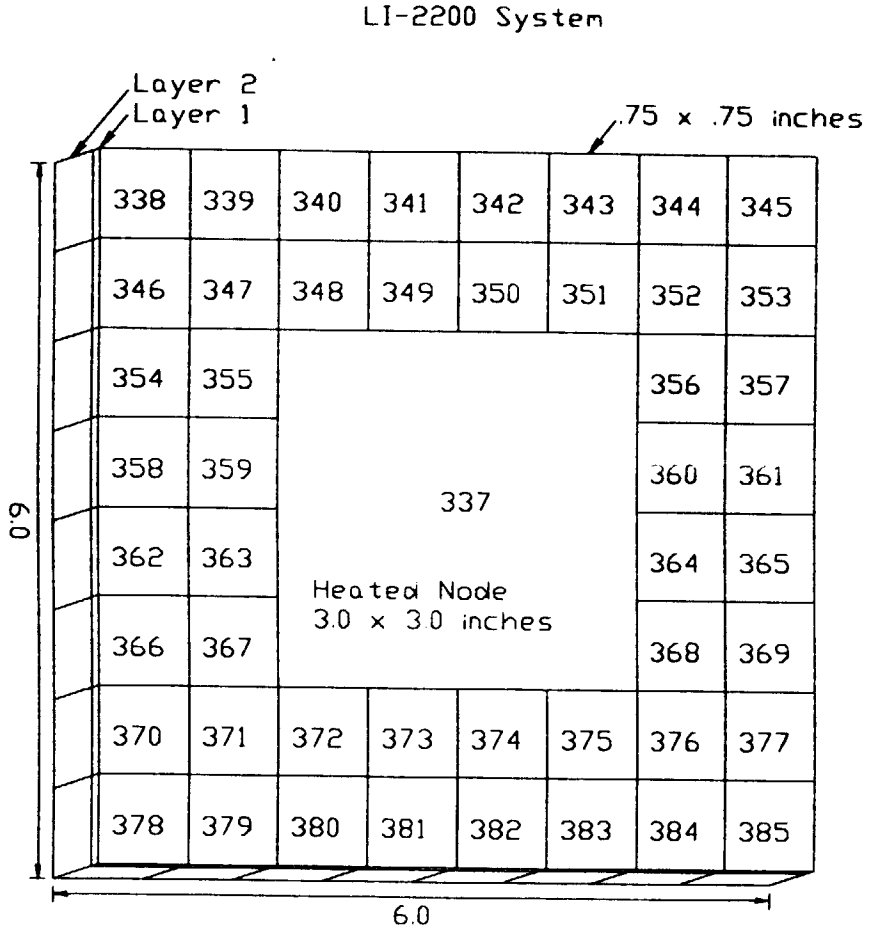

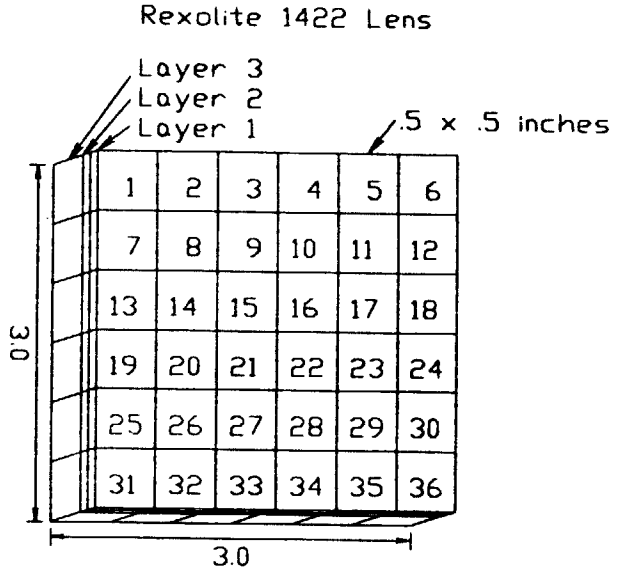

Rexolite 1422 Lens

	Thickness (in.)	Nodes
Layer 1	.002	1-36
Layer 2	.088	101-136
Layer 3	.910	201-236

LI-2200 System

	Thickness (in.)	Nodes
Layer 1	.020	337-385
Layer 2	.980	437-485

FIGURE 1 - THERMAL MODEL PATCH ASSIGNMENT AND LAYOUT

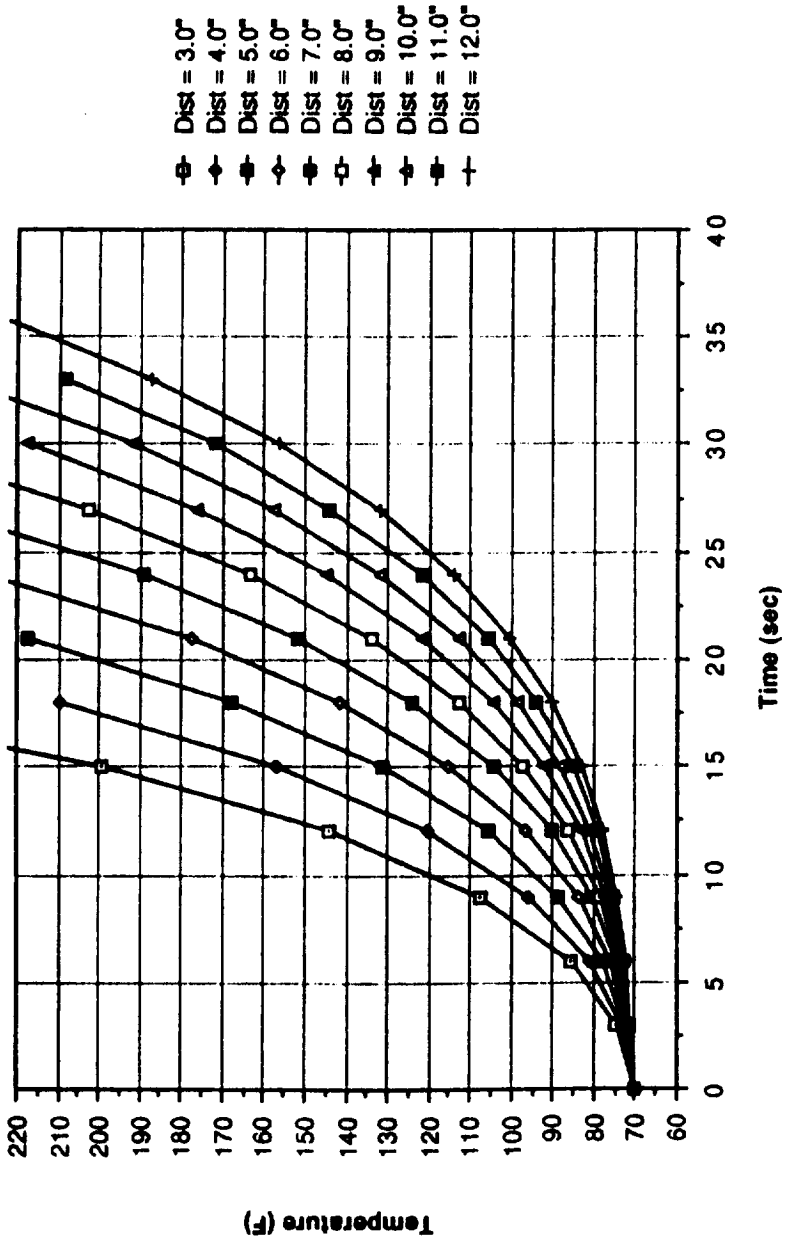

FIGURE 2 - REXOLITE 1422 LENS TEMPERATURE VERSUS TIME FOR VARIOUS LENS/SPECIMEN SEPARATIONS

FIGURE 2

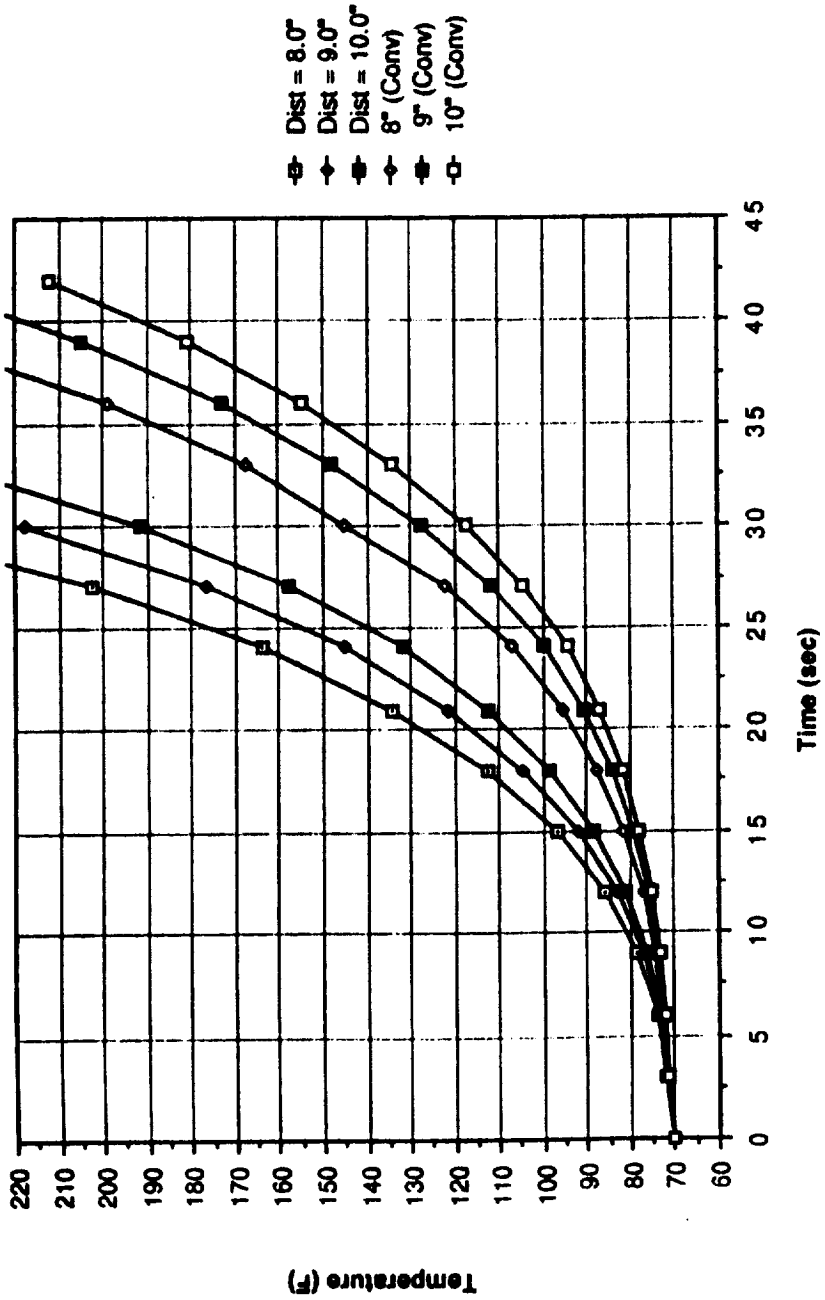

FIGURE 3 - REXOLITE 1422 LENS TEMPERATURE VERSUS TIME FOR VARIOUS LENS/SPECIMEN SEPARATIONS - WITH AND WITHOUT CONVECTION LOSSES

FIGURE 3

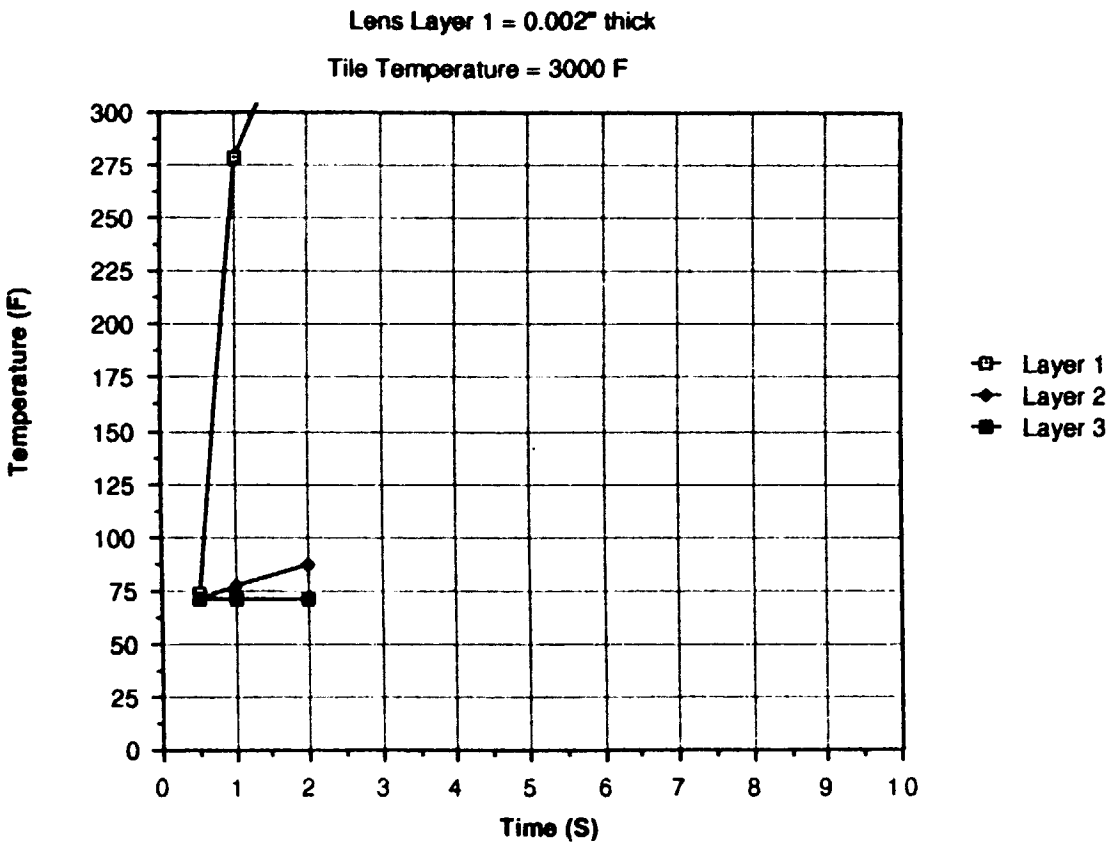

FIGURE 4 - REXOLITE 1422 LENS TEMPERATURE VERSUS TIME AFTER TRANSIENT EXPOSURE - EMISSIVITY = .8

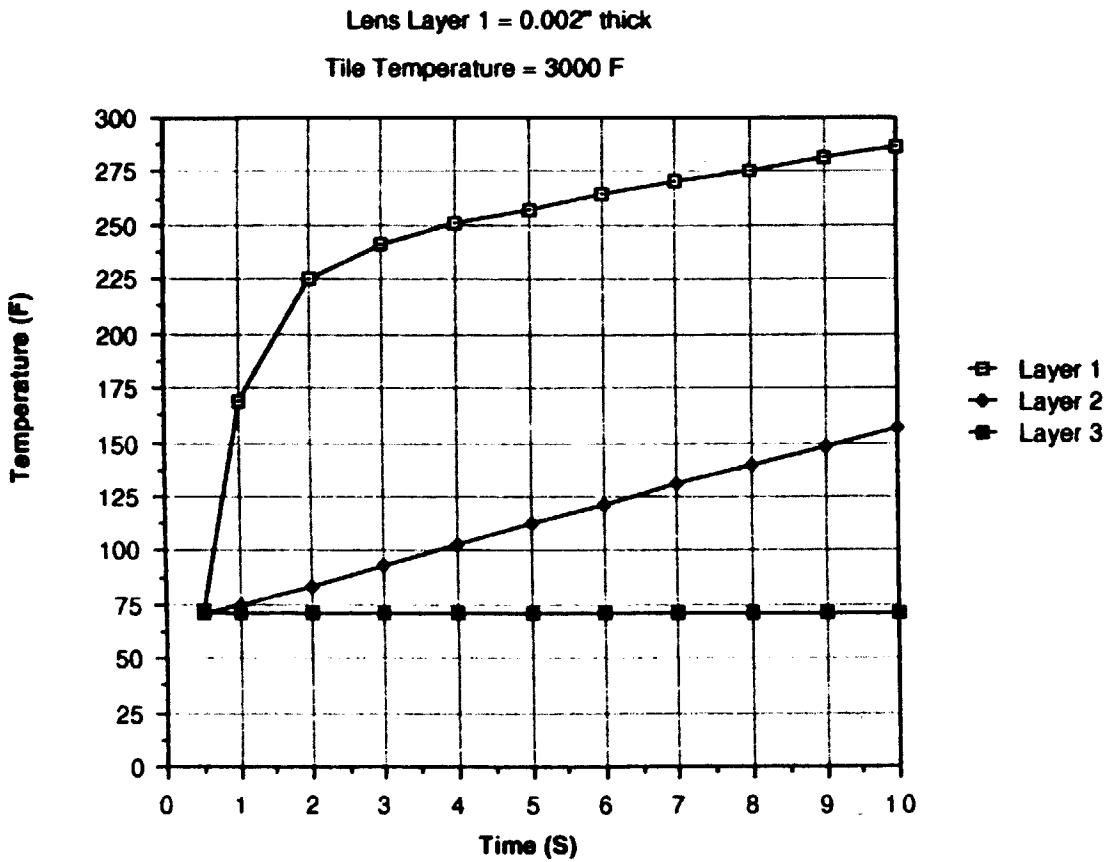

FIGURE 5 - REXOLITE 1422 LENS TEMPERATURE VERSUS TIME AFTER TRANSIENT EXPOSURE - EMISSIVITY = .38

1	2" LENS MOUNT
2	ANTENNA FEED
3	.5" LINEAR STAGE
4	ROD HOLDER & ROD
5	REAR LENS MOUNT
6	FORWARD LENS MOUNT
7	SPACER

8	MOUNTING PLATE
9	MOUNTING TABLE
10	2" LINEAR STAGE
11	SAMPLE HOLDER
12	TPS TILE SAMPLE
13	
14	

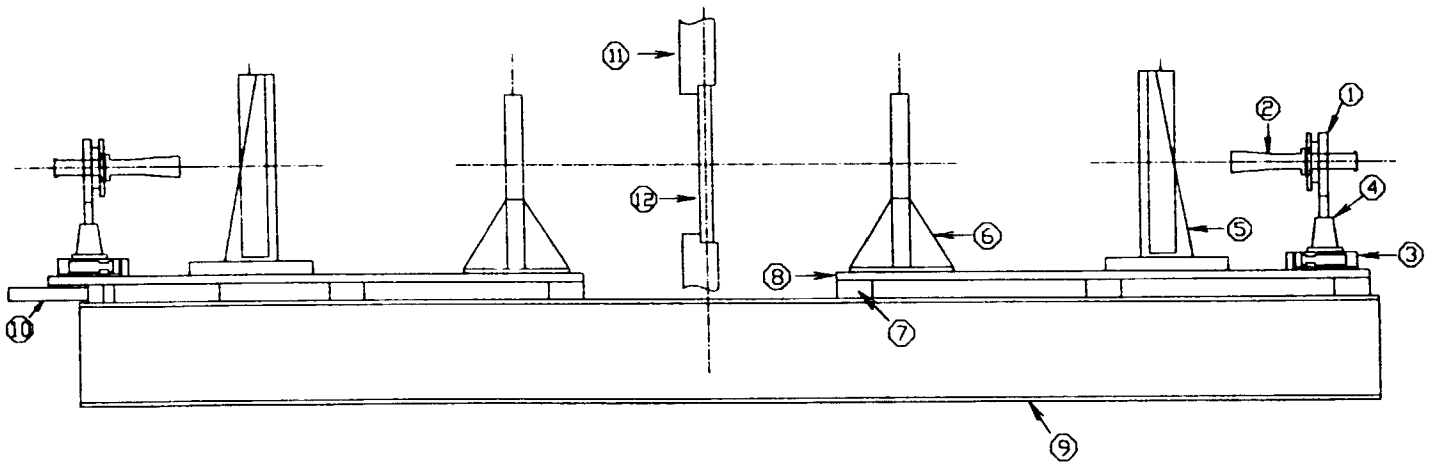

FIGURE 6 - ELEVATED TEMPERATURE ELECTROMAGNETIC CHARACTERIZATION SYSTEM SCHEMATIC DIAGRAM

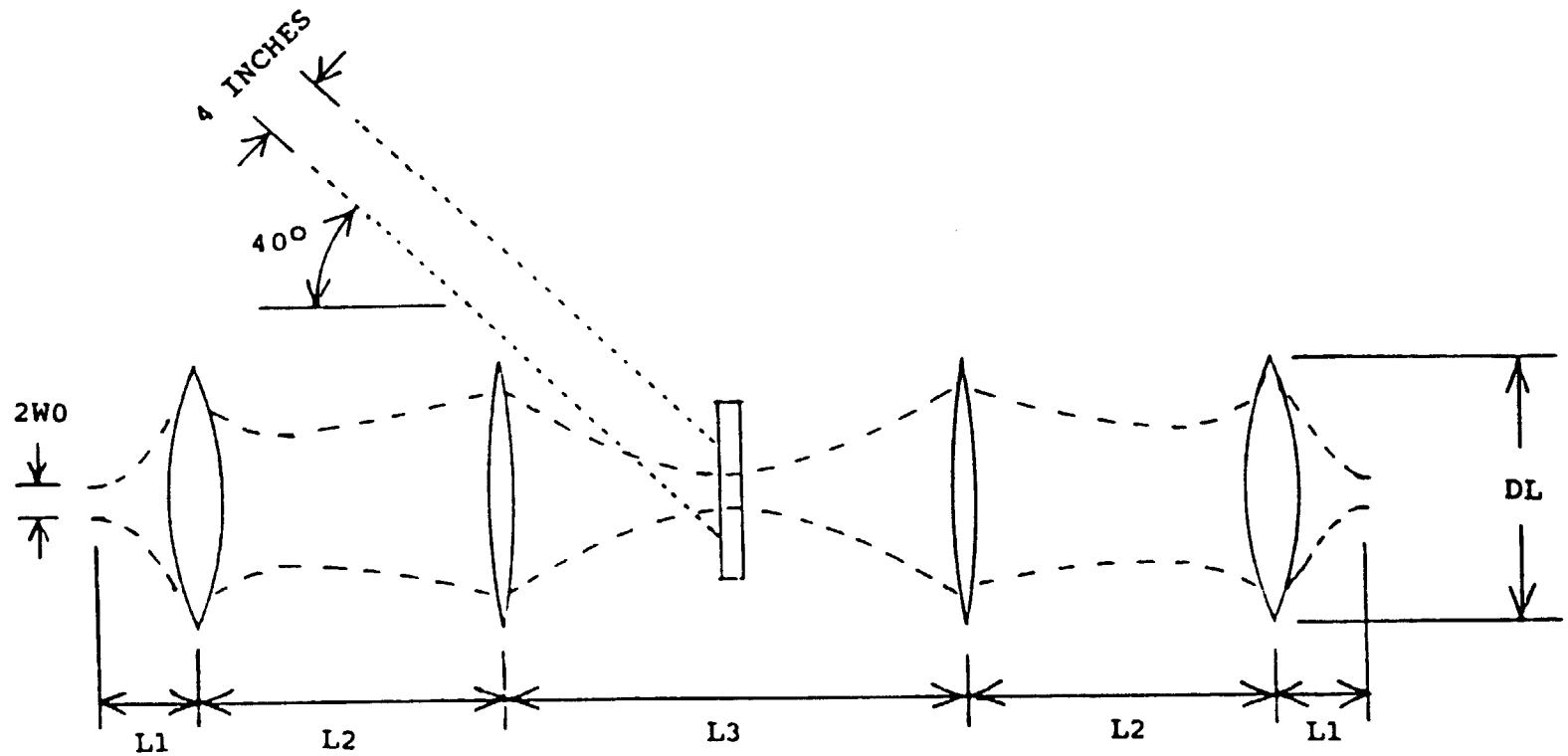

L1 = 4.071 INCHES
L2 = 14.982 INCHES
L3 = 21.823 INCHES

2W0 = 0.660 INCHES
DL = 7.000 INCHES

FIGURE 7 - DUAL LENS SPOT FOCUSING ANTENNA SYSTEM SCHEMATIC DIAGRAM

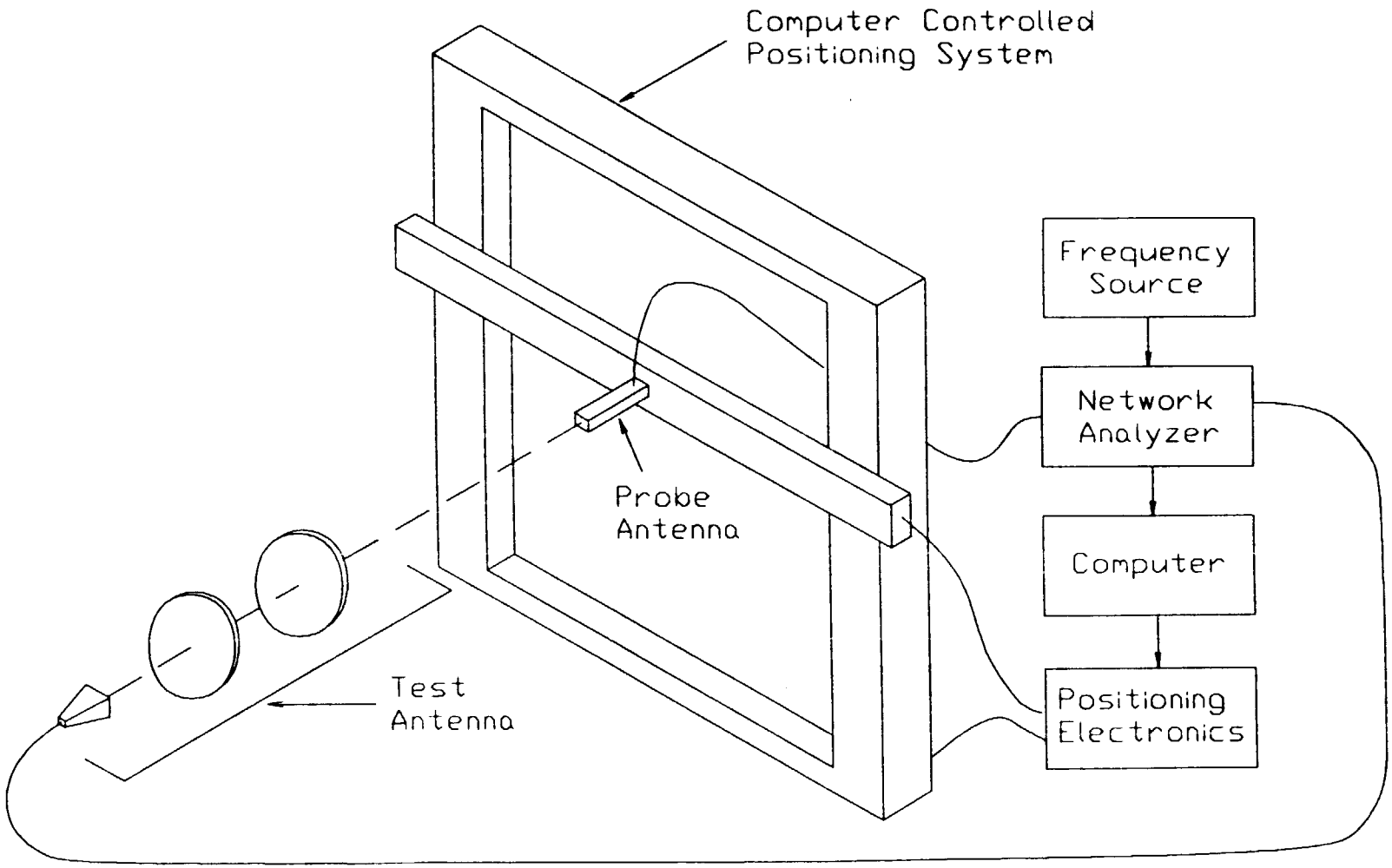

FIGURE 8 - SCHEMATIC DIAGRAM OF THE MICROWAVE AUTOMATED SCANNING SYSTEM USED TO OPTIMIZE THE DUAL LENS ANTENNAS

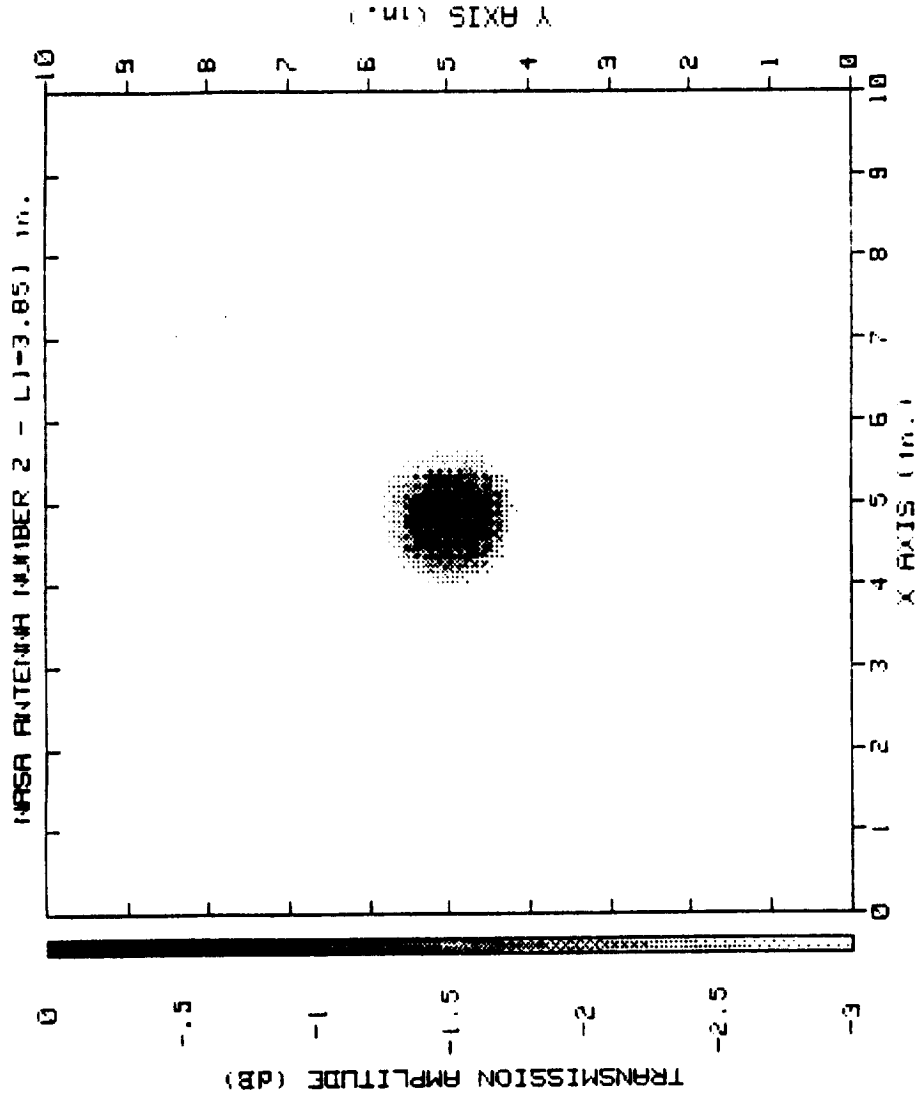

FIGURE 9 - HALF POWER SPOT SIZE OF AN OPTIMALLY ADJUSTED DUAL LENS ANTENNA AT 20 GHZ

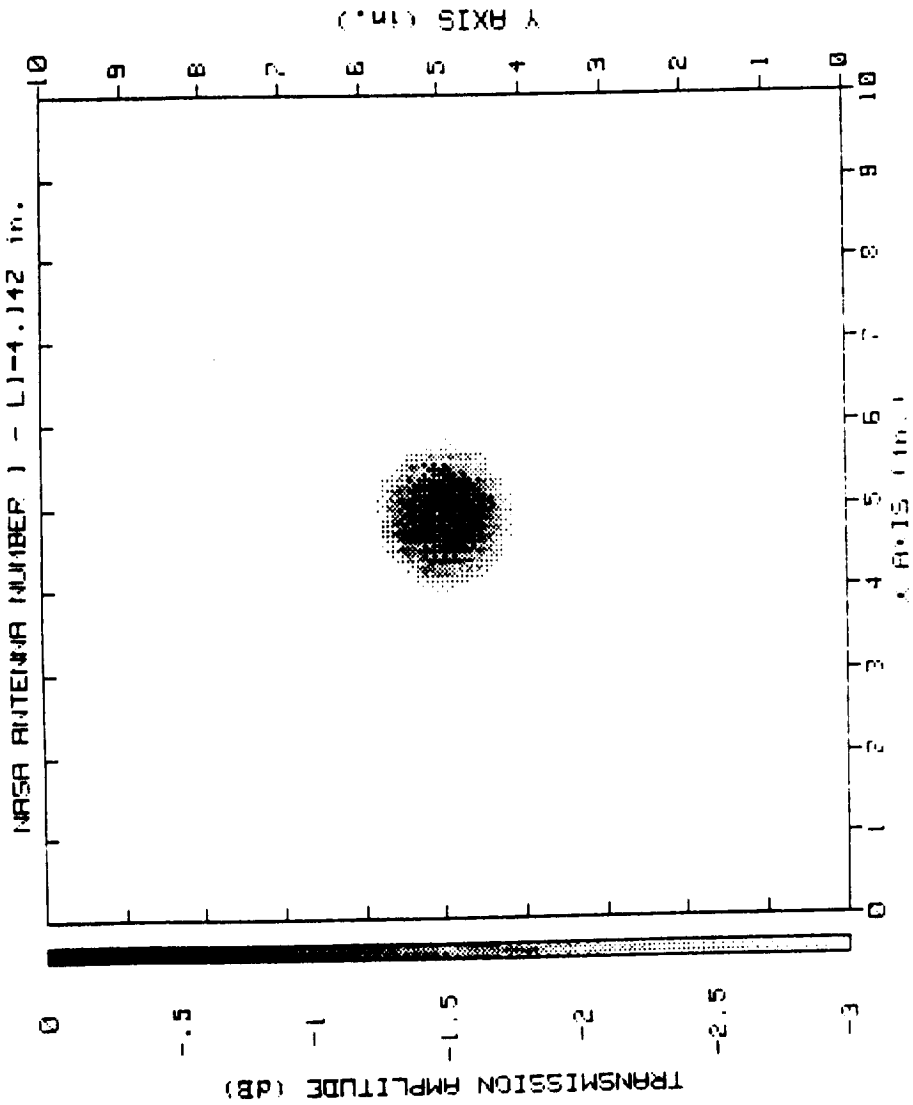

FIGURE 10 - HALF POWER SPOT SIZE OF A DE-FOCUSED DUAL LENS ANTENNA AT 20 GHZ

FIGURE 10

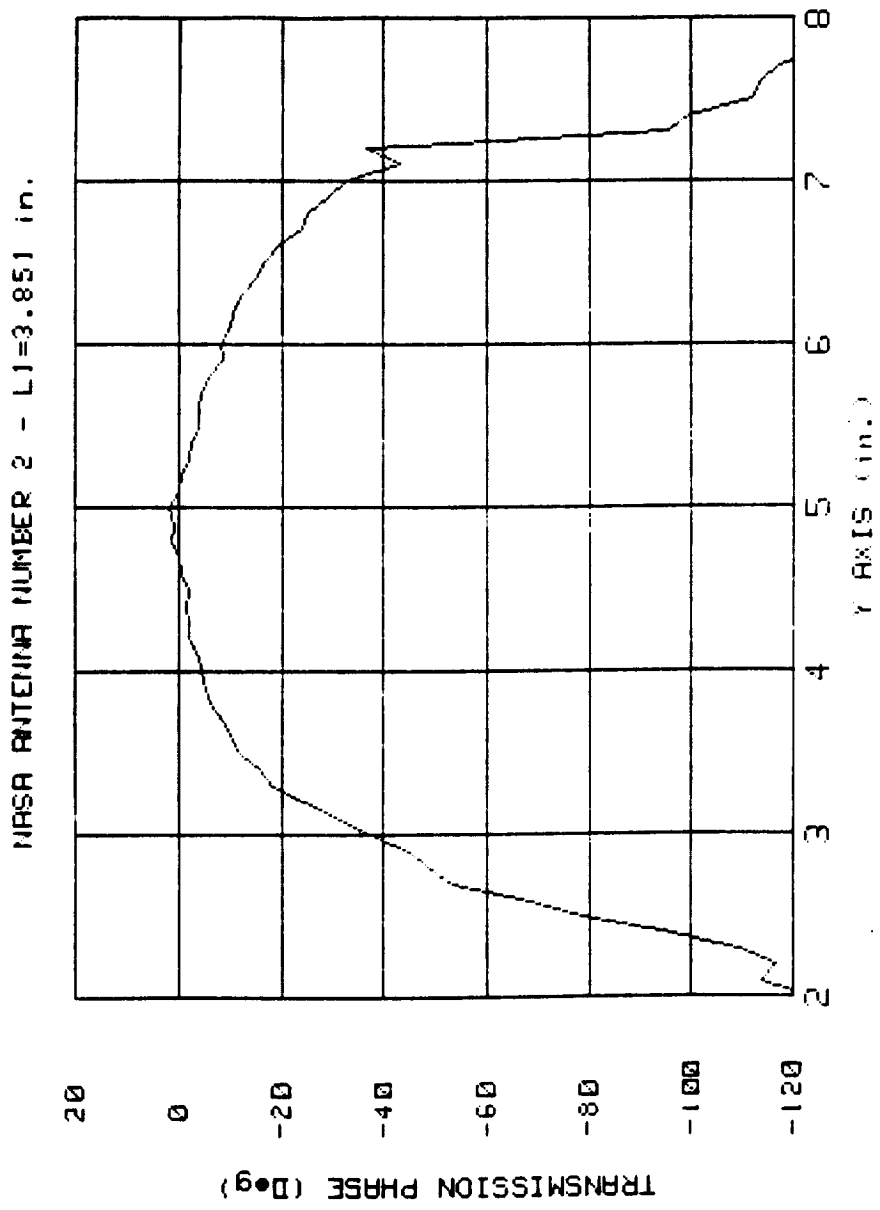

FIGURE 11 - PHASE TAPER OF AN OPTIMALLY ADJUSTED DUAL LENS ANTENNA AT 20 GHZ

FIGURE 11

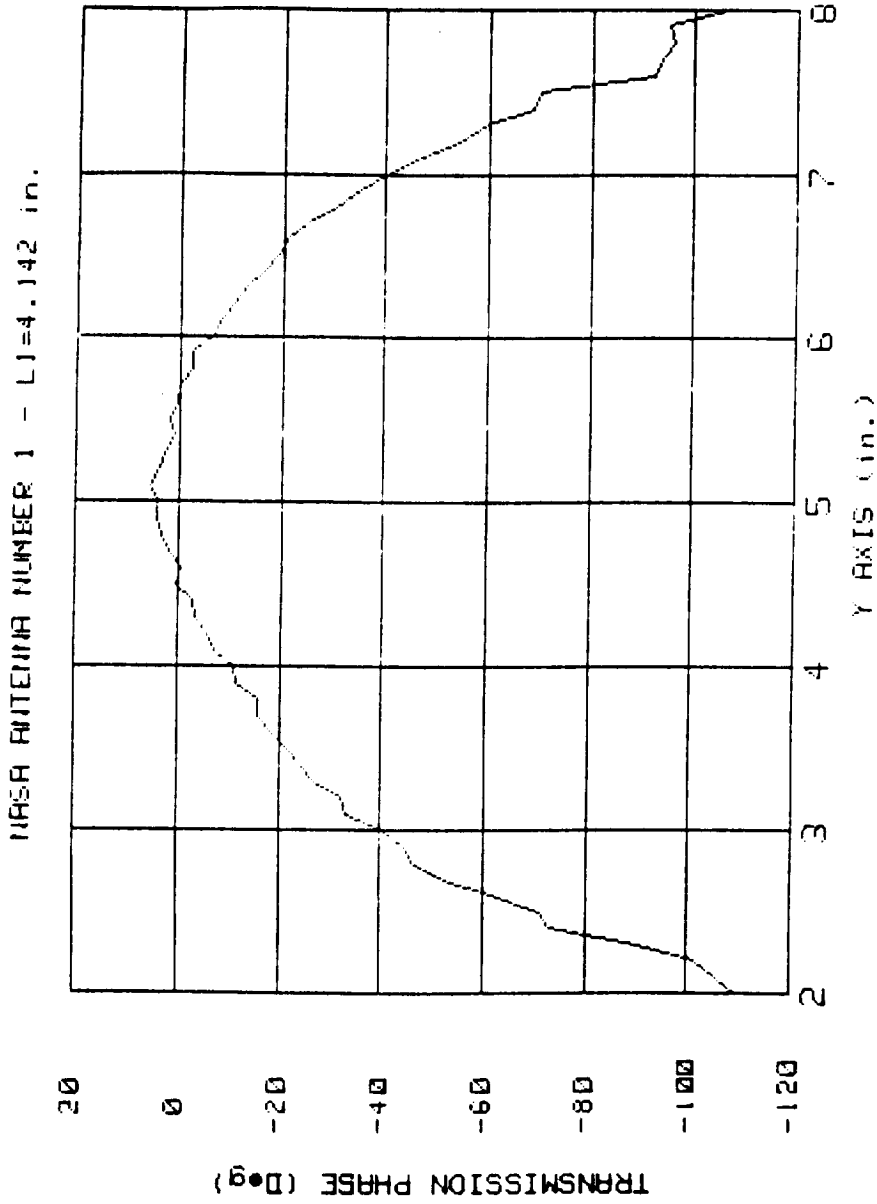

FIGURE 12 - PHASE TAPER OF A DE-FOCUSED DUAL LENS ANTENNA AT 20 GHZ

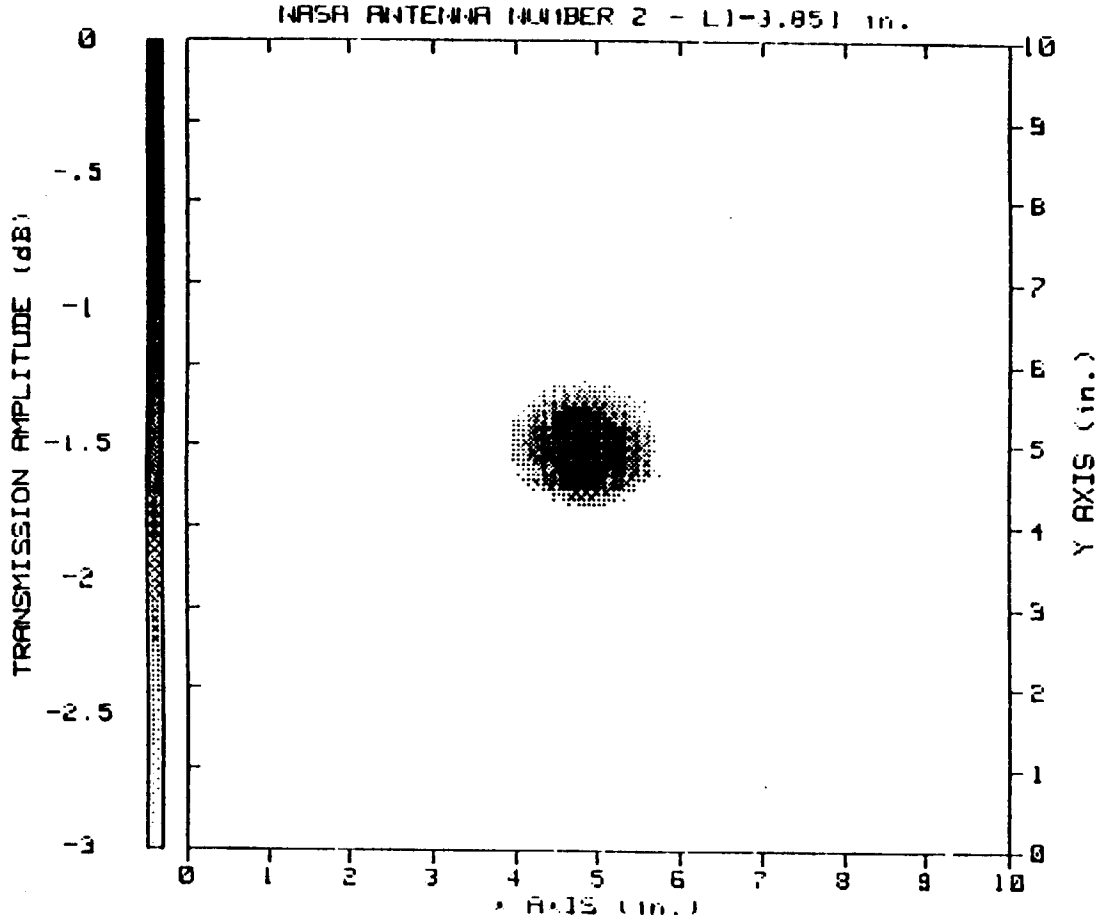

FIGURE 13 - HALF POWER SPOT SIZE OF AN OPTIMALLY ADJUSTED DUAL LENS ANTENNA AT 19 GHZ

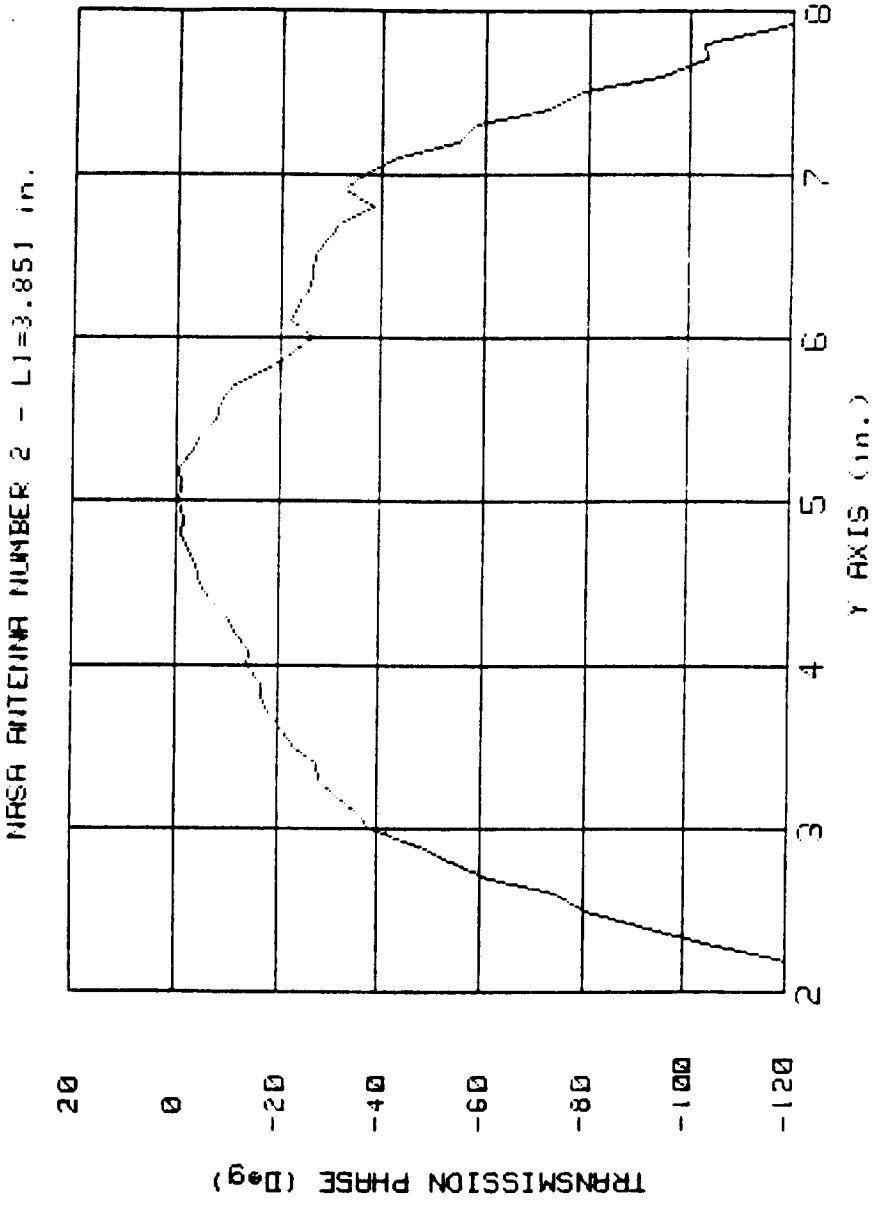

FIGURE 14 - PHASE TAPER OF AN OPTIMALLY ADJUSTED DUAL LENS ANTENNA AT 19 GHZ

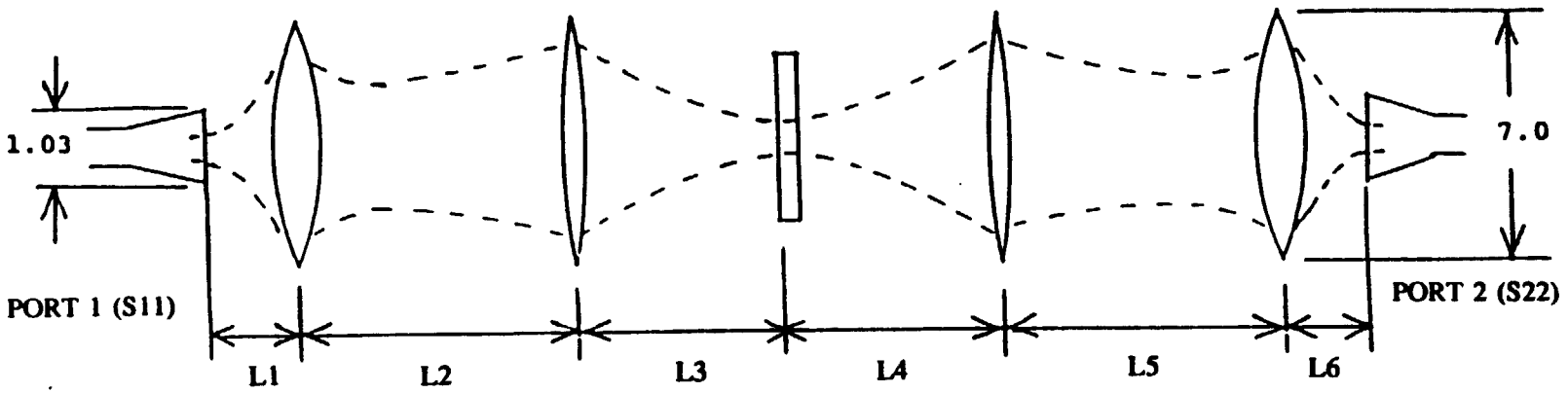

	Validation	Test
L1	3.894 in.	3.894 in.
L2	14.991 in.	14.991 in.
L3	10.562 in.	10.560 in.
L4	11.222 in.	11.229 in.
L5	14.991 in.	14.991 in.
L6	3.851 in.	3.851 in.

FIGURE 15 - ETEC SYSTEM COMPONENT LAYOUT

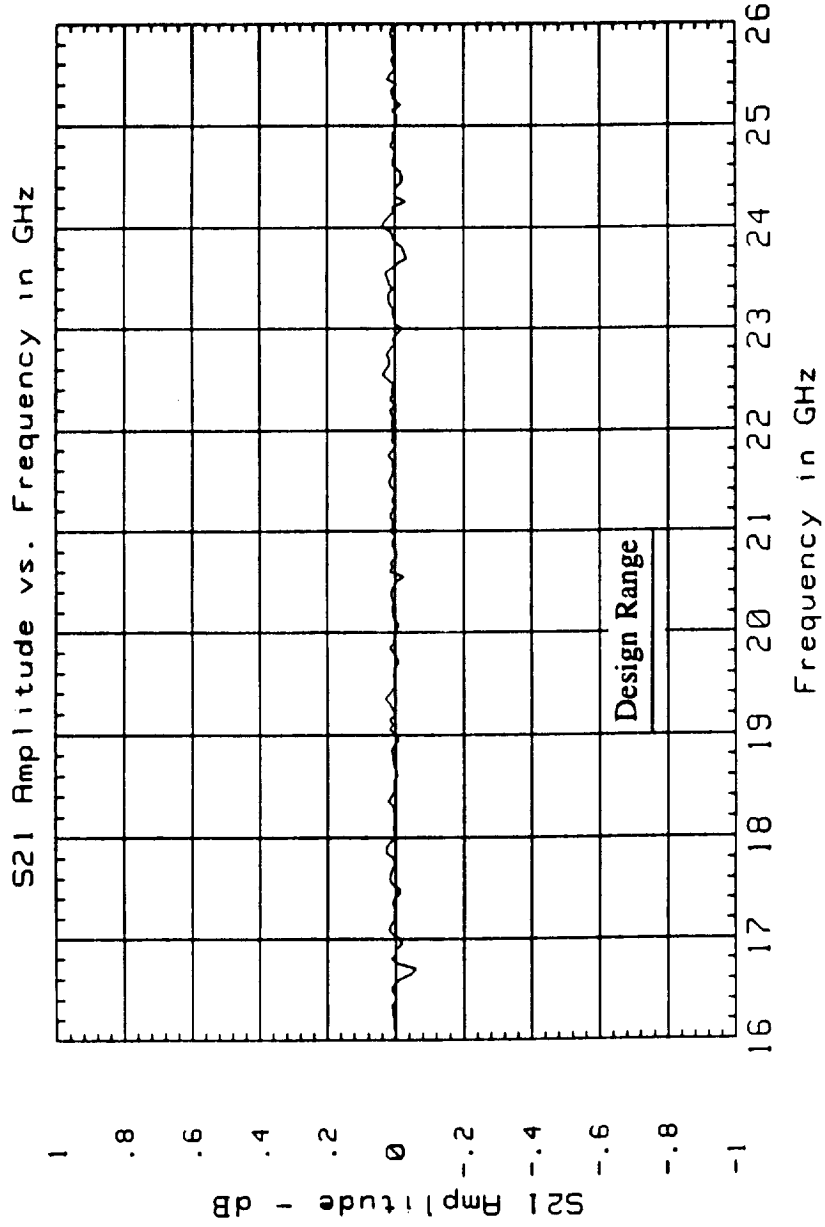

FIGURE 16 - TRANSMISSION AMPLITUDE OF THE EMPTY ETEC SYSTEM AFTER TRL CALIBRATION

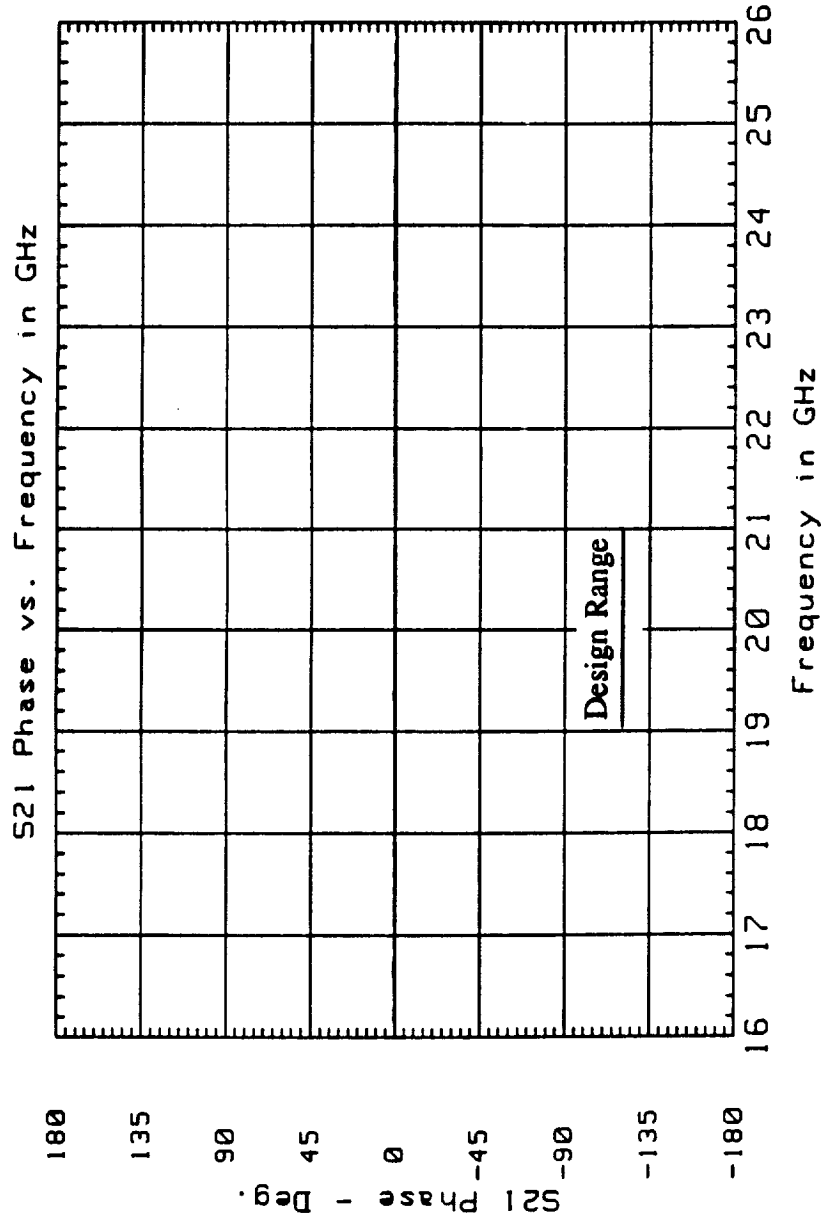

FIGURE 17 - TRANSMISSION PHASE OF THE EMPTY ETEC SYSTEM AFTER TRL CALIBRATION

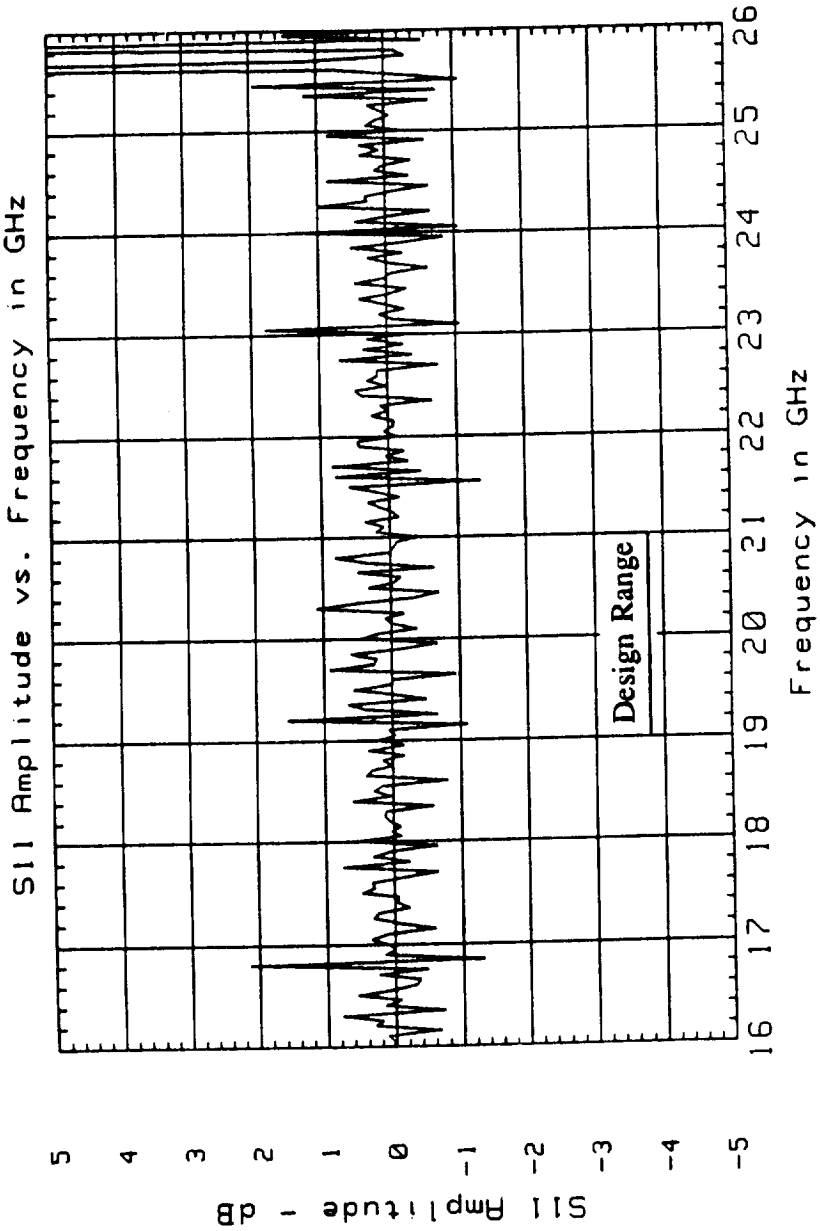

FIGURE 18 - REFLECTION AMPLITUDE FROM AN ALUMINUM PLATE IN THE ETEC SYSTEM AFTER TRL CALIBRATION

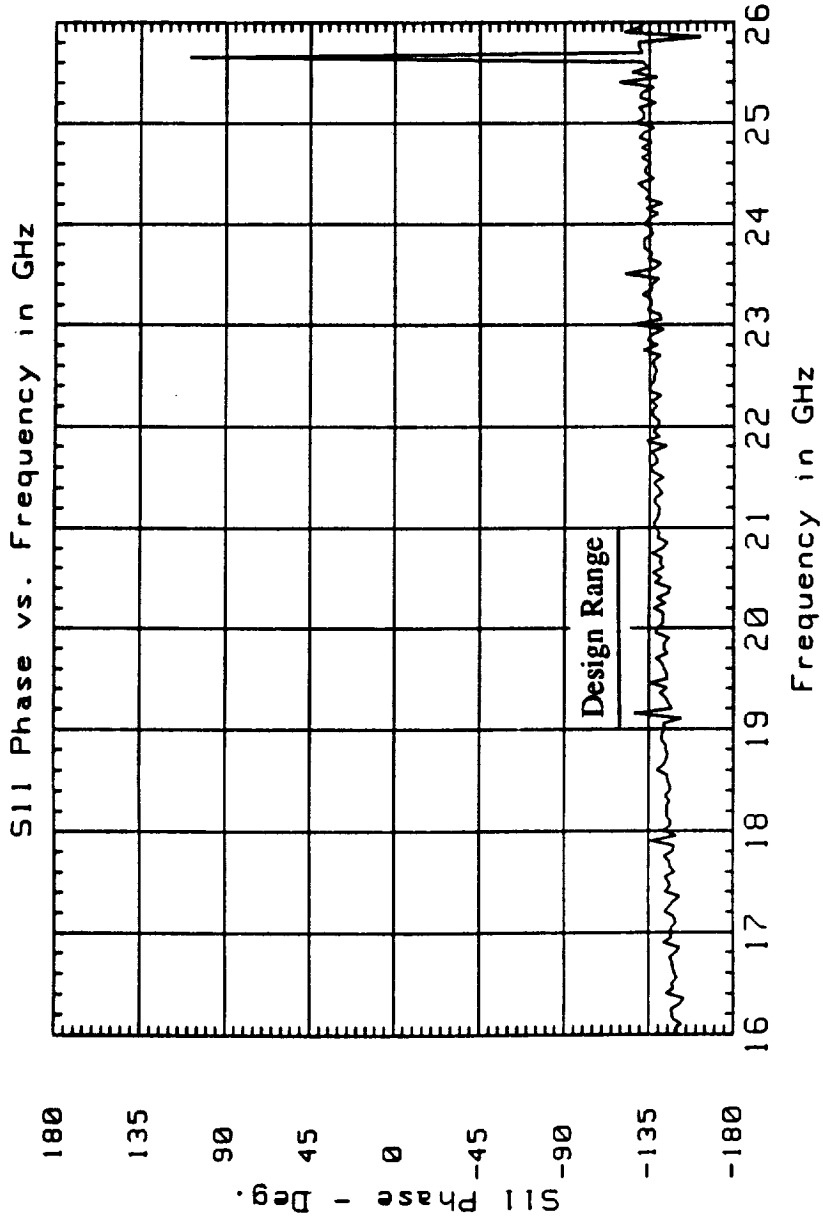

FIGURE 19 - REFLECTION PHASE FROM AN ALUMINUM PLATE IN THE ETEC SYSTEM AFTER TRL CALIBRATION

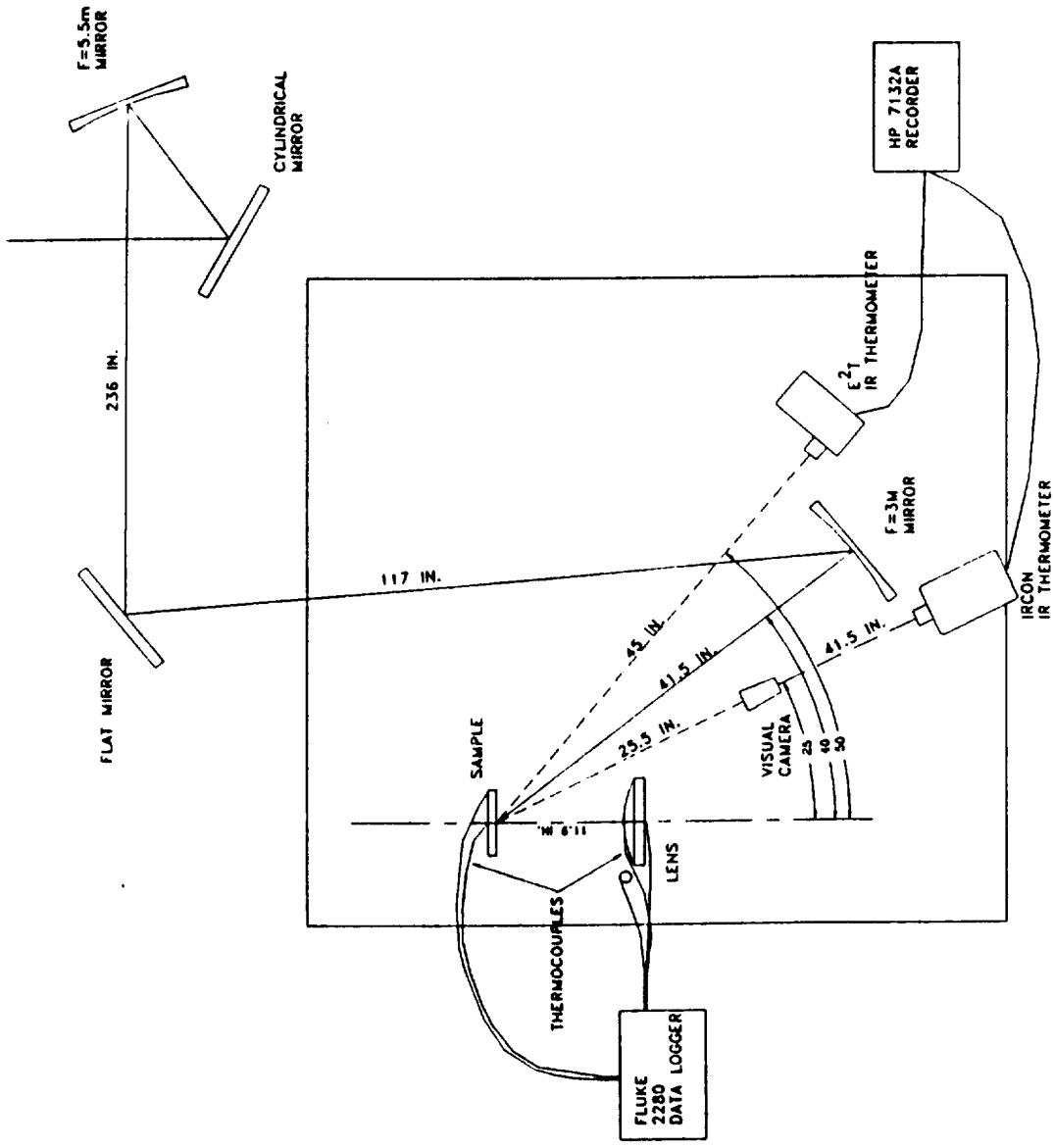

FIGURE 20 - LASER OPTICS AND EQUIPMENT LAYOUT FOR THE INITIAL LASER TESTS PERFORMED ON OCTOBER 23, 1991

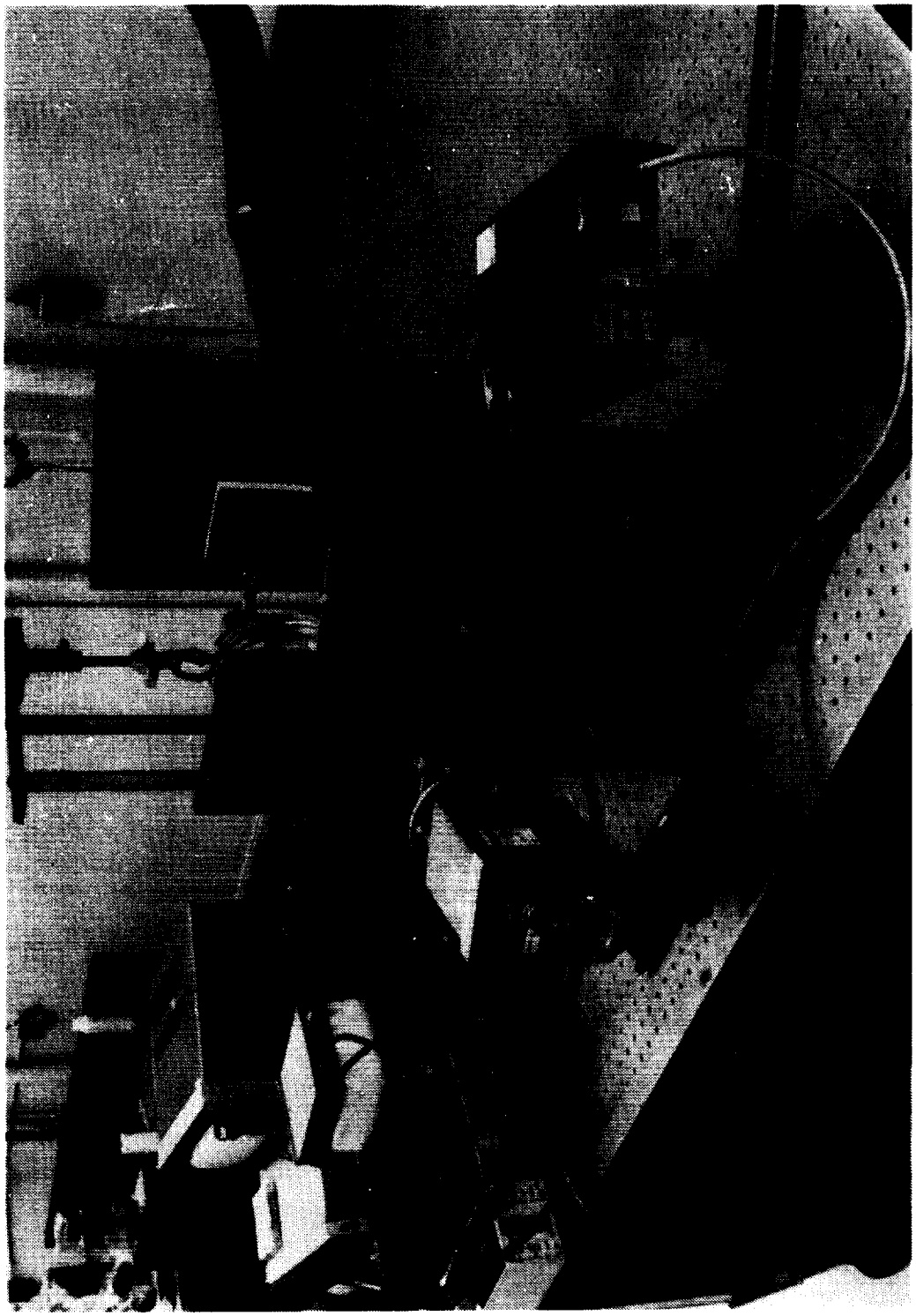

FIGURE 21 - PHOTOGRAPH OF THE EQUIPMENT LAYOUT USED FOR THE INITIAL LASER TESTS PERFORMED ON OCTOBER 23, 1991

ORIGINAL PAGE
BLACK AND WHITE PHOTOGRAPH

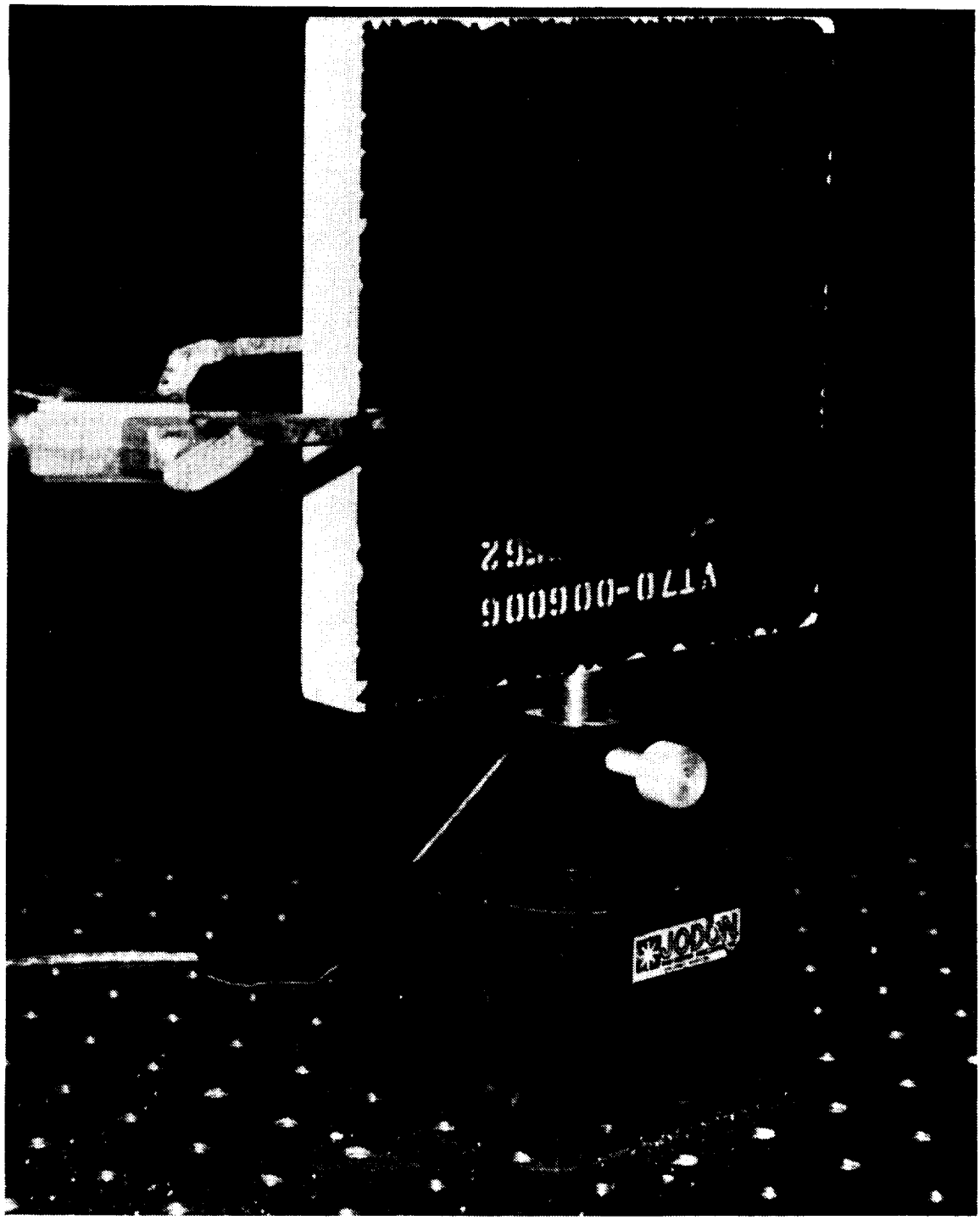

FIGURE 22 - LI-2200 SPECIMEN AFTER 11,567 WATT/3 SECOND EXPOSURE

ORIGINAL PAGE
BLACK AND WHITE PHOTOGRAPH

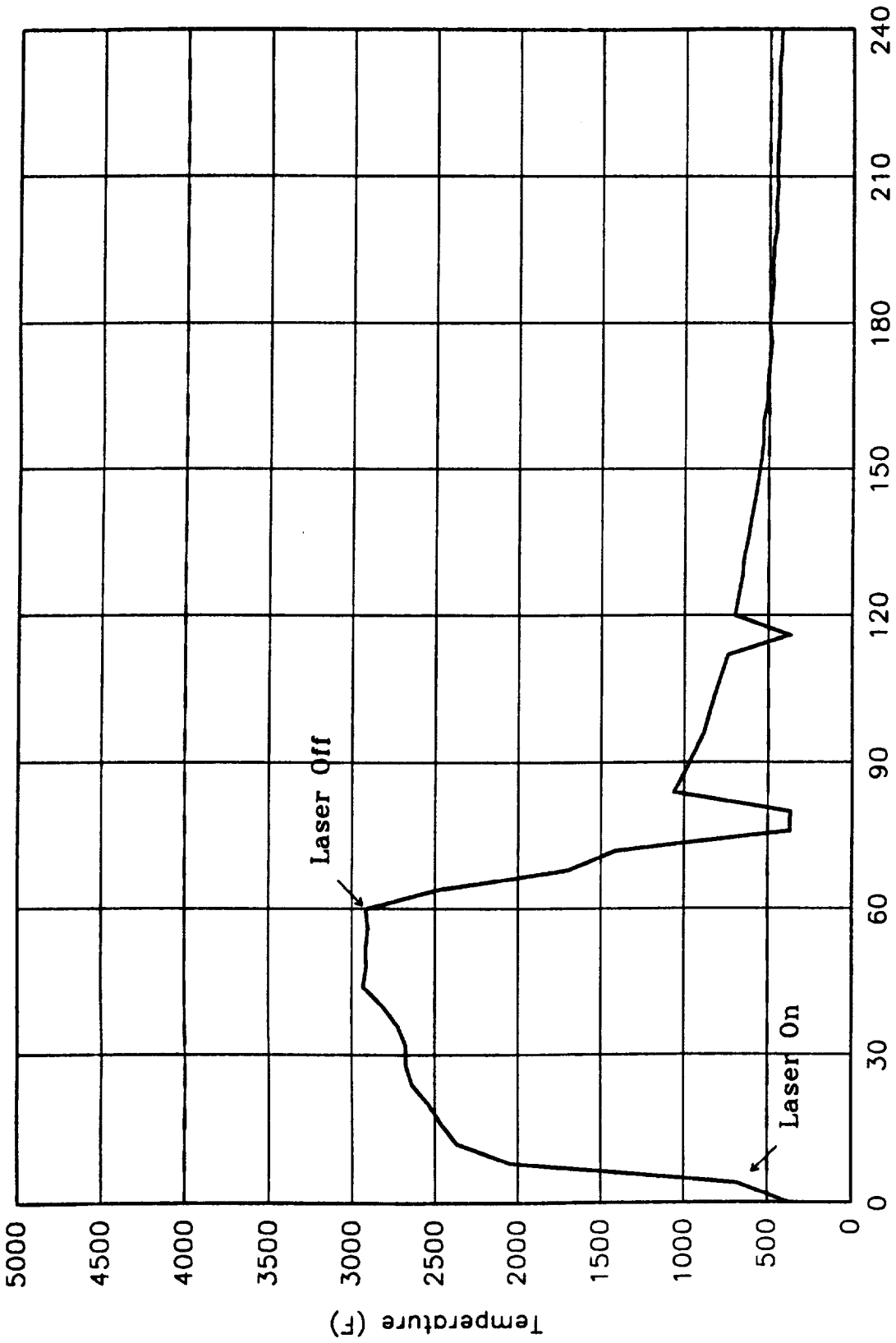

FIGURE 23 - LI-2200 SURFACE TEMPERATURE PROFILE FOR A 6,800 WATT LASER EXPOSURE

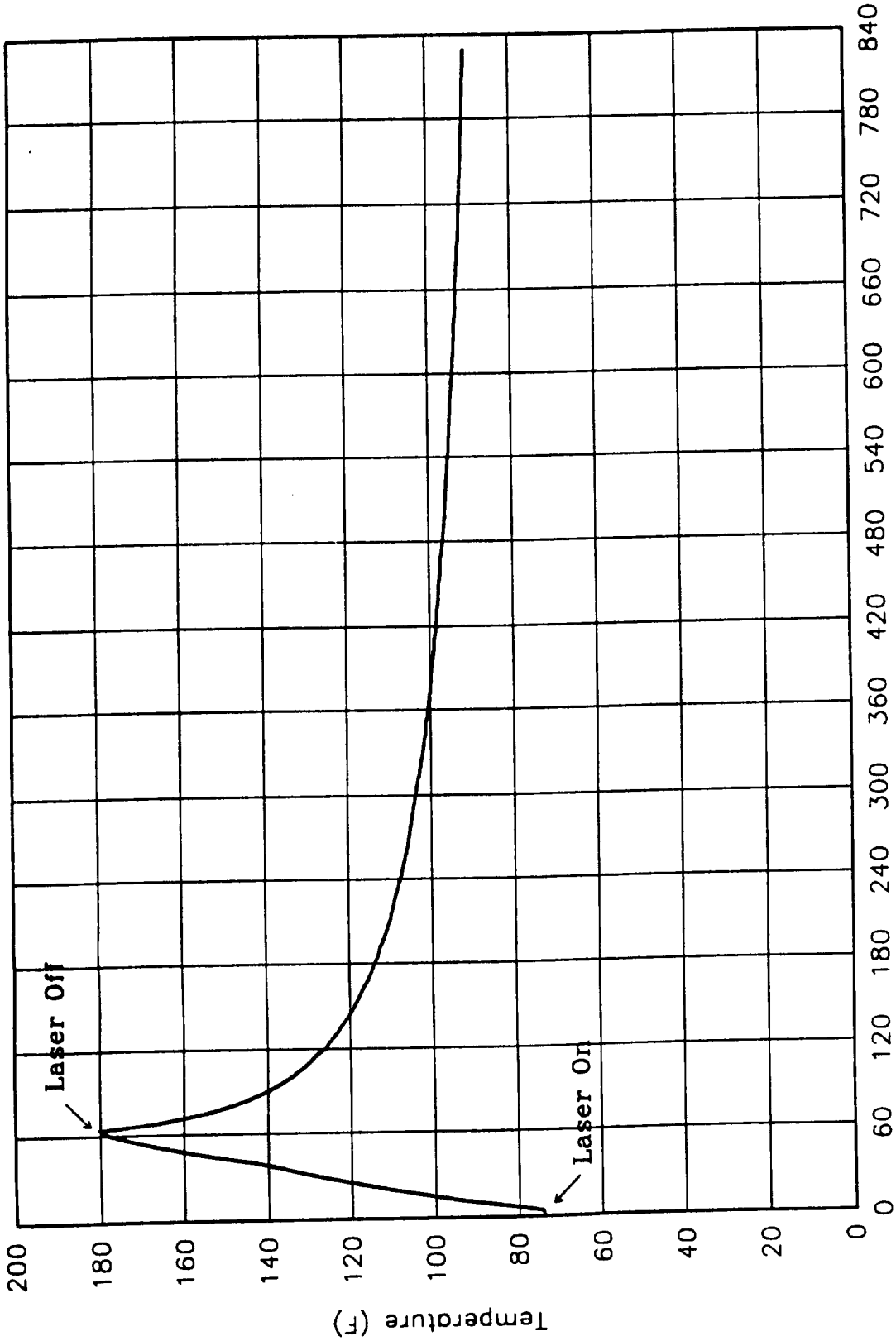

FIGURE 24 - FORWARD LENS FRONT SURFACE TEMPERATURE PROFILE FOR A 6,800 WATT LASER EXPOSURE

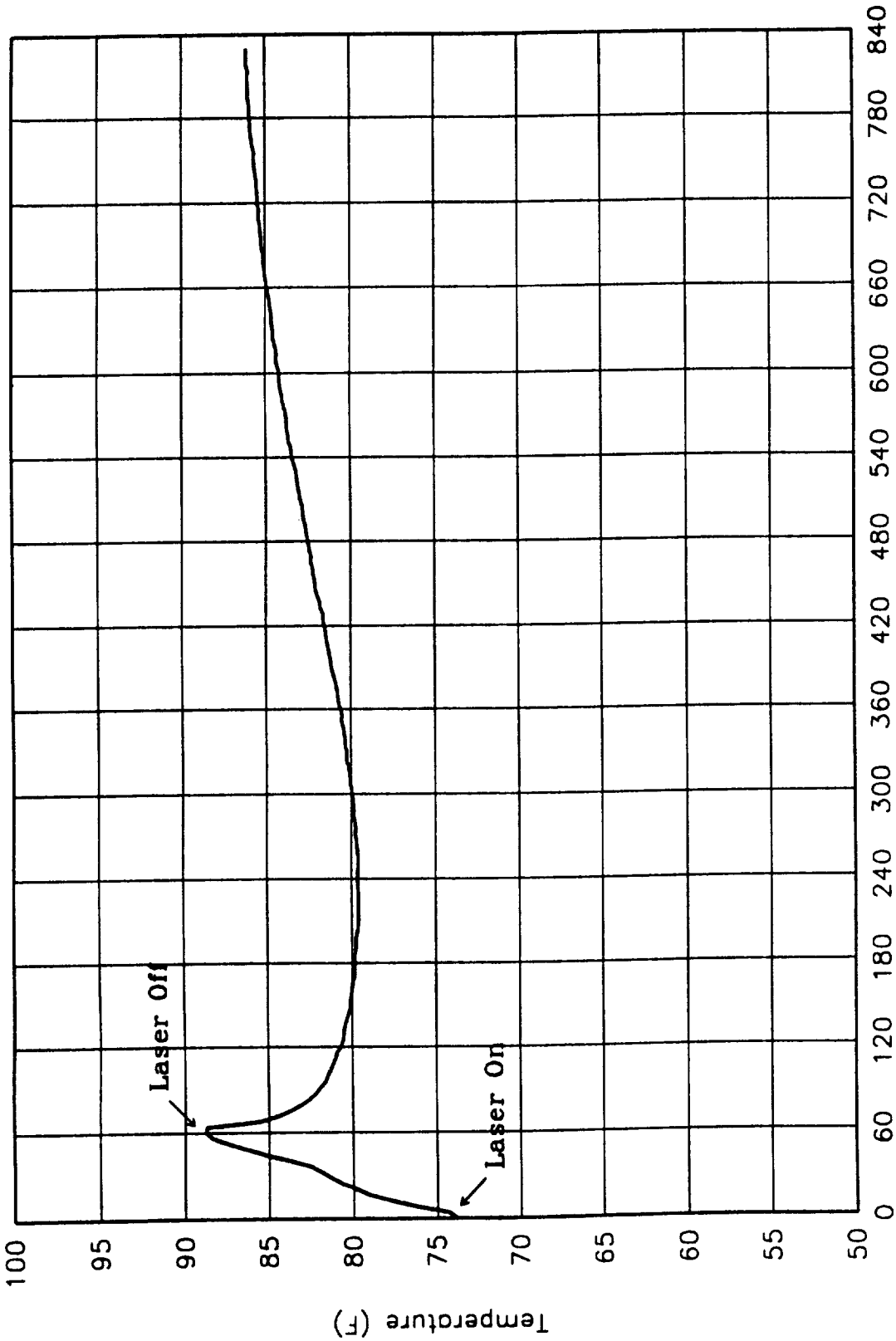

FIGURE 25 - FORWARD LENS REAR SURFACE TEMPERATURE PROFILE FOR A 6,800 WATT LASER EXPOSURE

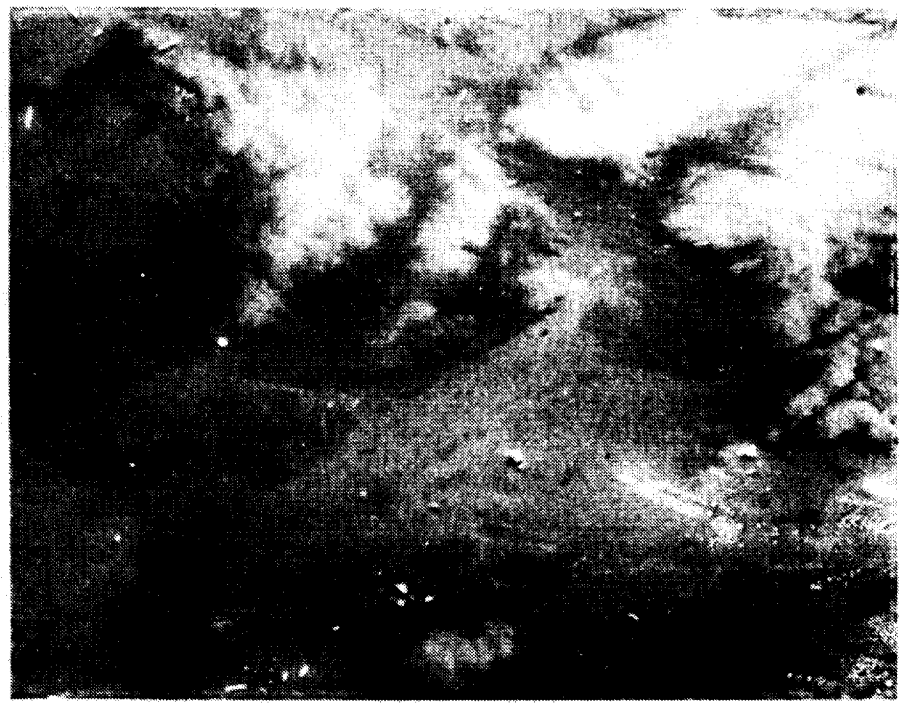

FIGURE 26 - 200X MICROPHOTOGRAPH OF LASER DAMAGED RCG COATING

ORIGINAL PAGE
BLACK AND WHITE PHOTOGRAPH

FIGURE 27 - 200X SEM MICROPHOTOGRAPH OF UNDAMAGED RCG COATING

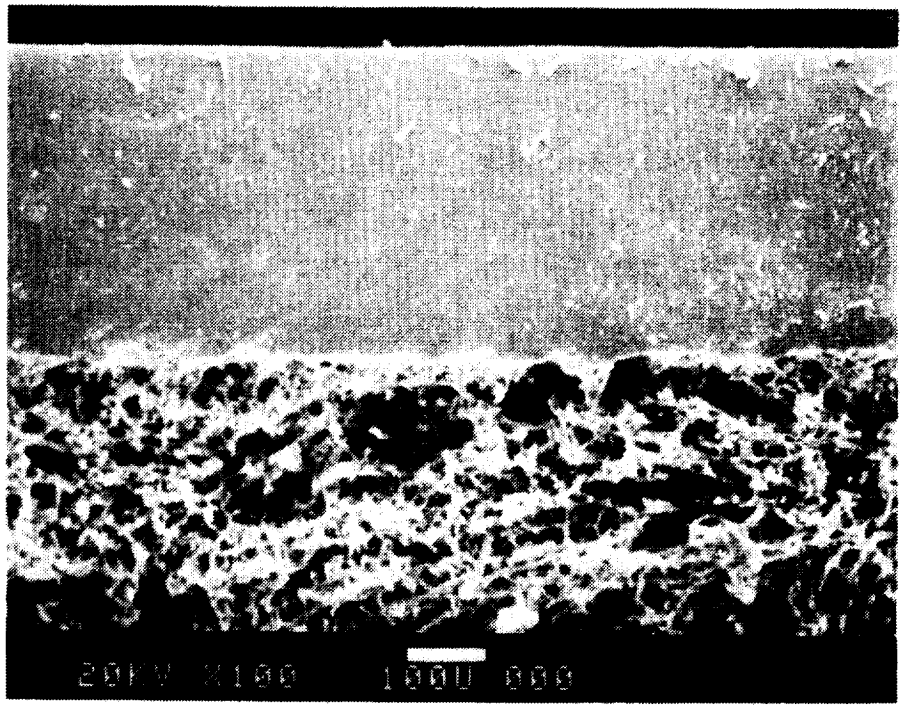

FIGURE 28 - 100X MICROPHOTOGRAPH OF LASER DAMAGED RCG COATING/SUBSTRATE INTERFACE

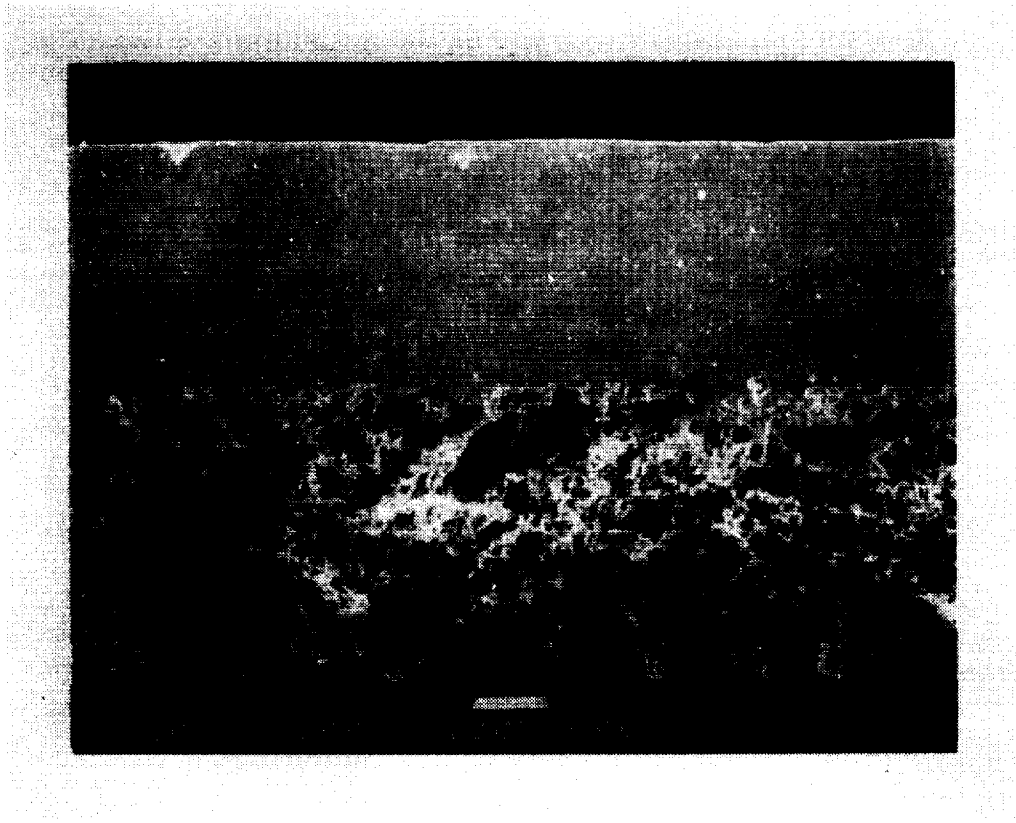

FIGURE 29 - 100X SEM MICROPHOTOGRAPH OF UNDAMAGED RCG COATING/SUBSTRATE INTERFACE

ORIGINAL PAGE
BLACK AND WHITE PHOTOGRAPH

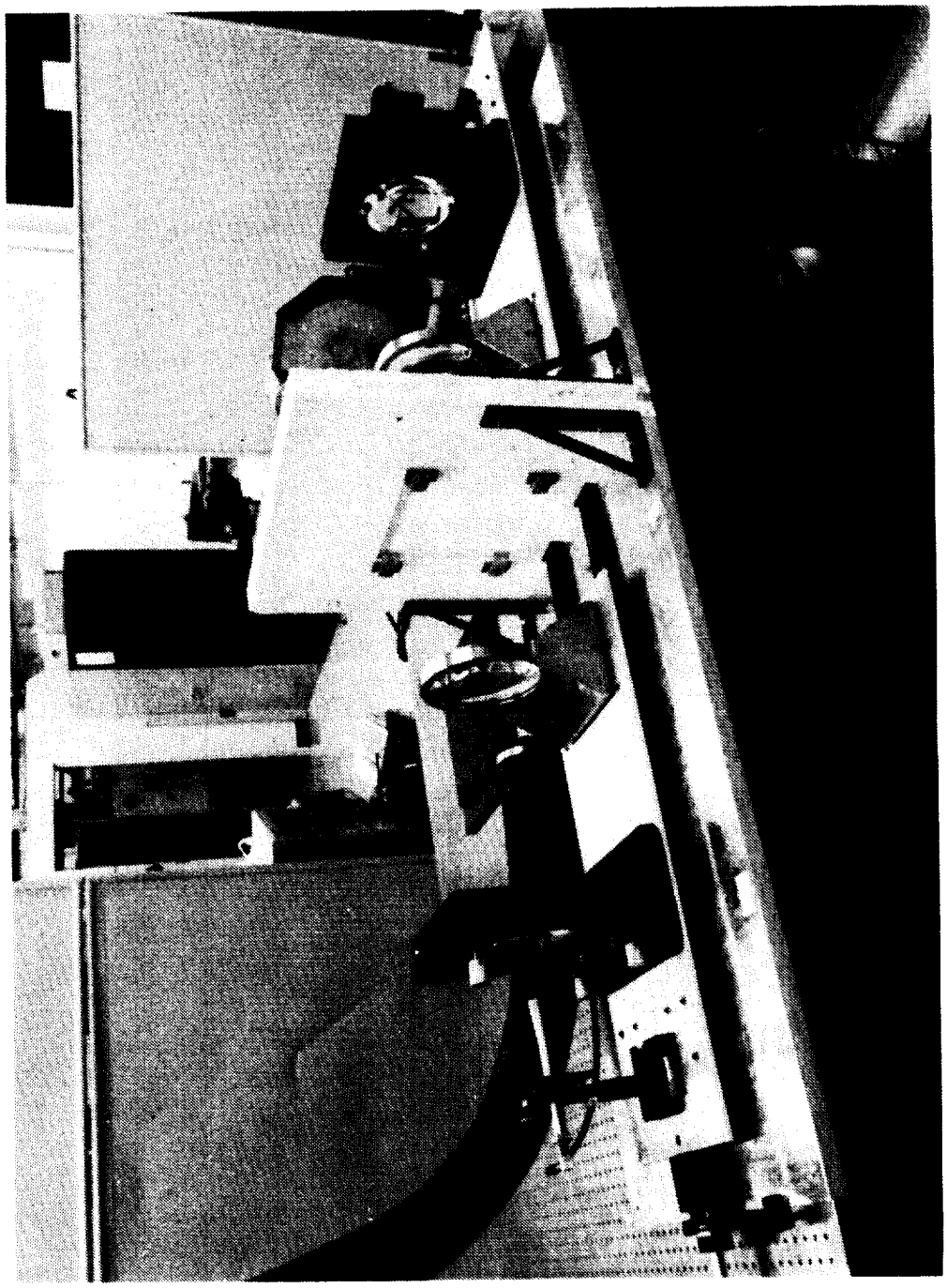

FIGURE 30 - ETEC SYSTEM PRIOR TO ELEVATED TEMPERATURE TESTING

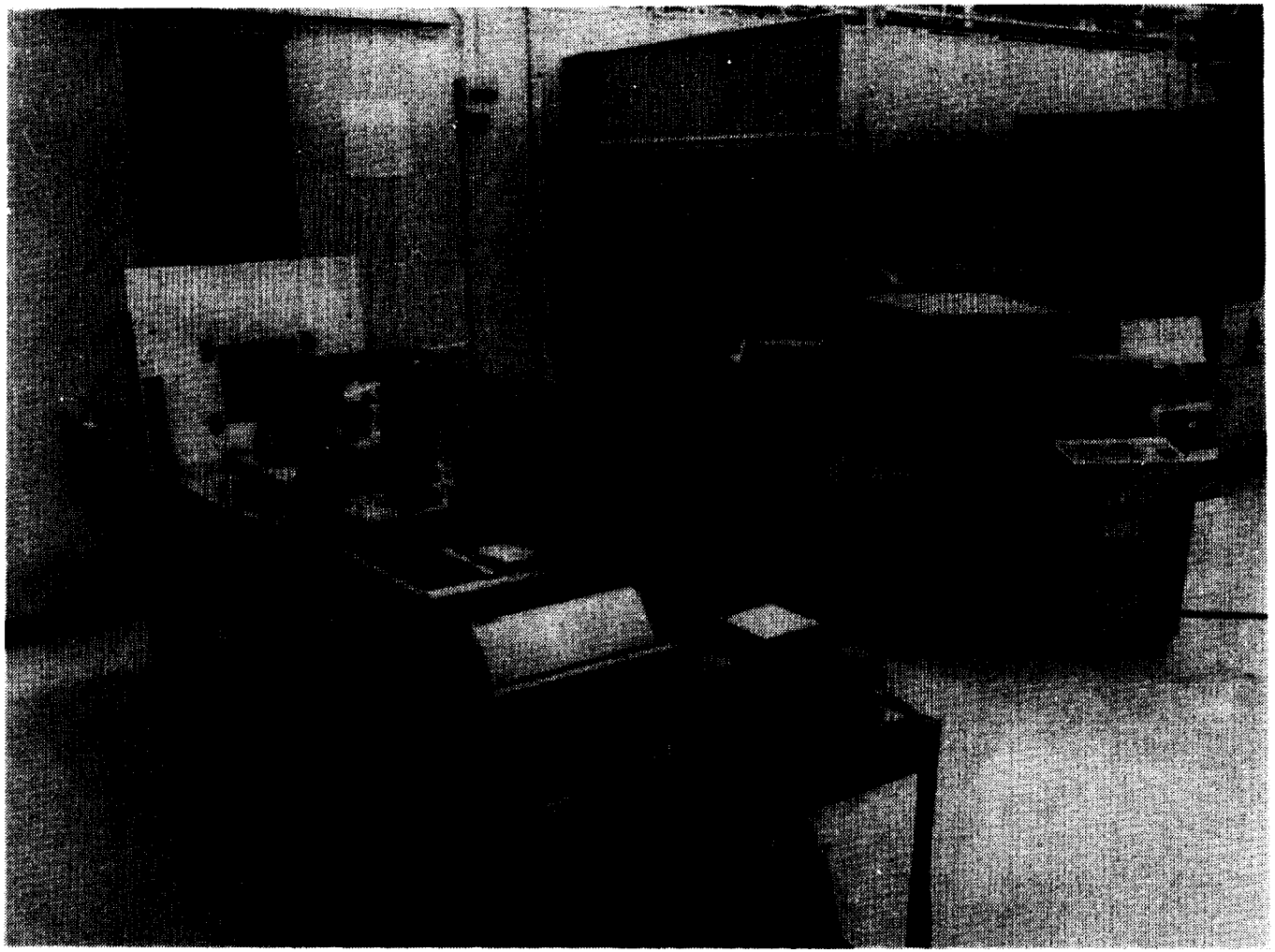

FIGURE 31 - PHOTOGRAPH OF THE EQUIPMENT LAYOUT USED FOR THE ELEVATED TEMPERATURE TESTING PERFORMED ON NOVEMBER 18-19, 1991

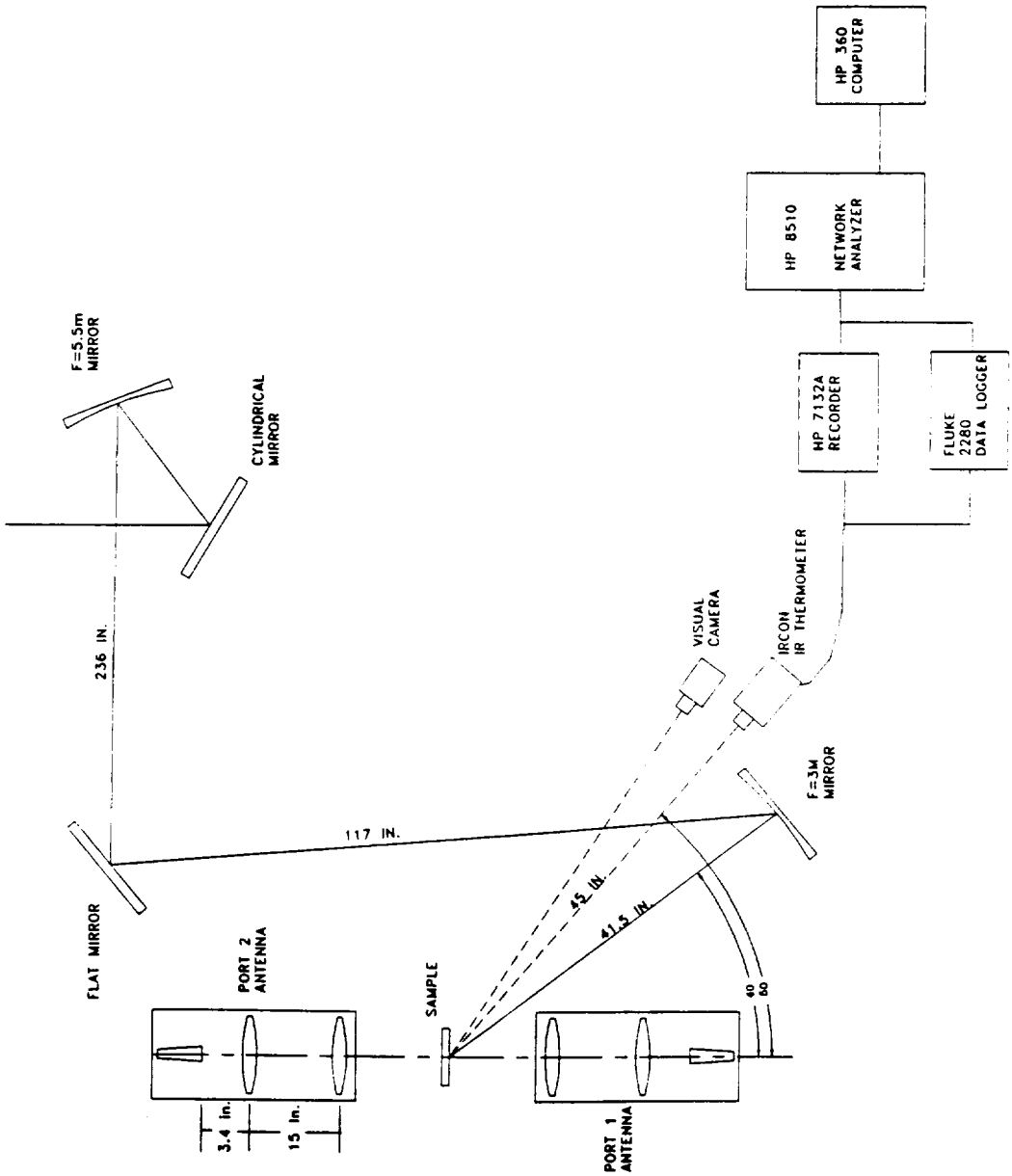

FIGURE 32 - LASER OPTICS AND EQUIPMENT LAYOUT FOR THE ELEVATED TEMPERATURE TESTING PERFORMED ON NOVEMBER 18-19, 1991

Tile : 159849-003-1044
Target Temperature : 1000 F.

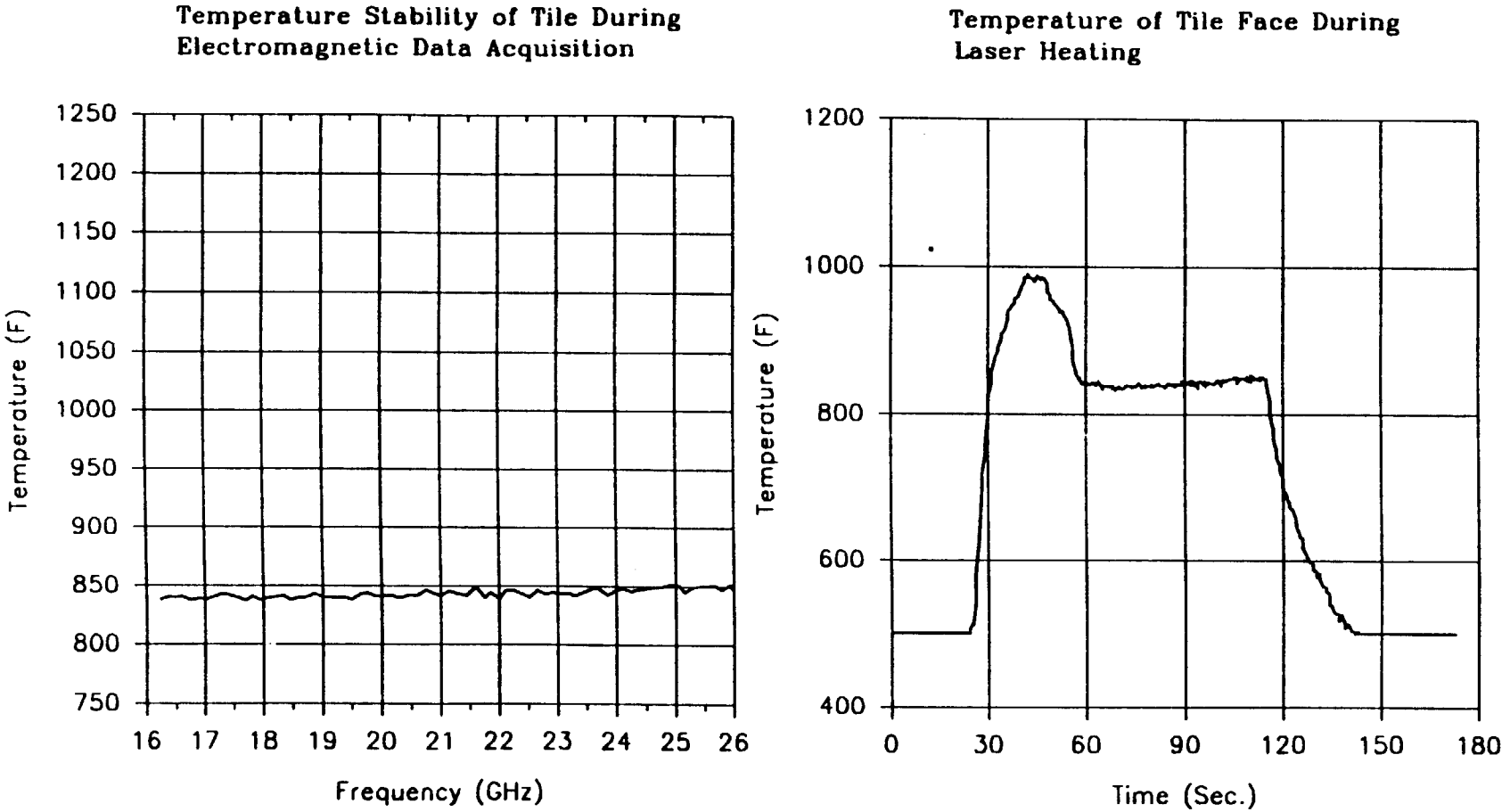

FIGURE 33 - LI-2200 SURFACE TEMPERATURE PROFILES FOR THE 1000°F TEST

Tile : 159849-003-1043
Target Temperature : 1500 F.

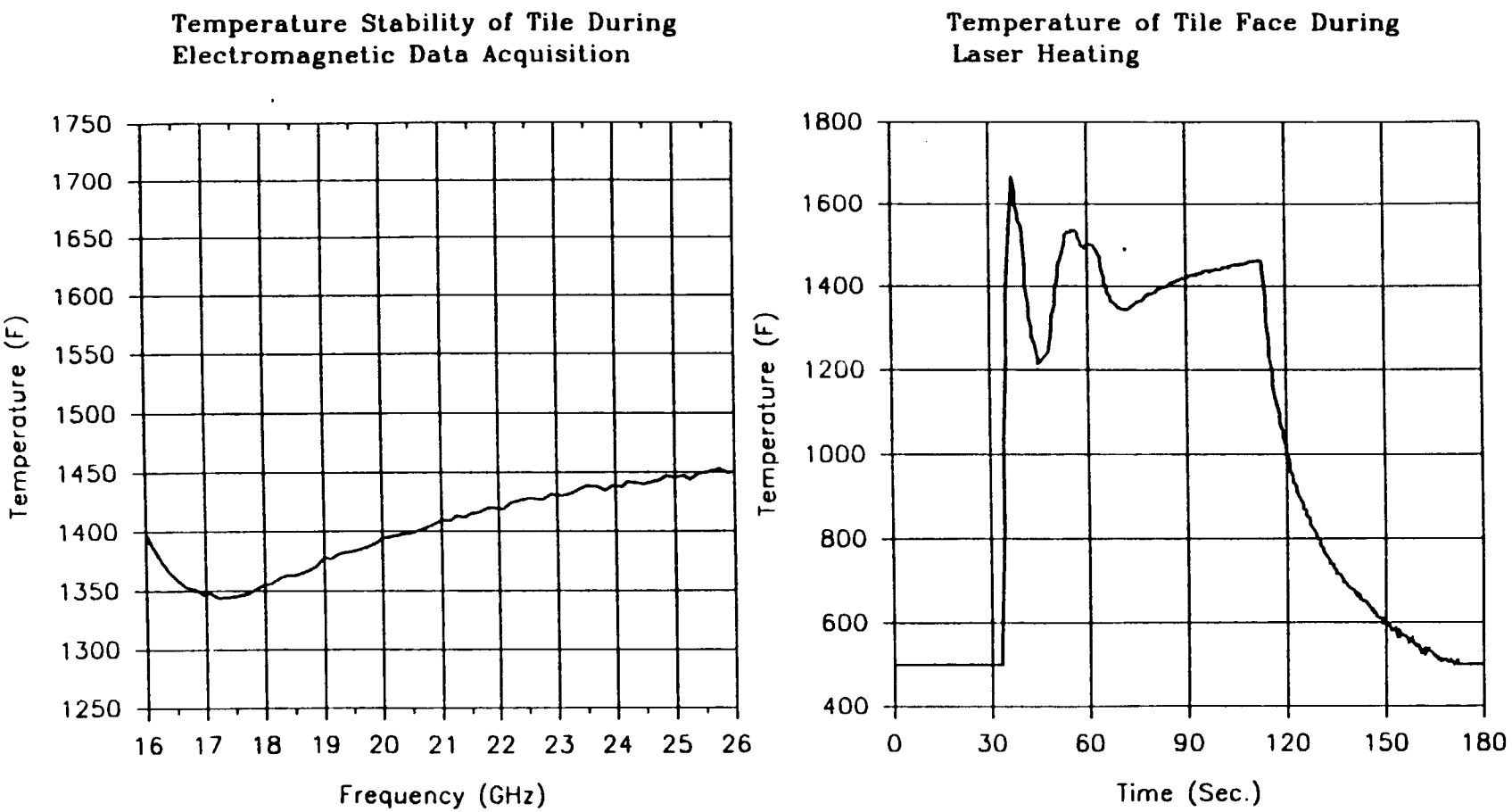

FIGURE 34 - LI-2200 SURFACE TEMPERATURE PROFILES FOR THE 1500°F TEST

Tile : 159849-003-1038
Target Temperature : 2000 F.

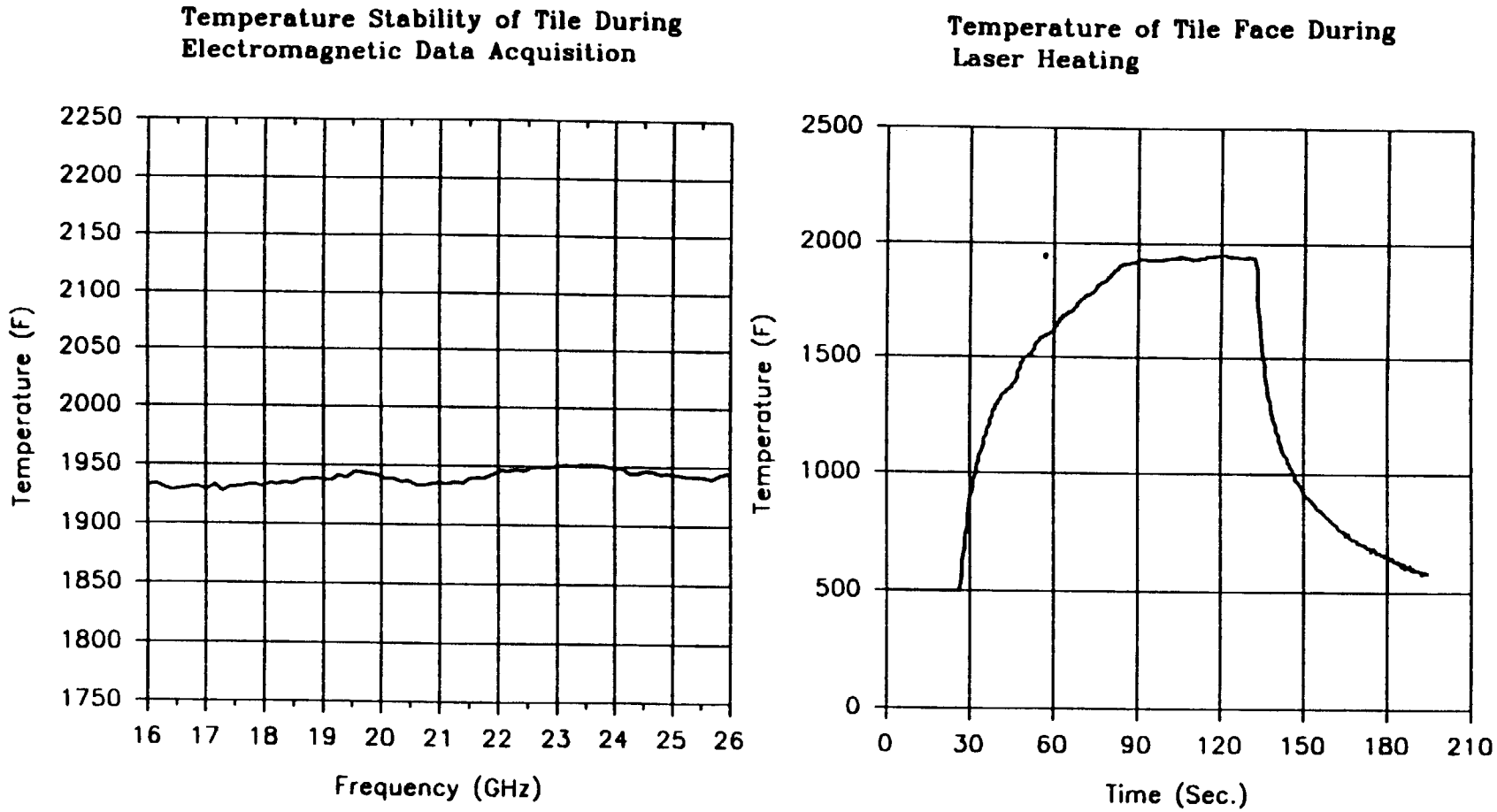

FIGURE 35 - LI-2200 SURFACE TEMPERATURE PROFILES FOR THE 2000°F TEST

Tile : 159849-003-1046
Target Temperature : 2200 F.

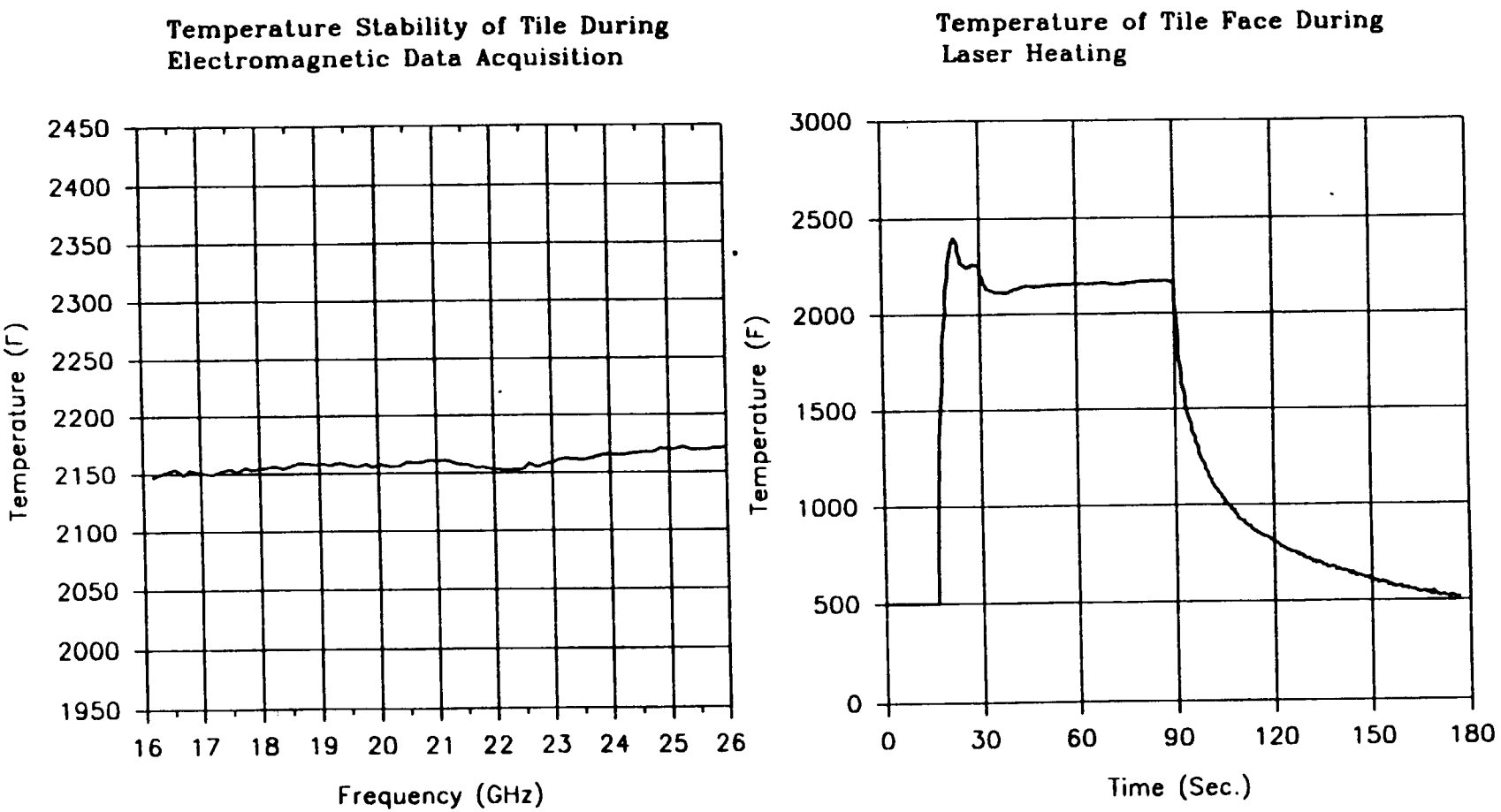

FIGURE 36 - LI-2200 SURFACE TEMPERATURE PROFILES FOR THE 2200°F TEST

Tile : 159849-003-1048
Target Temperature : 2400 F.

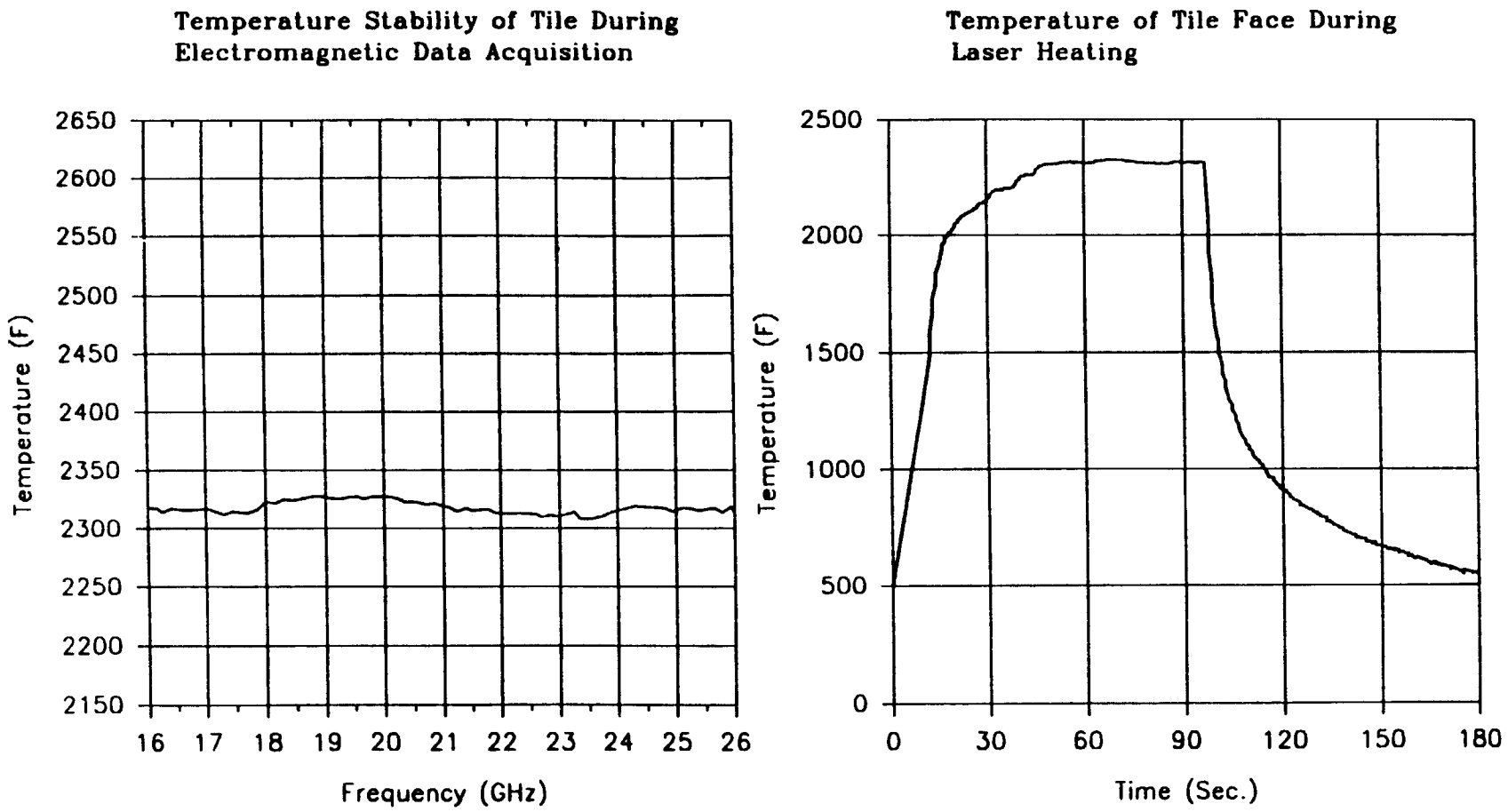

FIGURE 37 - LI-2200 SURFACE TEMPERATURE PROFILES FOR THE 2400°F TEST

Tile : 159849-003-1042
Target Temperature : 2600 F.

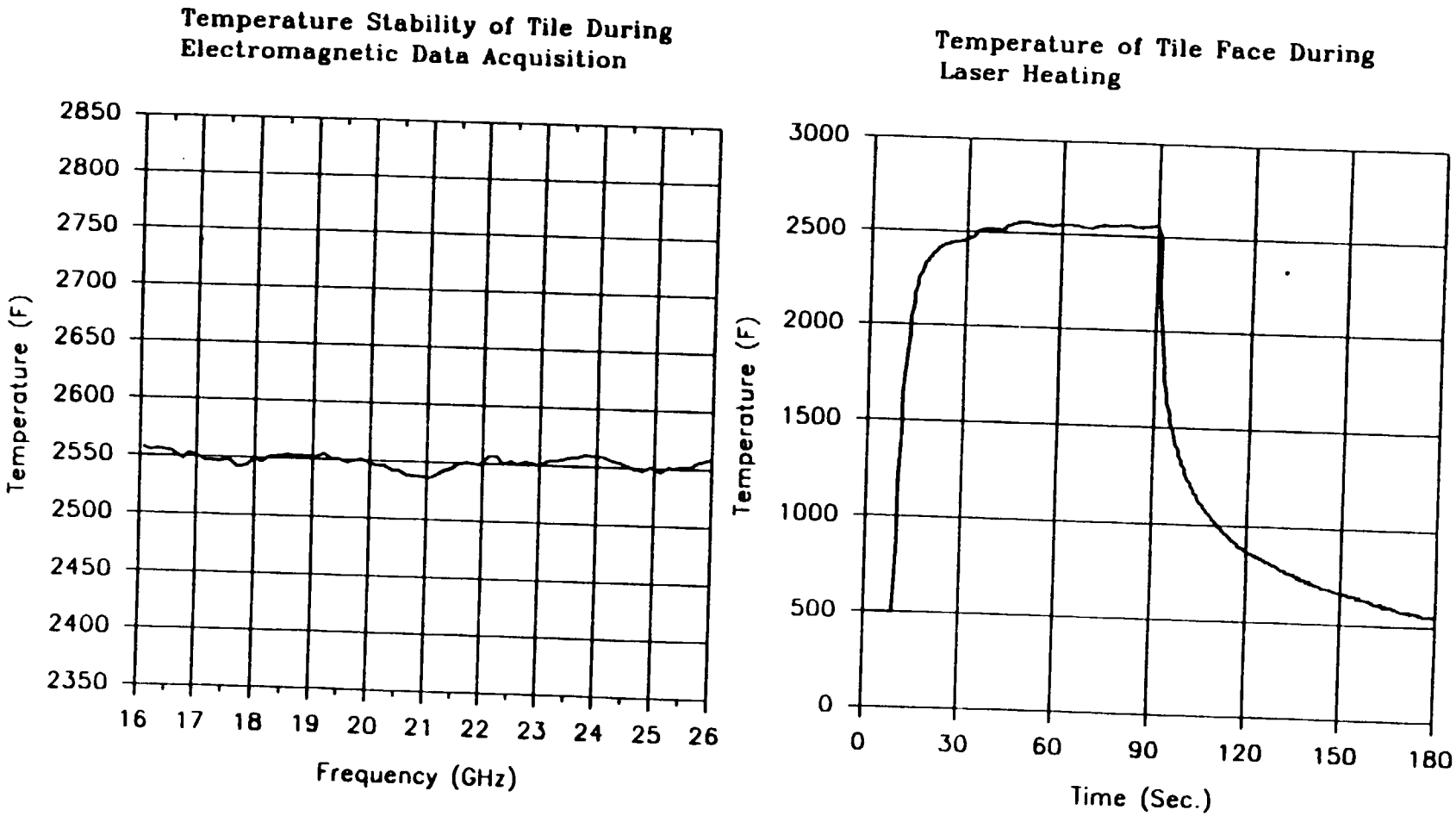

FIGURE 38 - LI-2200 SURFACE TEMPERATURE PROFILES FOR THE 2600°F TEST

Tile : 159849-003-1037
Target Temperature : 2700 F.

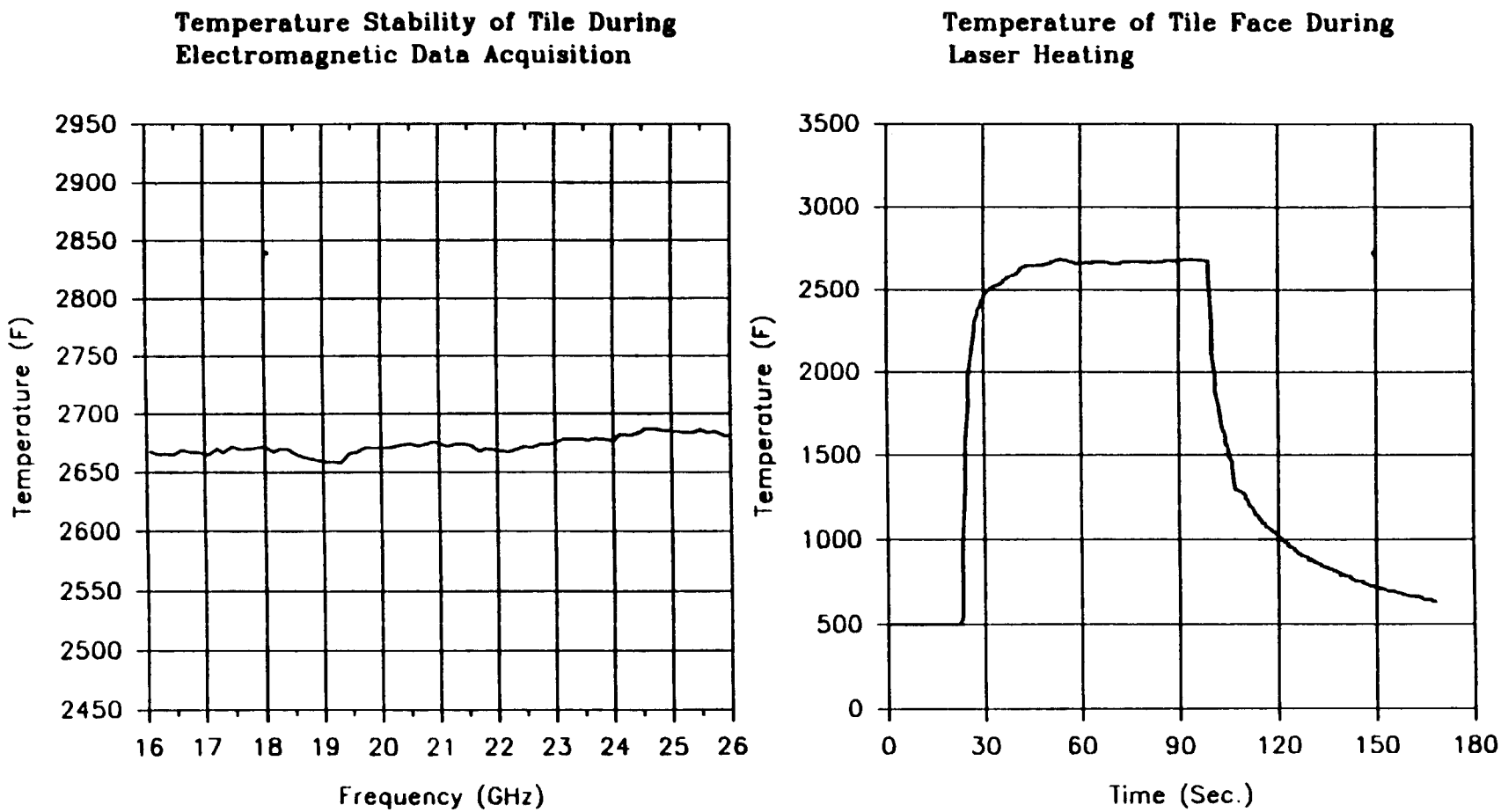

FIGURE 39 - LI-2200 SURFACE TEMPERATURE PROFILES FOR THE 2700°F TEST

Tile : 159849-003-1040
Target Temperature : 2800 F.

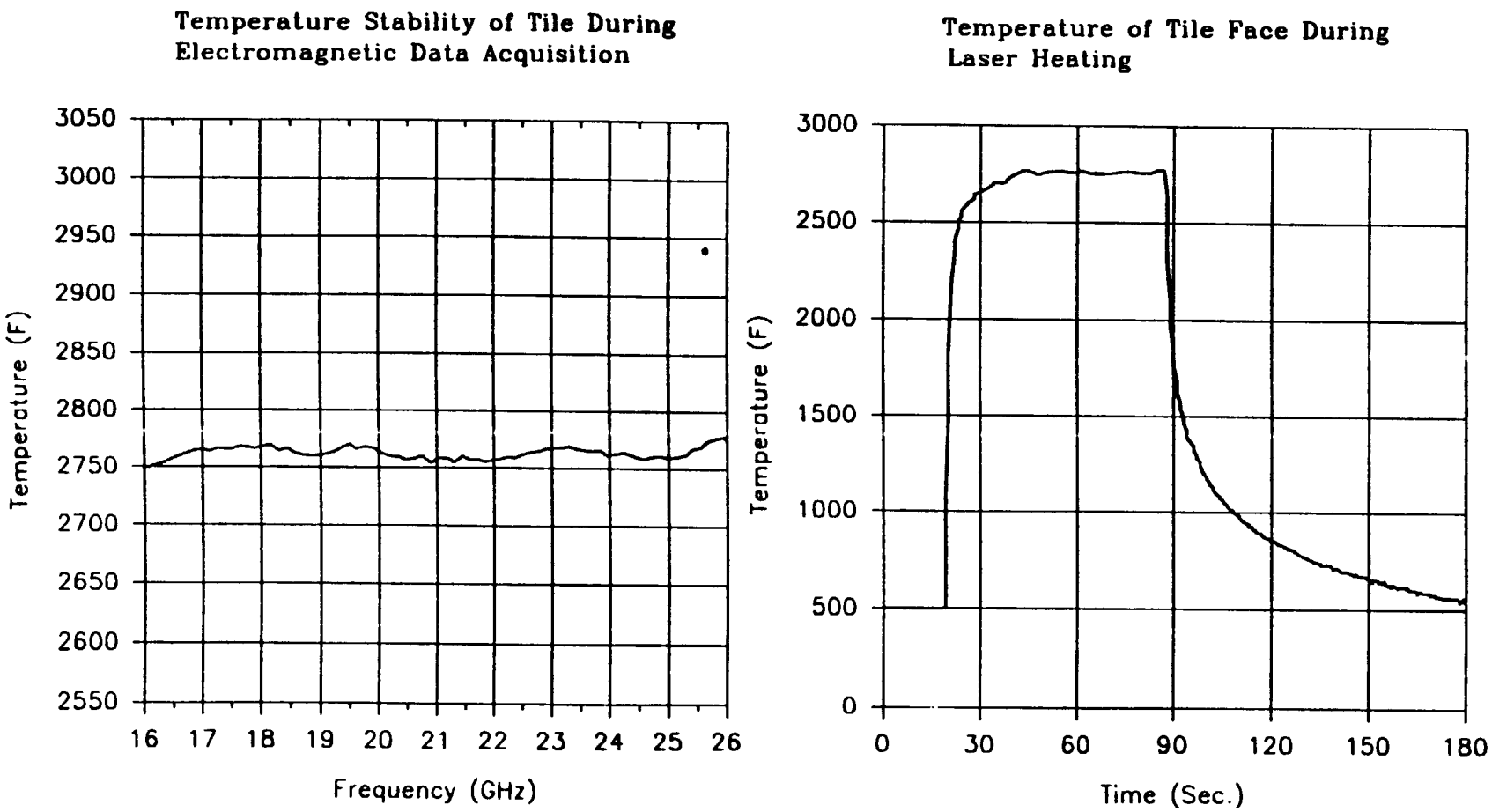

FIGURE 40 - LI-2200 SURFACE TEMPERATURE PROFILES FOR THE 2800°F TEST

Tile : 159849-003-1039
Target Temperature : 2900 F.

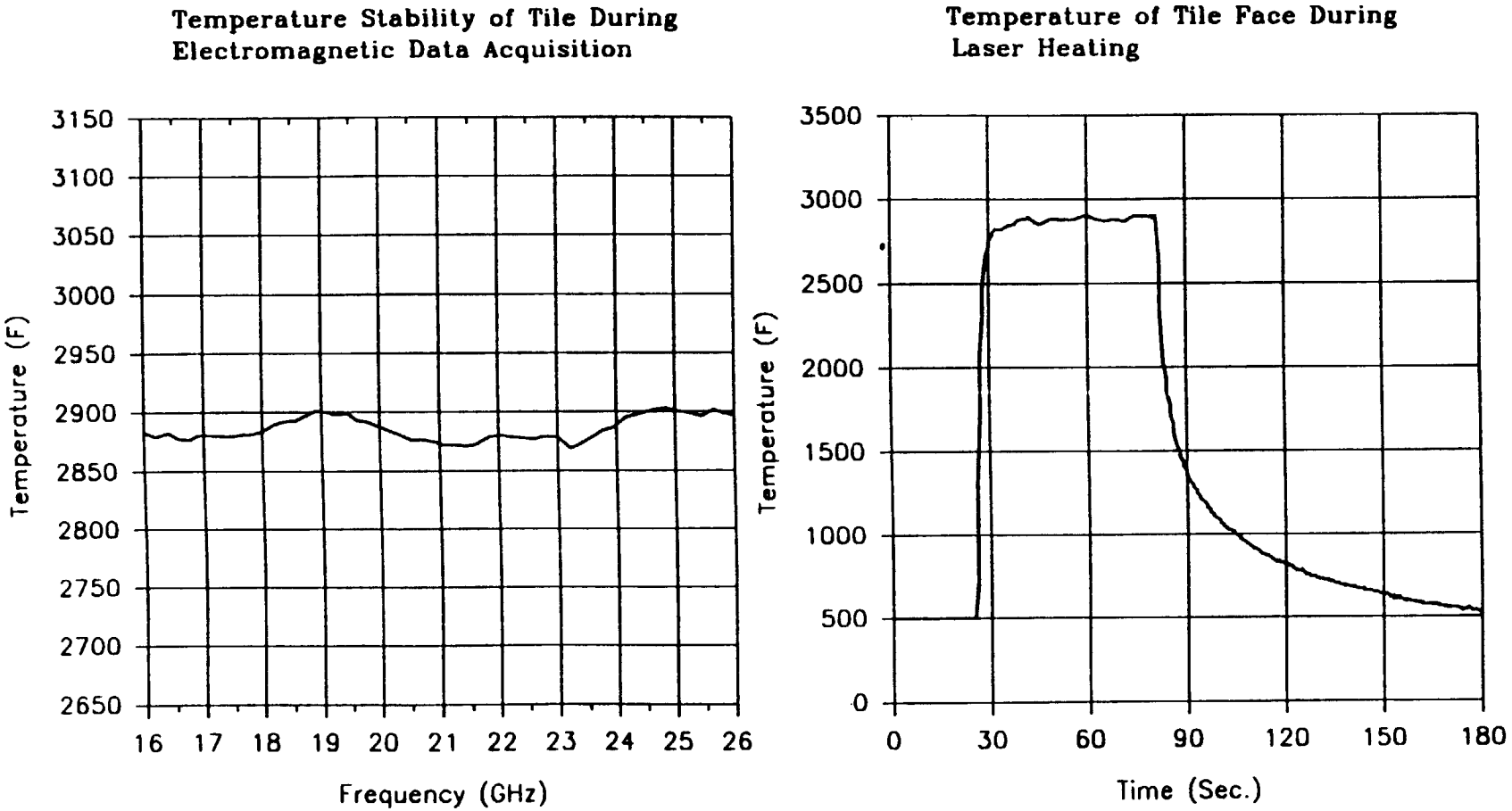

FIGURE 41 - LI-2200 SURFACE TEMPERATURE PROFILES FOR THE 2900°F TEST

Tile : 159849-003-1036
Target Temperature : 3000 F.

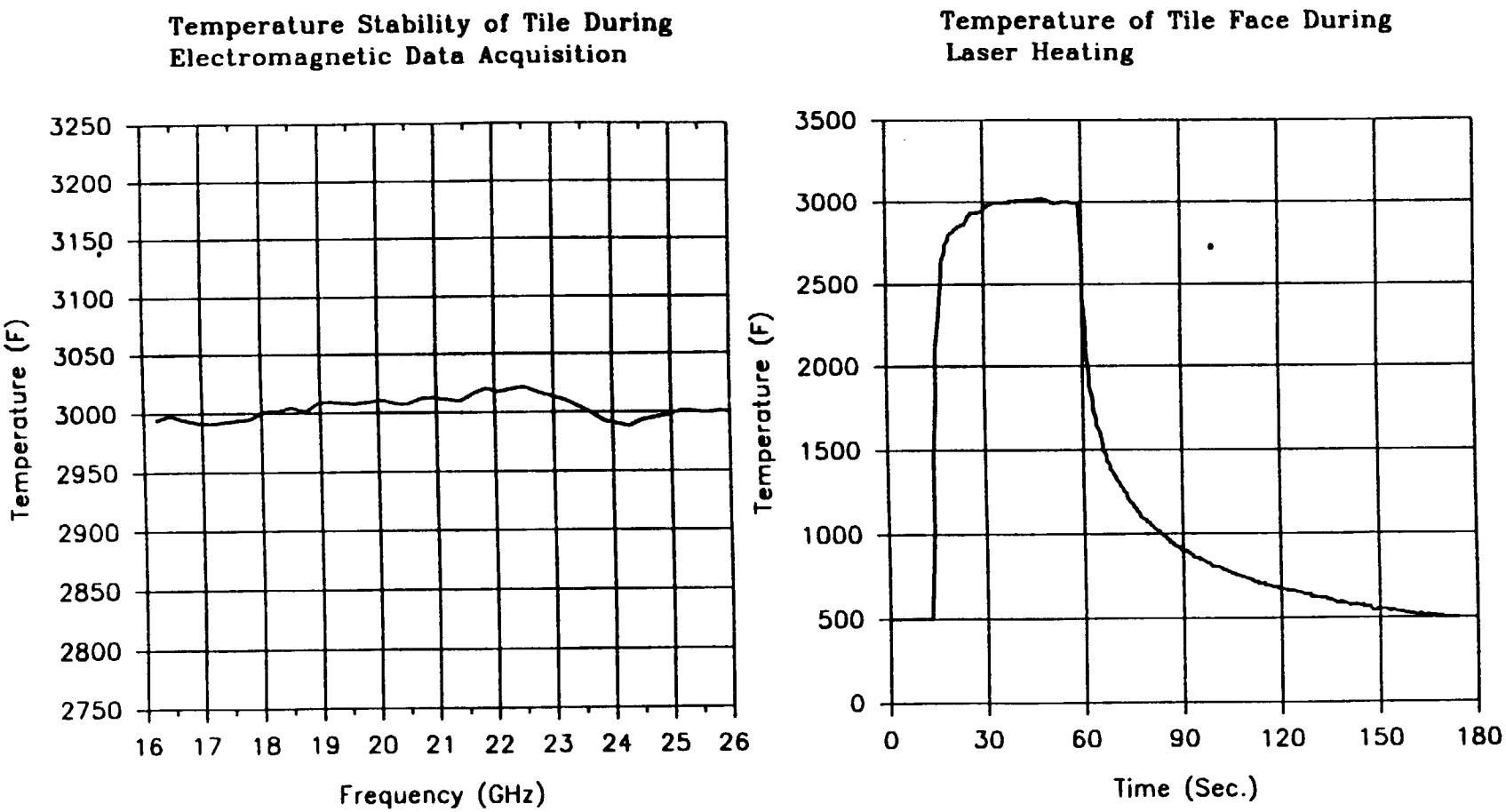

FIGURE 42 - LI-2200 SURFACE TEMPERATURE PROFILES FOR THE 3000°F TEST

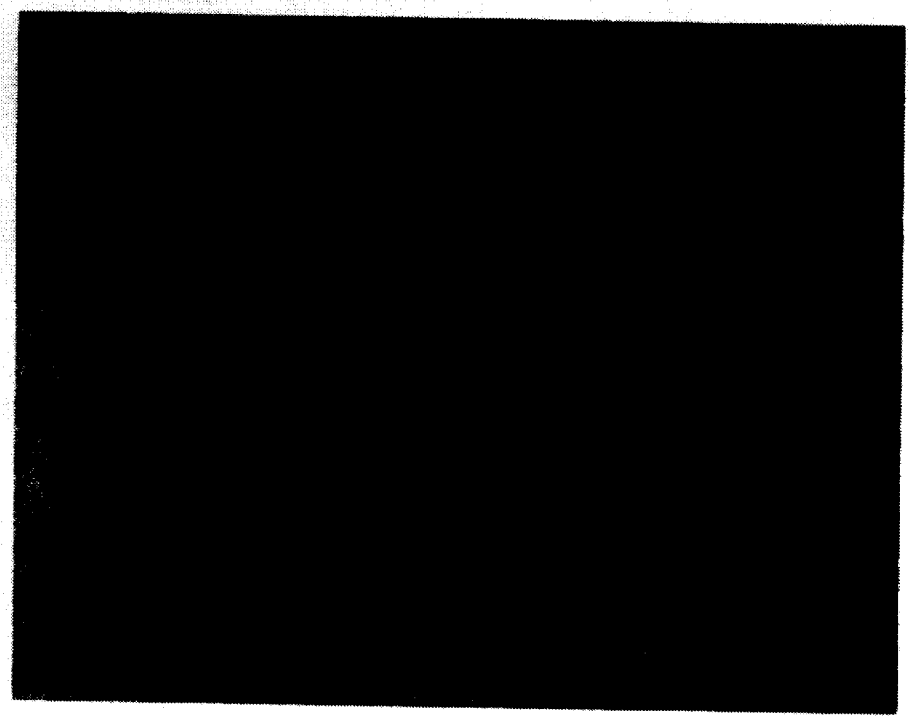

TILE 159849-003-1036

FIGURE 43 - 2X OPTICAL MICROPHOTOGRAPH OF A TYPICAL CRACKING PATTERN

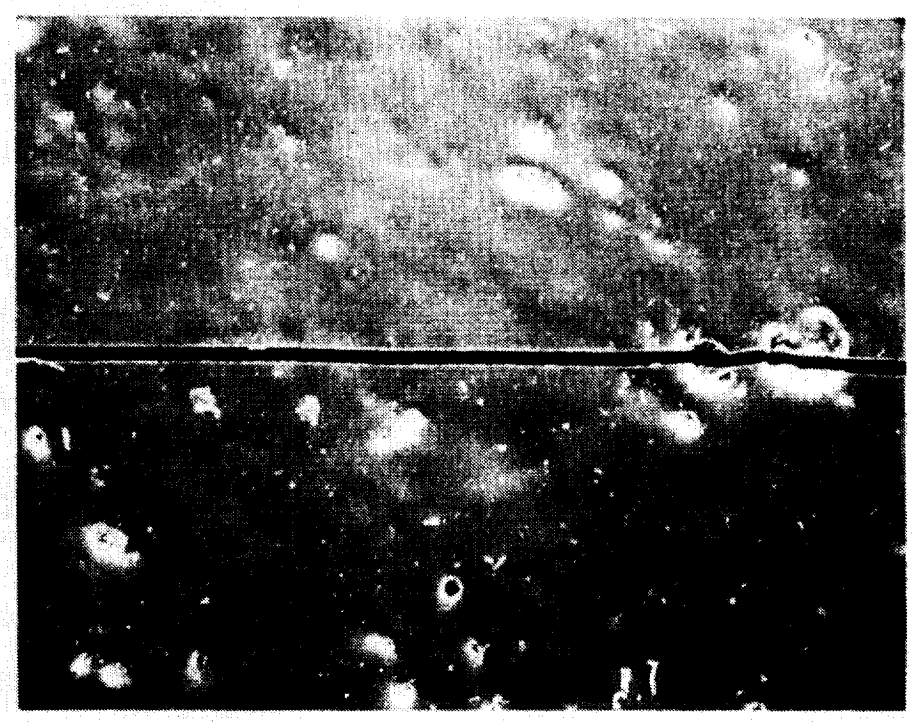

TILE 159849-003-1036

FIGURE 44 - 100X SEM MICROPHOTOGRAPH OF THE RCG COATING DISPLAYING A TYPICAL CRACK

FIGURE 45 - 50X SEM MICROPHOTOGRAPH OF THE RCG COATING/SUBSTRATE INTERFACE DISPLAYING A TYPICAL CRACK

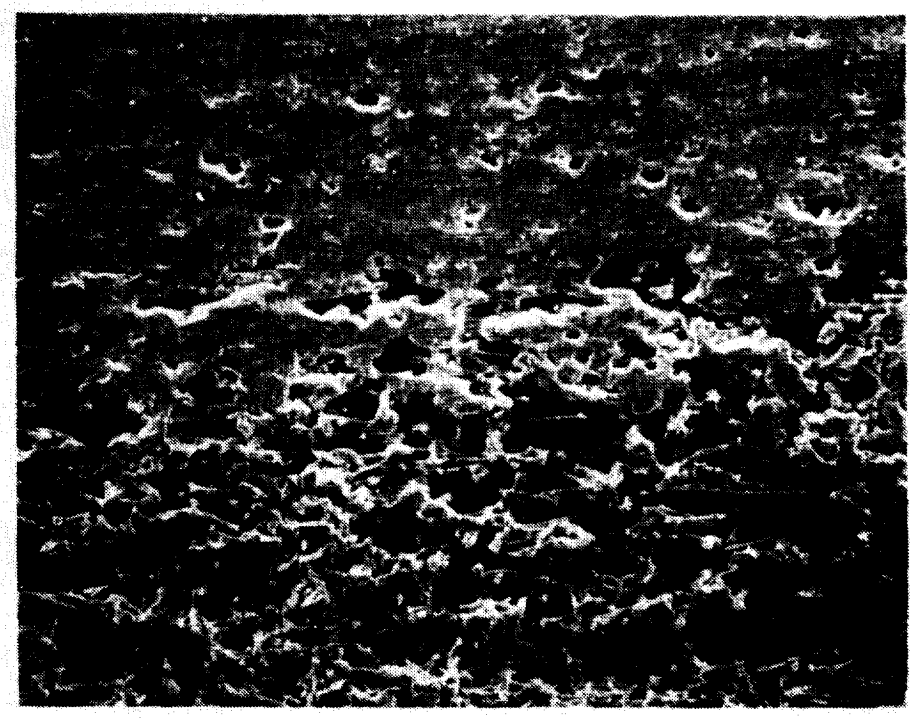

TILE 159849-003-1041

FIGURE 46 - 200X SEM MICROPHOTOGRAPH OF THE RCG COATING/SUBSTRATE INTERFACE DISPLAYING RCG FLOW

FIGURE 47 - 500X SEM MICROPHOTOGRAPH OF THE SUBSTRATE MATERIAL DISPLAYING FIBER BREAKAGE

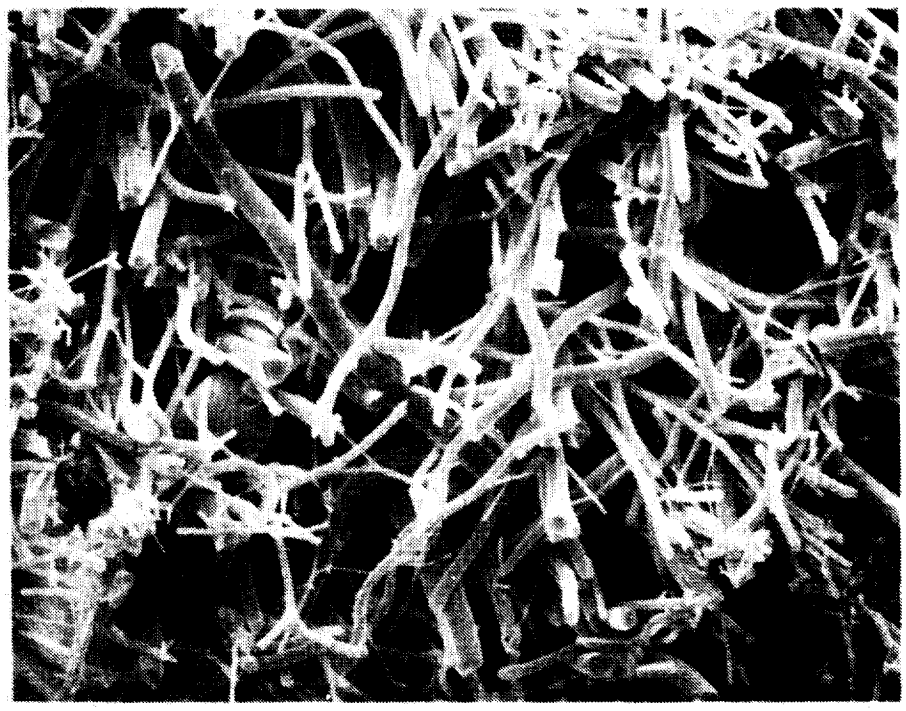

TILE 159849-003-1041

FIGURE 48 - 500X SEM MICROPHOTOGRAPH OF THE SUBSTRATE MATERIAL DISPLAYING NO FIBER BREAKAGE

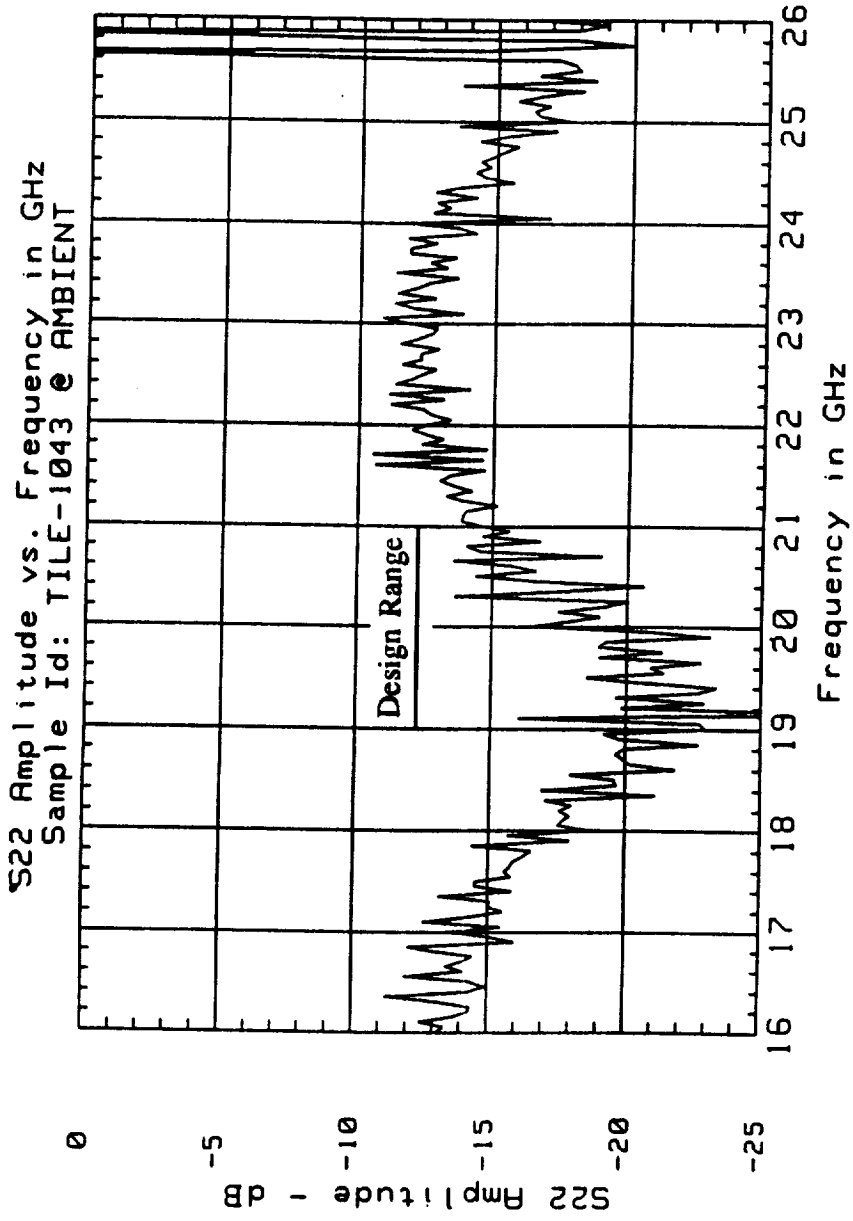

FIGURE 49 - UNPROCESSED S22 AMPLITUDE OF THE LI-2200 SYSTEM WITH THE RCG COATING FACING PORT 1

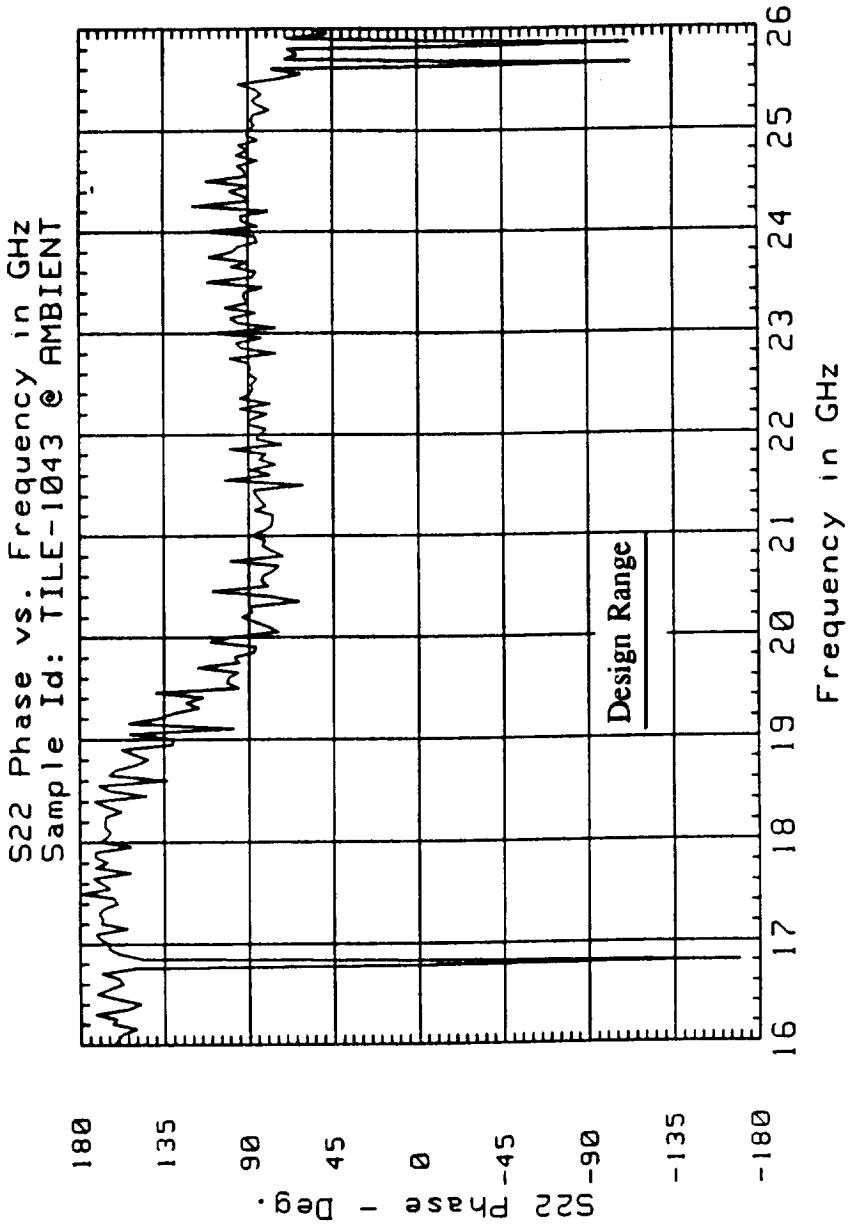

FIGURE 50 - UNPROCESSED S22 PHASE OF THE LI-2200 SYSTEM WITH THE RCG COATING FACING PORT 1

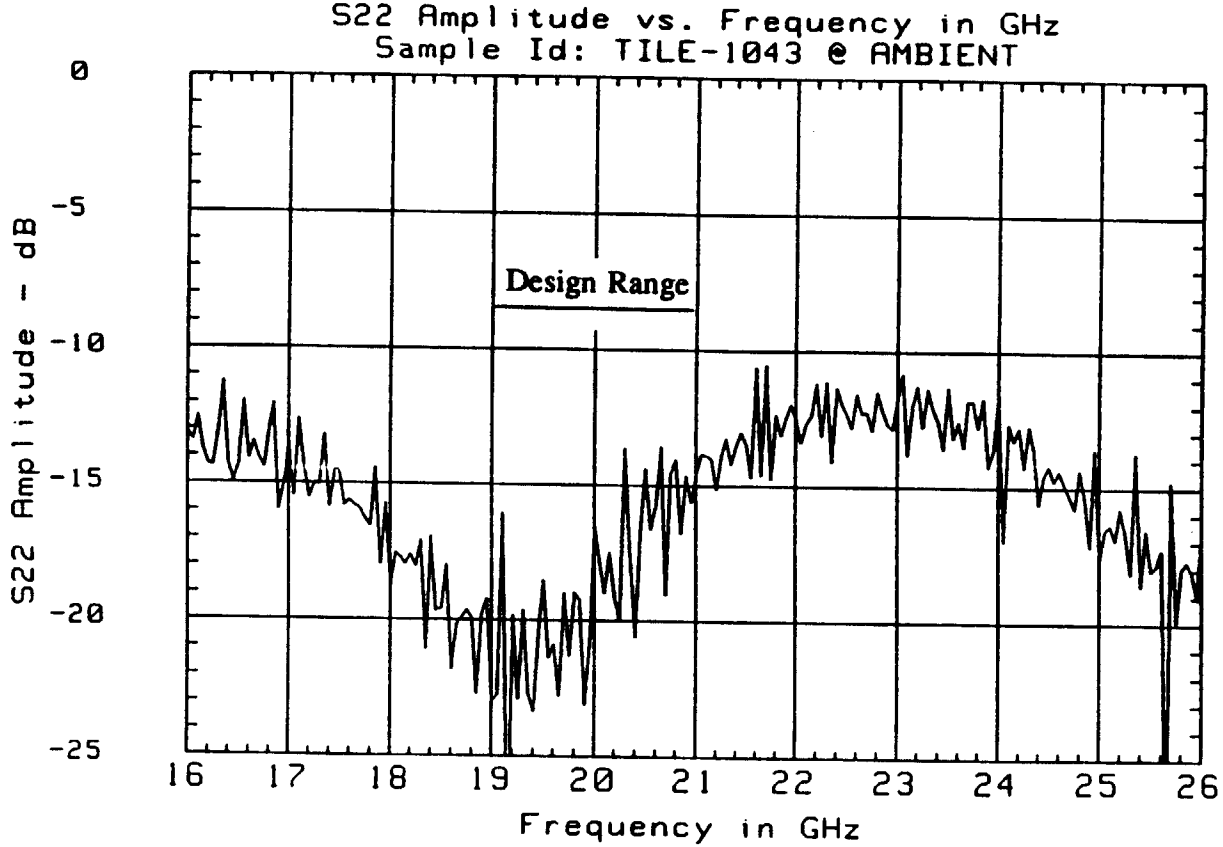

FIGURE 51 - S22 AMPLITUDE OF THE LI-2200
SYSTEM WITH THE RCG COATING FACING PORT 1 AFTER REMOVAL OF NON-REPETITIVE SPIKES

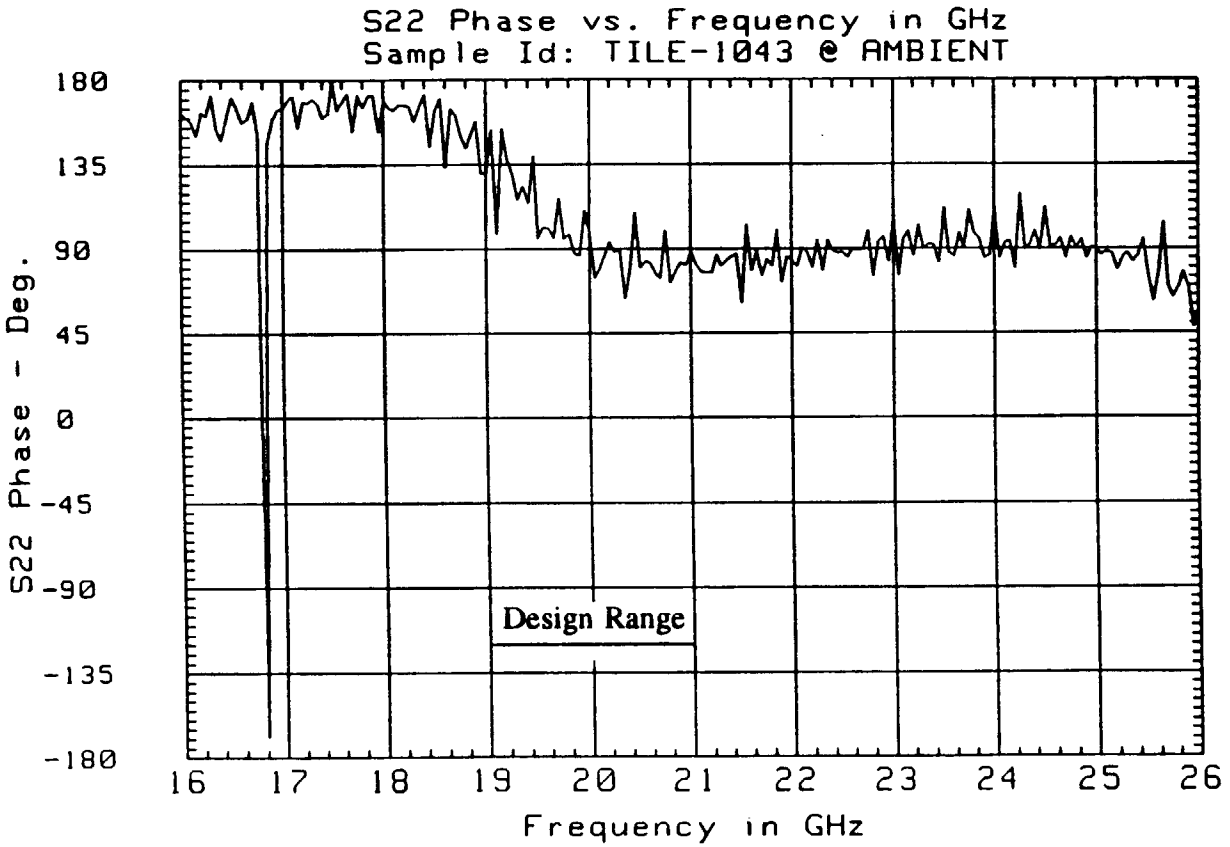

FIGURE 52 - S22 PHASE OF THE LI-2200
SYSTEM WITH THE RCG COATING FACING PORT 1 AFTER REMOVAL OF NON-REPETITIVE SPIKES

```
Thru Reference File Name      : T10_THRU
Reflect Reference File Name   : T10_METAL
Thickness of Reference Plane :  .062 inches.

Sliding Aperture Width        :  21  points.
Glitch Detection Threshold    :  3  standard deviations.
Number of Passes              :  2

Gate Span (nS)                :  1  nanoseconds.


De-glitching Report for S11 of TILE-1043 @ 1000


De-glitching Report for S22 of TILE-1043 @ 1000

Glitch corrected at : 25.65 GHz
Glitch corrected at : 25.85 GHz

De-glitching Report for S21 of TILE-1043 @ 1000

Glitch corrected at : 25.65 GHz
Glitch corrected at : 25.85 GHz

De-glitching Report for S12 of TILE-1043 @ 1000

Glitch detected at : 19.2 GHz
Glitch corrected at : 25.65 GHz
Glitch corrected at : 25.85 GHz
```

FIGURE 53 - DATA PROCESSING REPORT

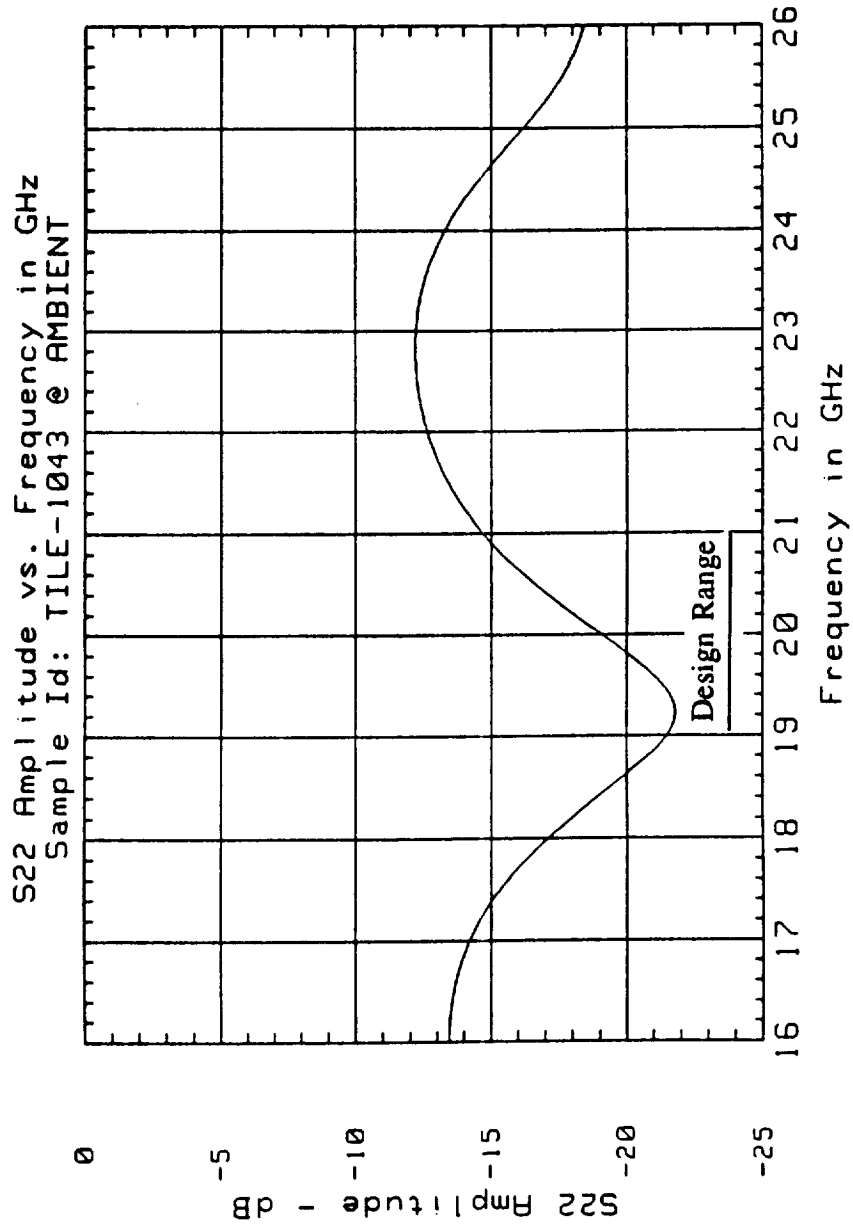

FIGURE 54 - S22 AMPLITUDE OF THE LI-2200 SYSTEM WITH THE RCG COATING FACING PORT 1 AFTER COMPLETION OF THE DATA PROCESSING PROCEDURE

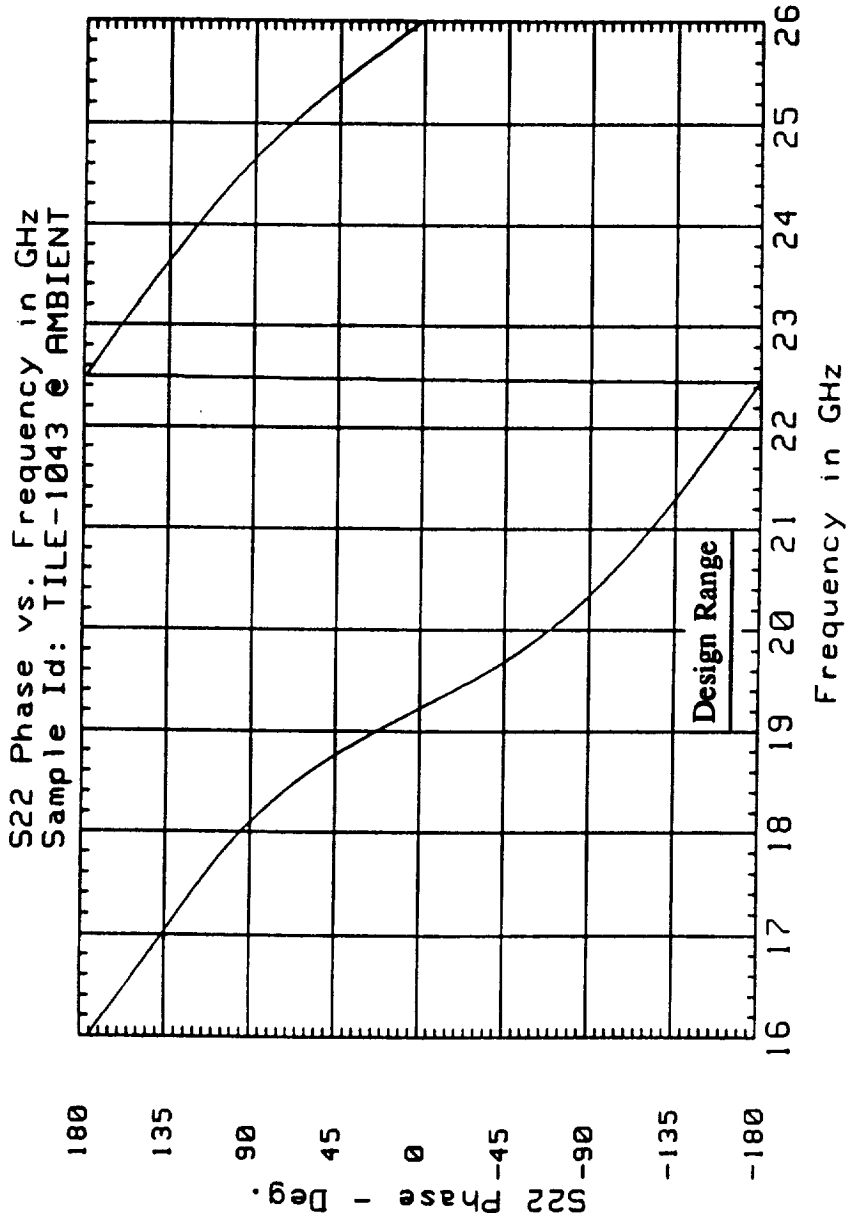

FIGURE 55 - S22 PHASE OF THE LI-2200 SYSTEM WITH THE RCG COATING FACING PORT 1 AFTER COMPLETION OF THE DATA PROCESSING PROCEDURE

FIGURE 55

C-2

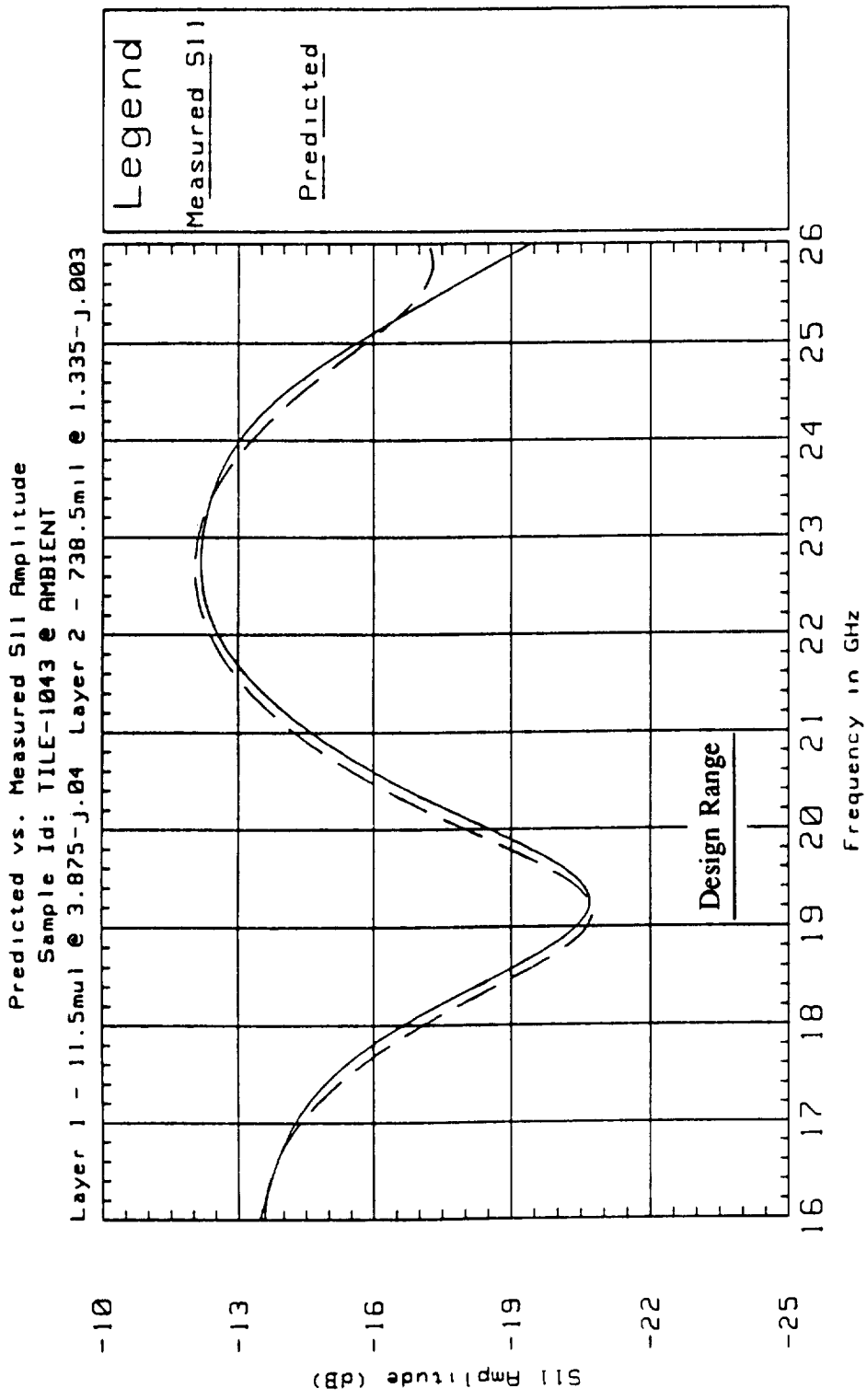

FIGURE 56 - MEASURED AND PREDICTED S11 AMPLITUDE OF THE LI-2200 SYSTEM WITH THE RCG COATING FACING PORT 1

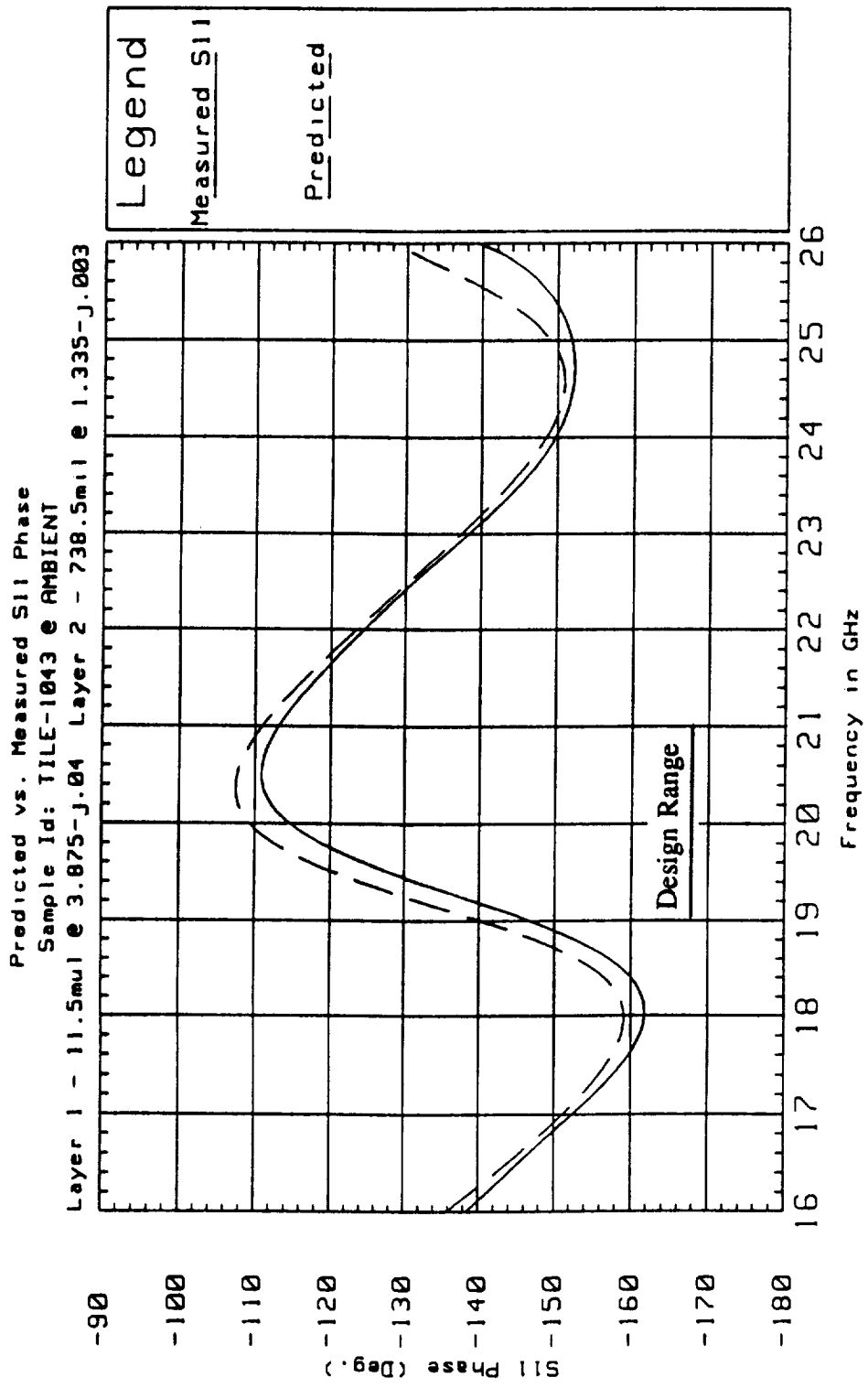

FIGURE 57 - MEASURED AND PREDICTED S11 PHASE OF THE LI-2200 SYSTEM WITH THE RCG COATING FACING PORT 1

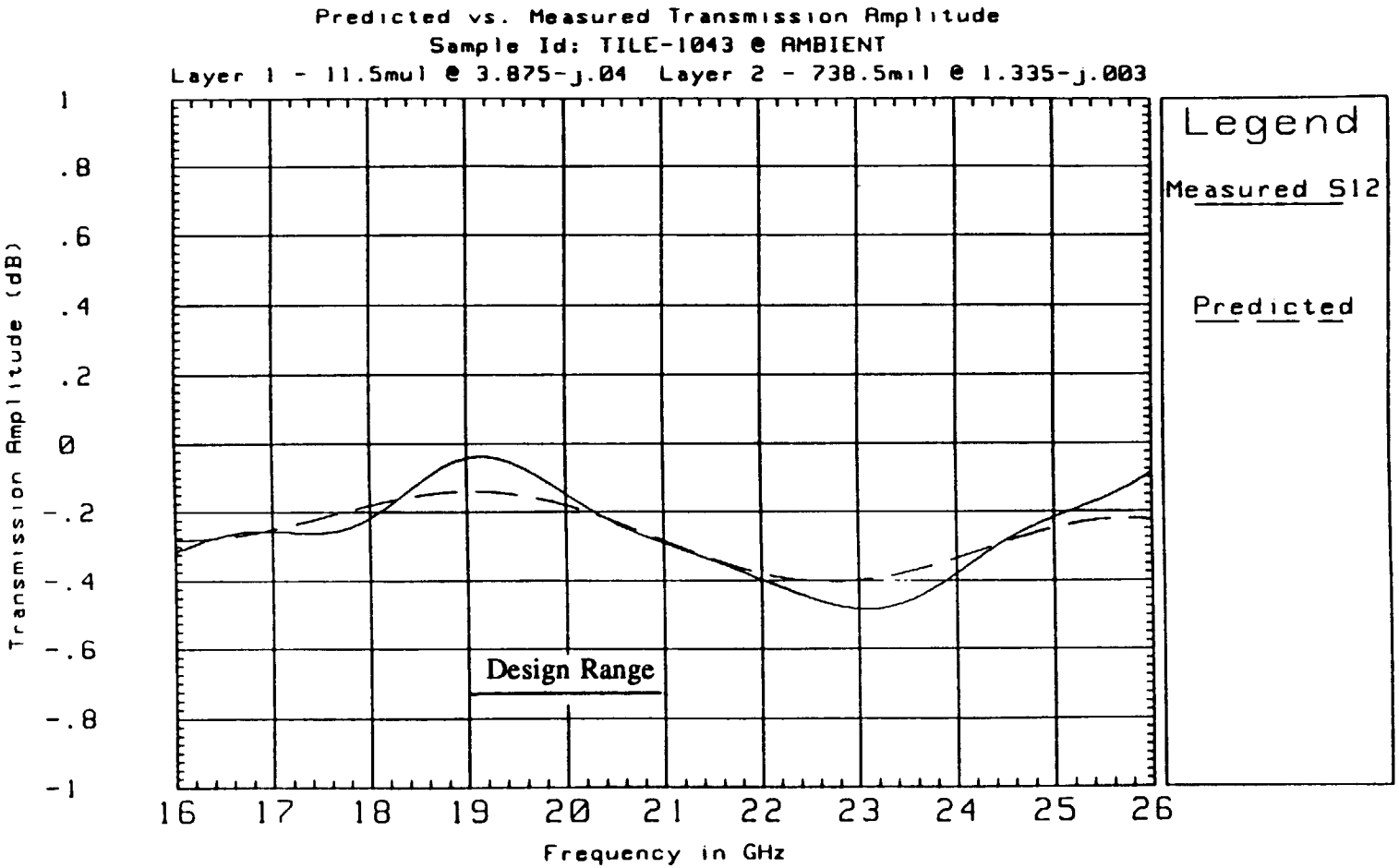

FIGURE 58 - MEASURED AND PREDICTED S21 AMPLITUDE OF THE LI-2200 SYSTEM WITH THE RCG COATING FACING PORT 1

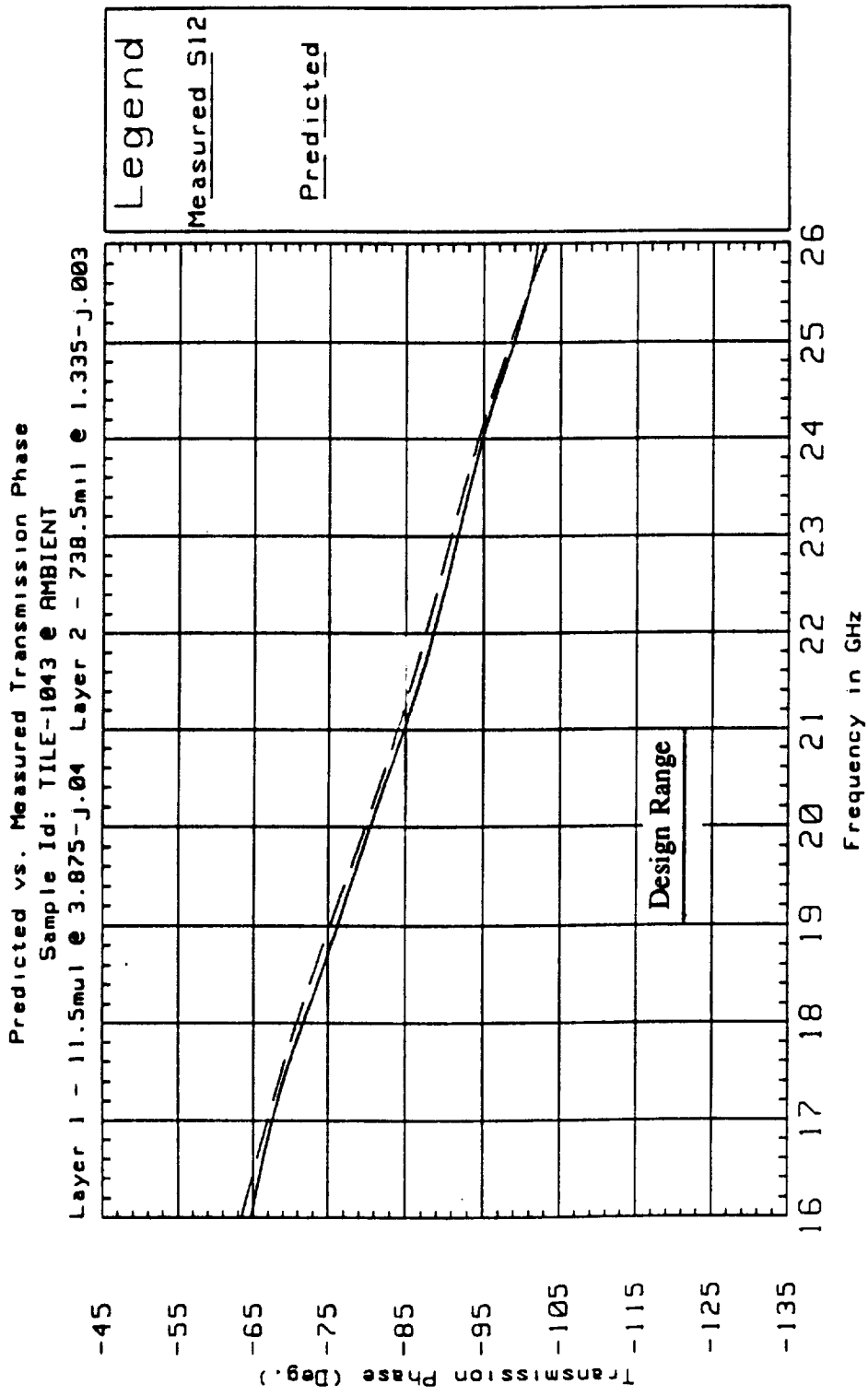

FIGURE 59 - MEASURED AND PREDICTED S21 PHASE OF THE LI-2200 SYSTEM WITH THE RCG COATING FACING PORT 1

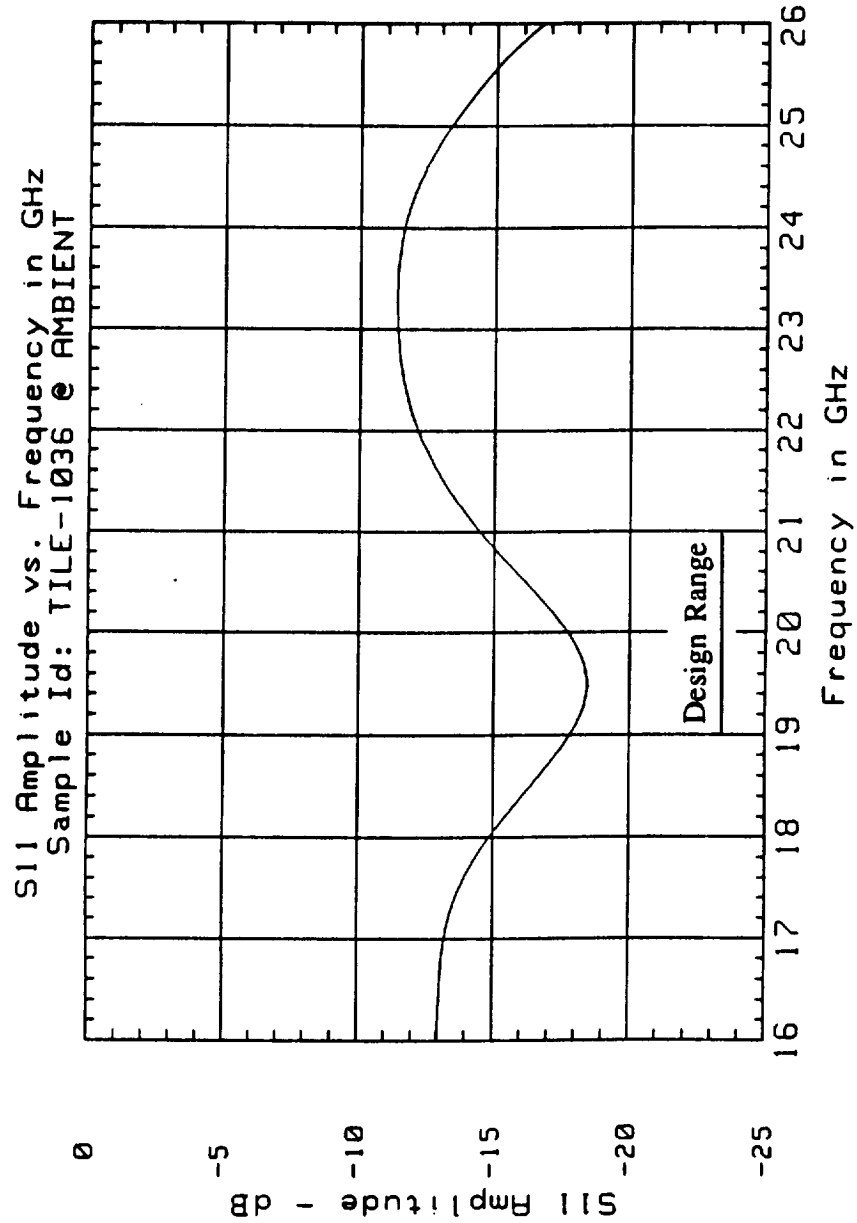

FIGURE 60 - S11 AMPLITUDE MEASURED FOR LI-2200
TITLE NUMBER 159849-003-1036 AT ROOM TEMPERATURE

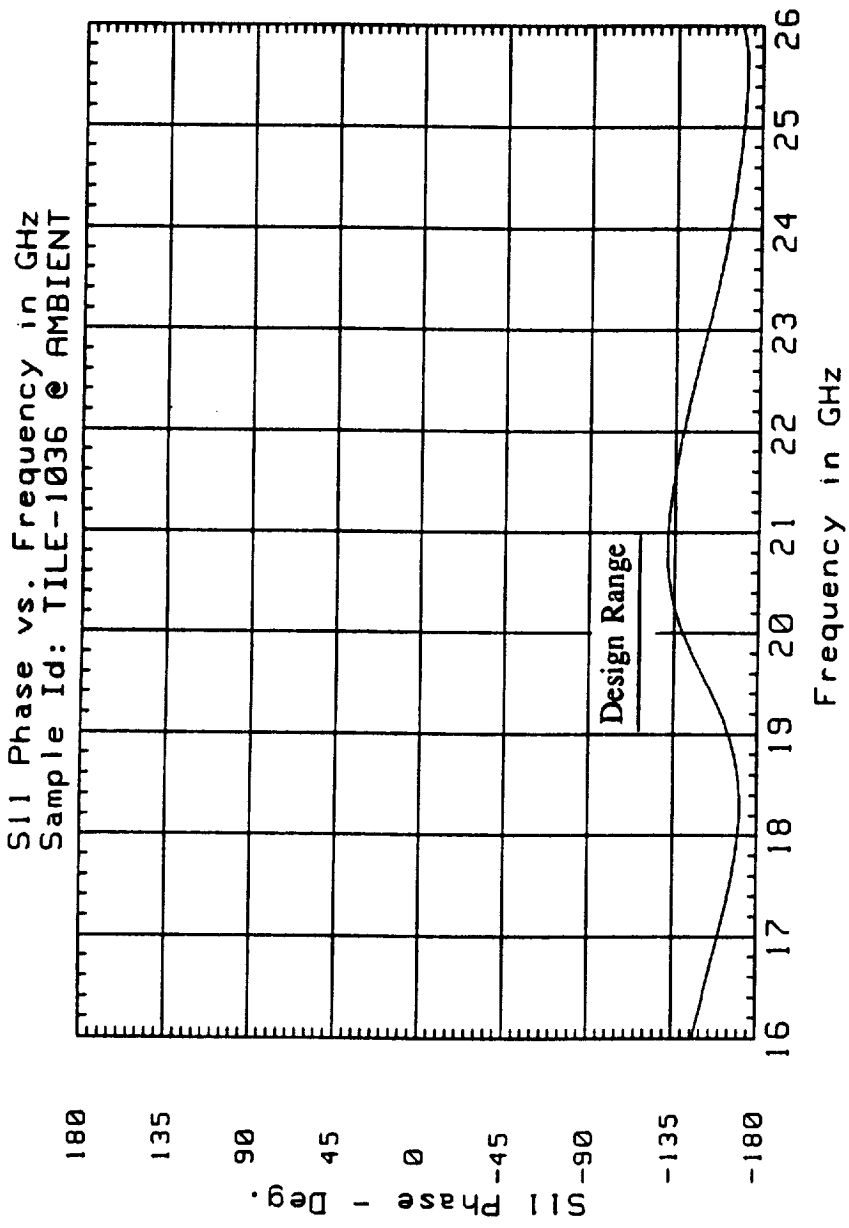

FIGURE 61 - S11 PHASE MEASURED FOR LI-2200
TITLE NUMBER 159849-003-1036 AT ROOM TEMPERATURE

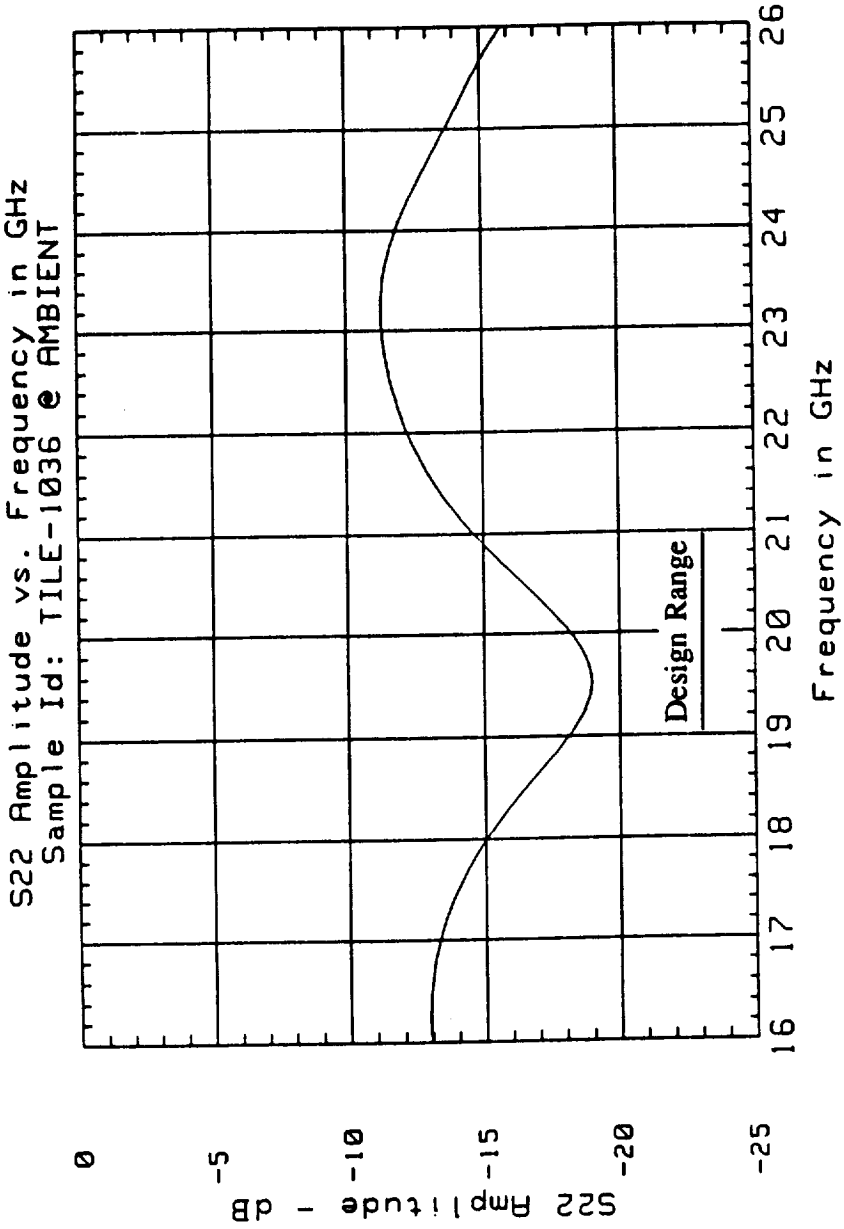

FIGURE 62 - S22 AMPLITUDE MEASURED FOR LI-2200
TITLE NUMBER 159849-003-1036 AT ROOM TEMPERATURE

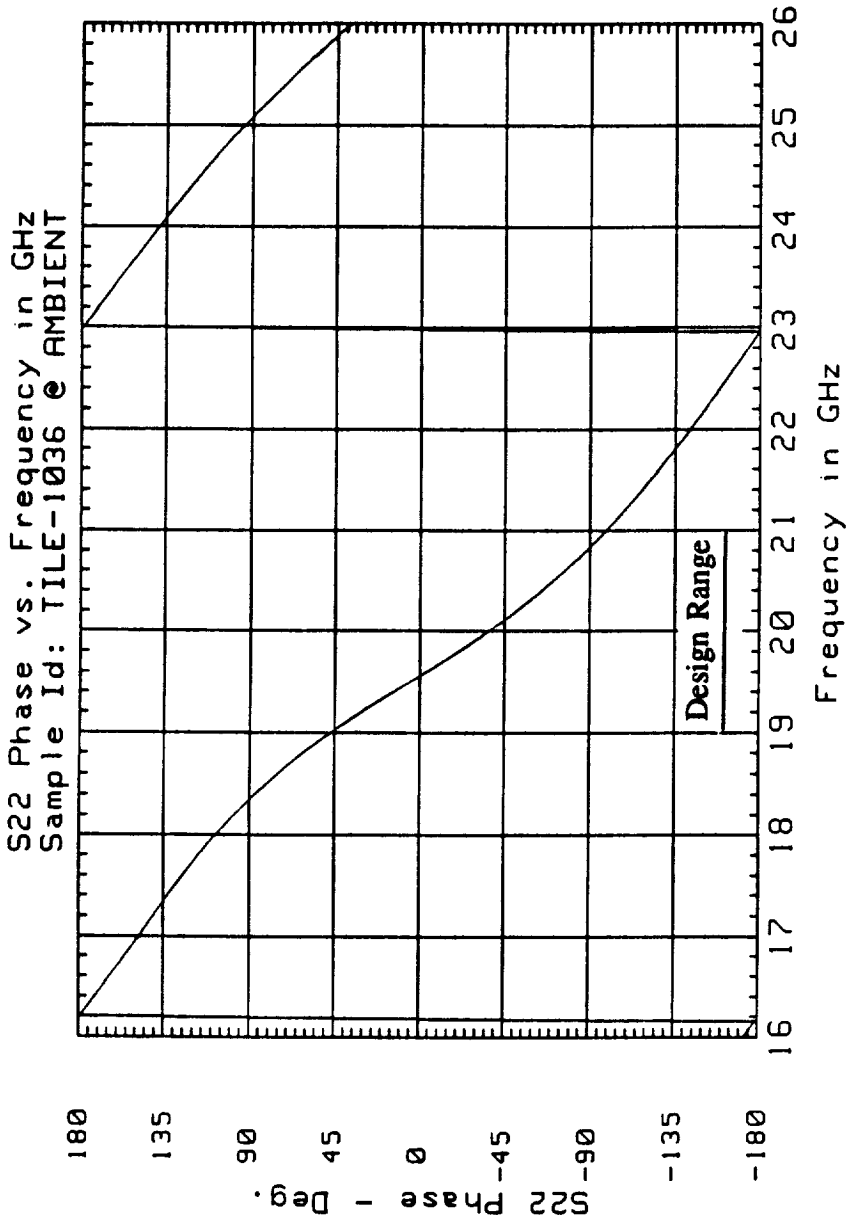

FIGURE 63 - S22 PHASE MEASURED FOR LI-2200
TITLE NUMBER 159849-003-1036 AT ROOM TEMPERATURE

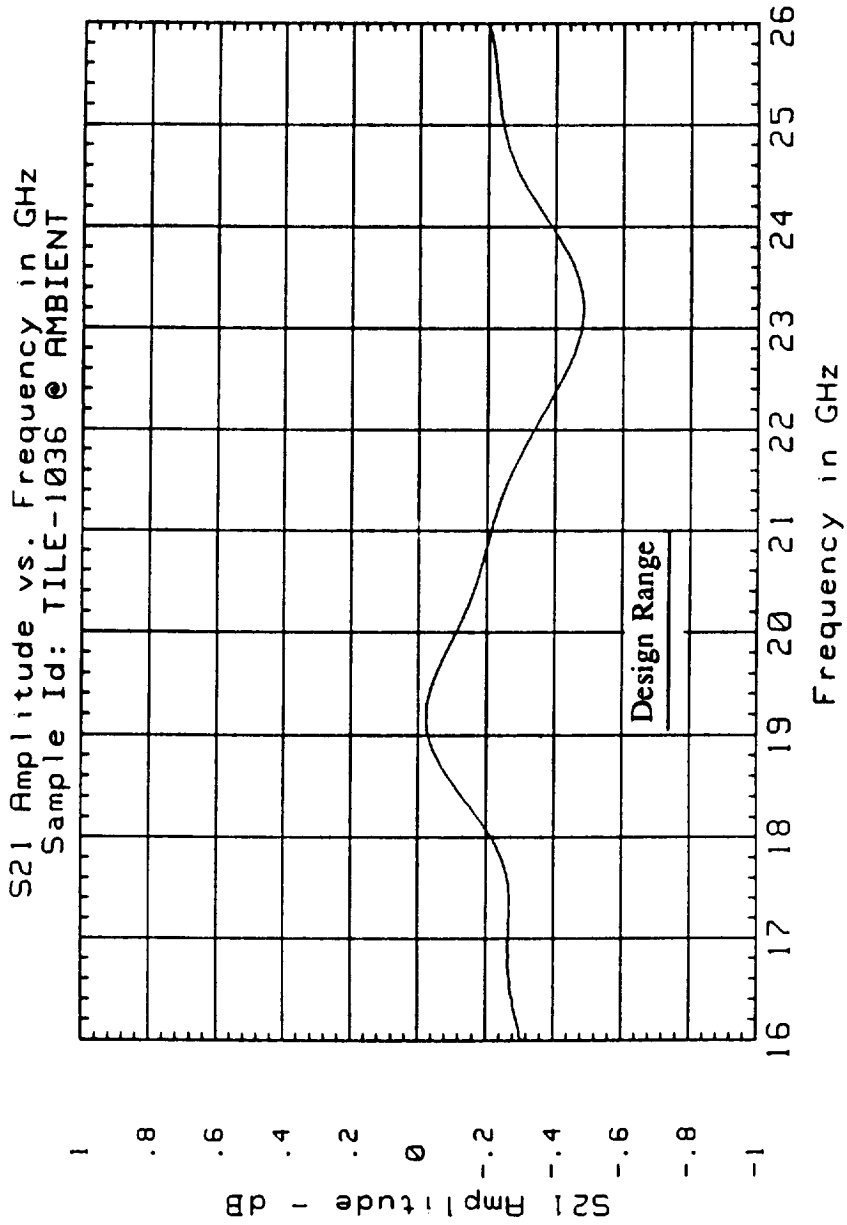

FIGURE 64 - S21 AMPLITUDE MEASURED FOR LI-2200
TITLE NUMBER 159849-003-1036 AT ROOM TEMPERATURE

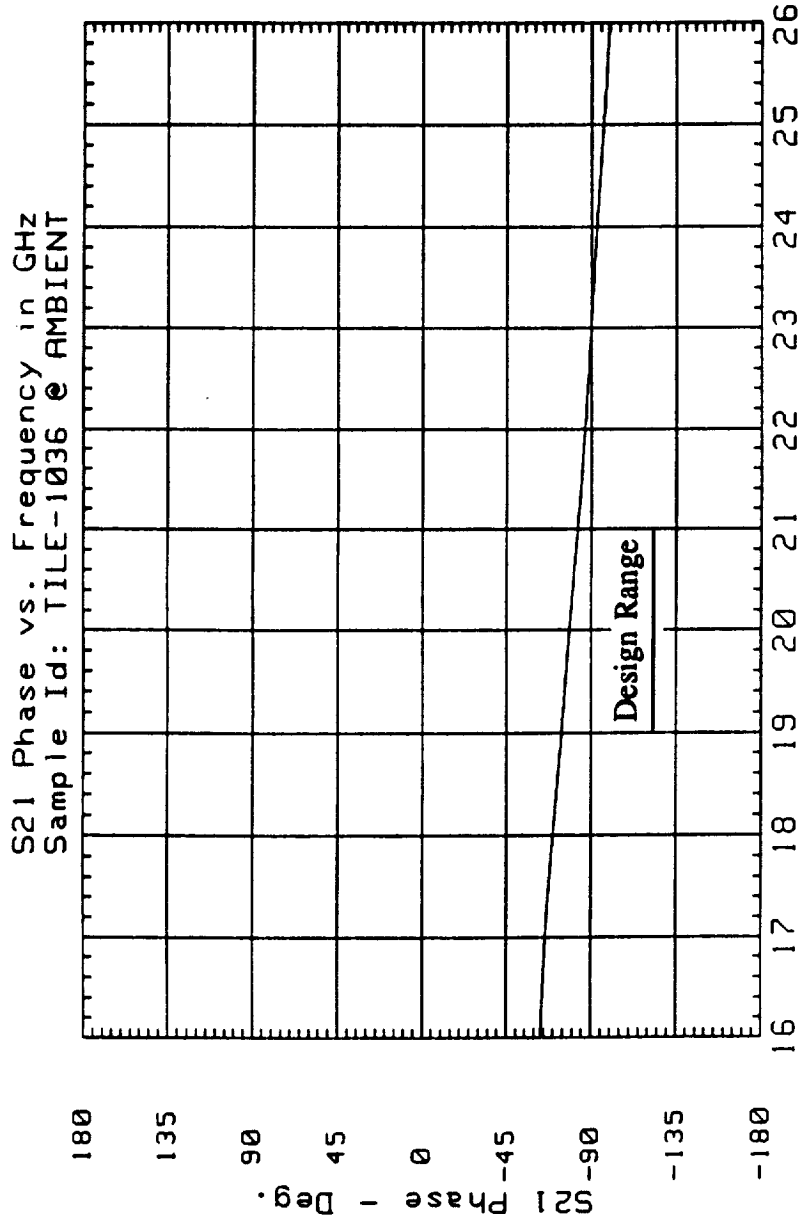

FIGURE 65 - S21 PHASE MEASURED FOR LI-2200
TITLE NUMBER 159849-003-1036 AT ROOM TEMPERATURE

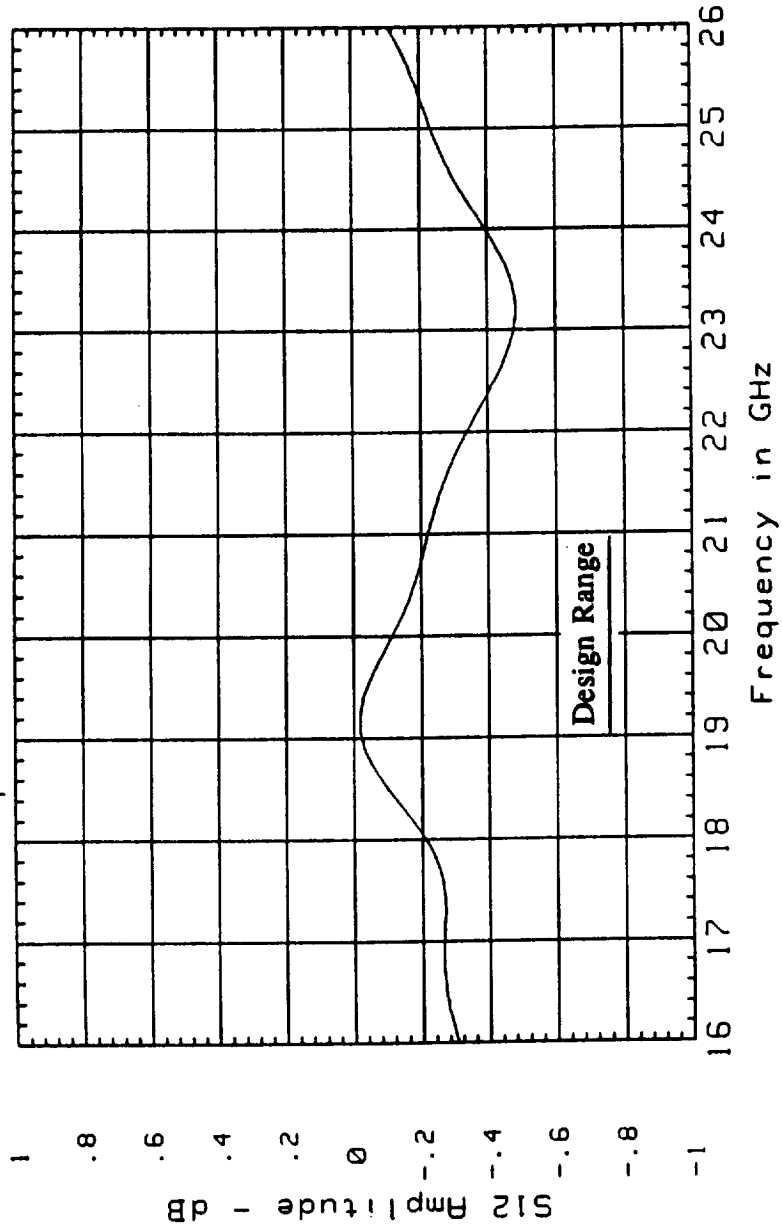

FIGURE 66 - S12 AMPLITUDE MEASURED FOR LI-2200
TITLE NUMBER 159849-003-1036 AT ROOM TEMPERATURE

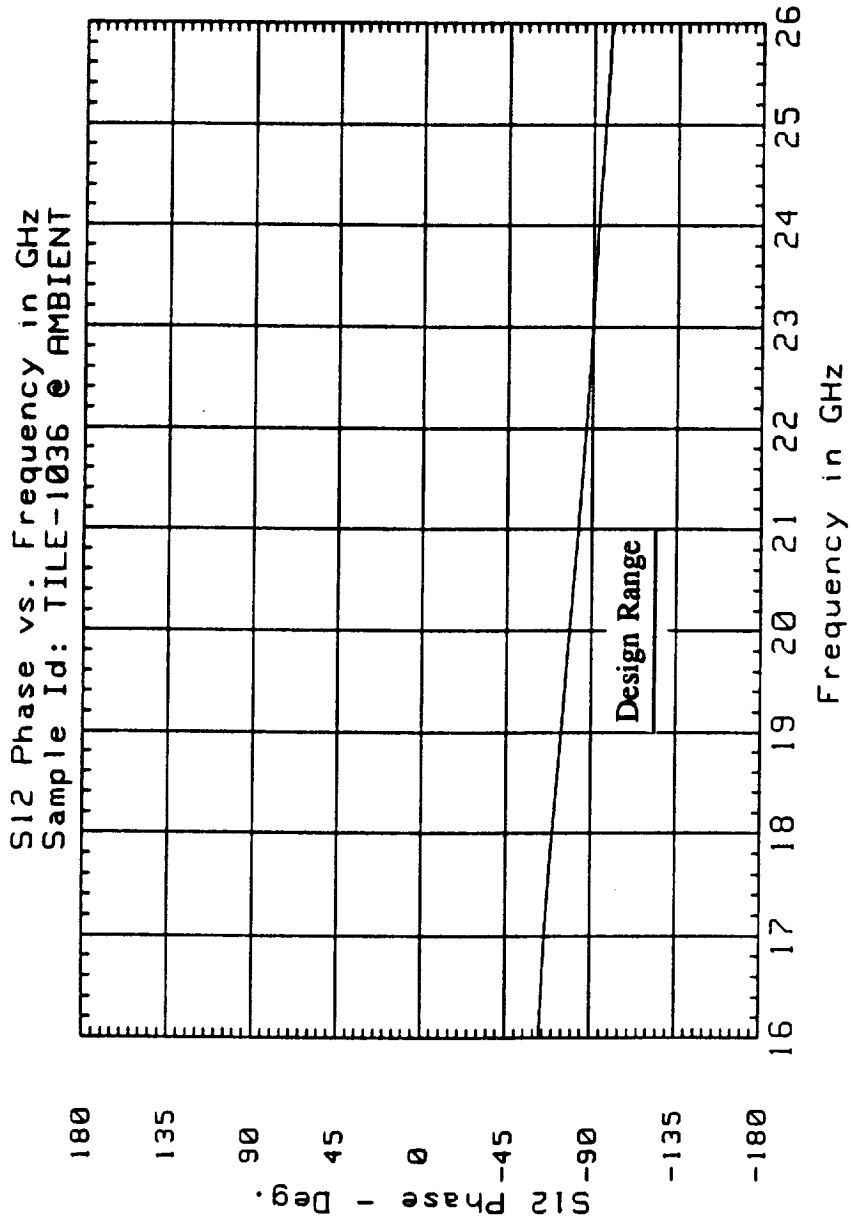

FIGURE 67 - S12 PHASE MEASURED FOR LI-2200
TITLE NUMBER 159849-003-1036 AT ROOM TEMPERATURE

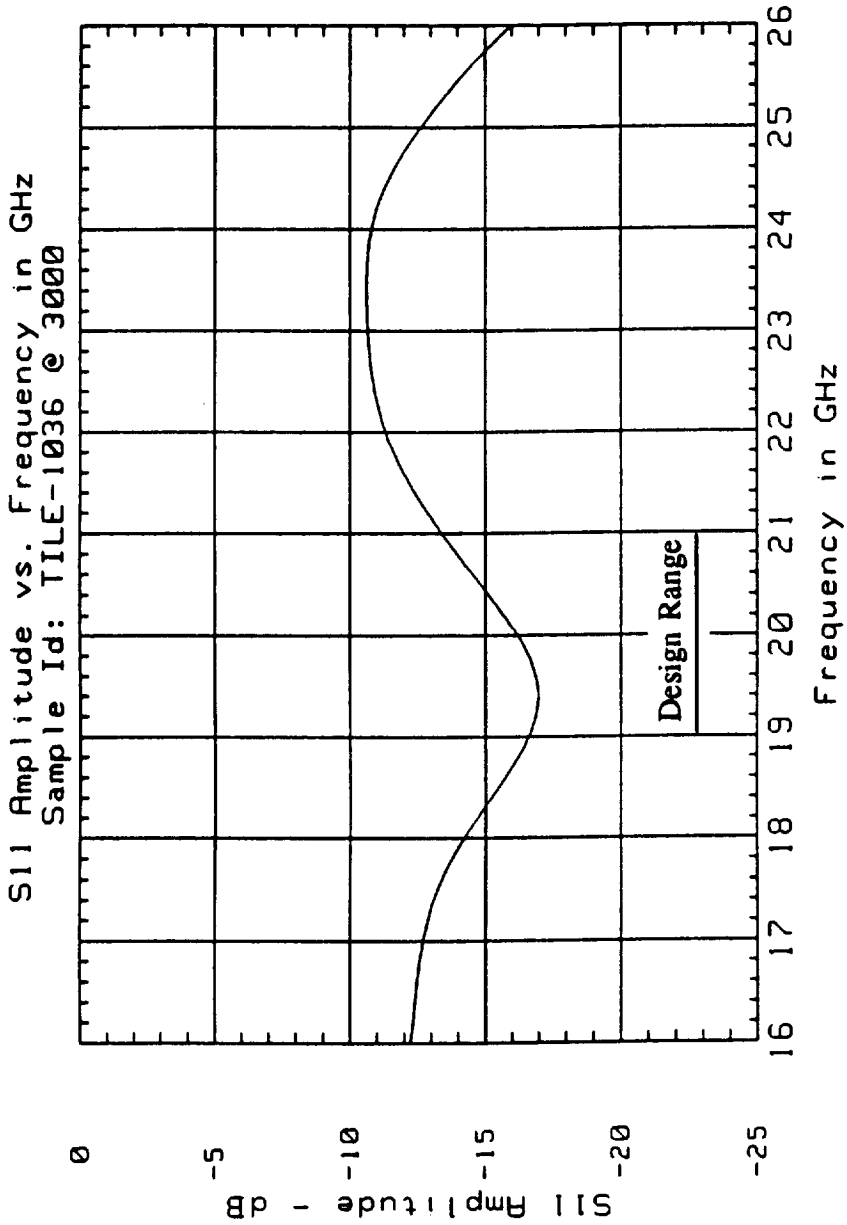

FIGURE 68 - S11 AMPLITUDE MEASURED FOR LI-2200
TITLE NUMBER 159849-003-1036 AT 3000°F

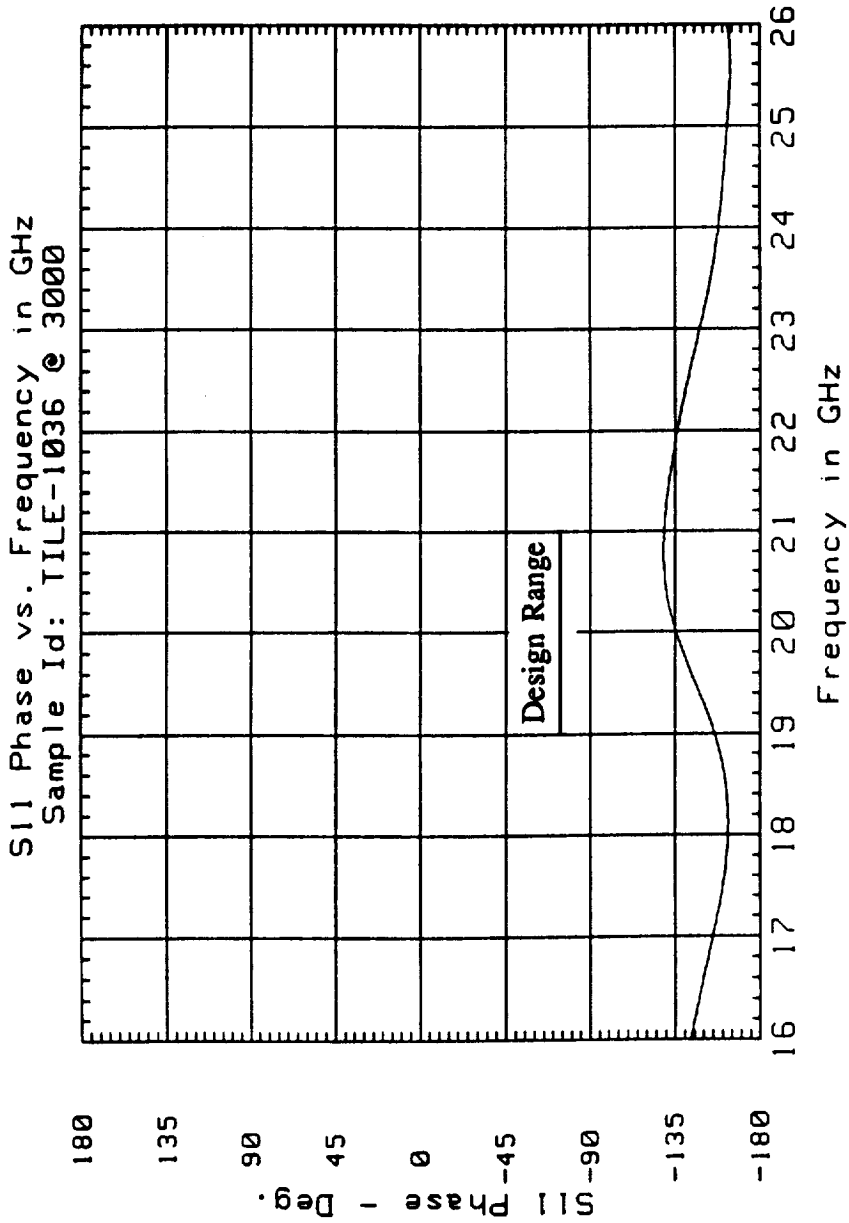

FIGURE 69 - S11 PHASE MEASURED FOR LI-2200
TITLE NUMBER 159849-003-1036 AT 3000°F

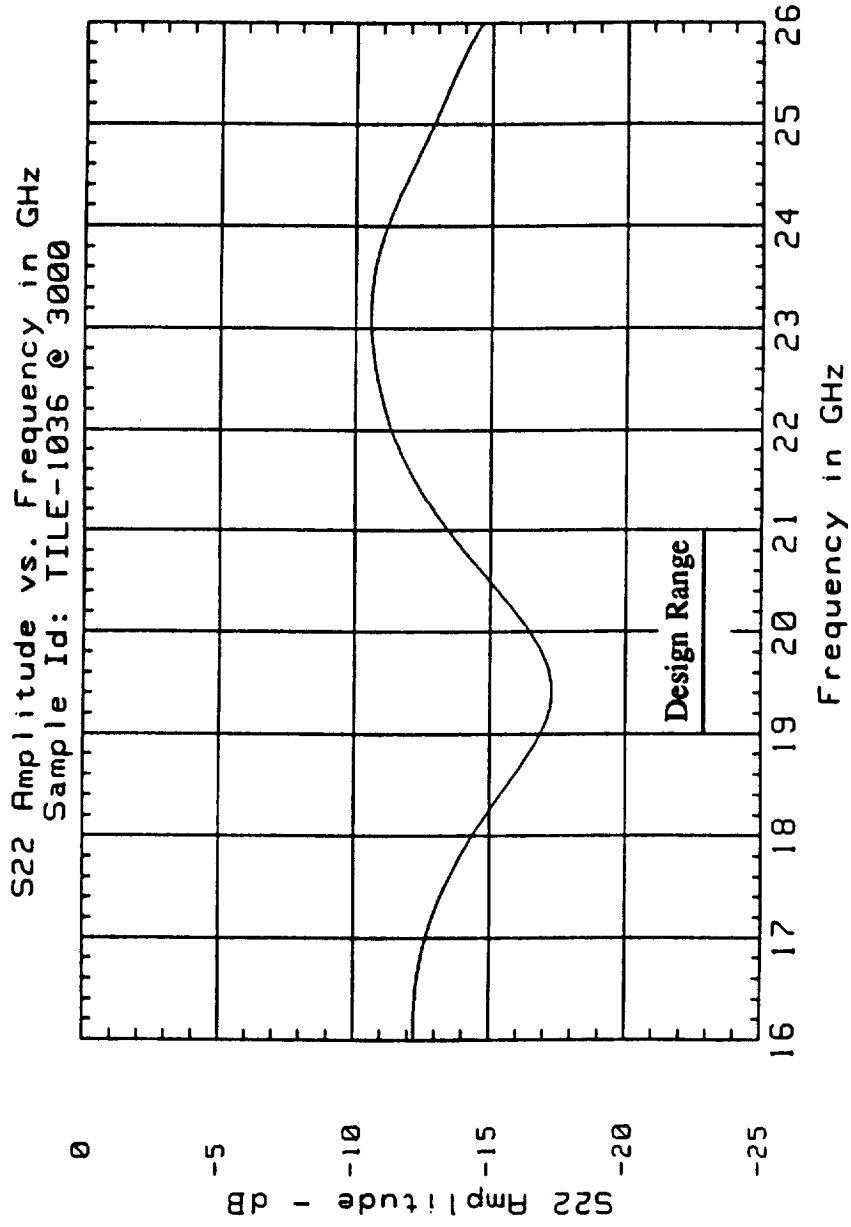

FIGURE 70 - S22 AMPLITUDE MEASURED FOR LI-2200
TITLE NUMBER 159849-003-1036 AT 3000°F

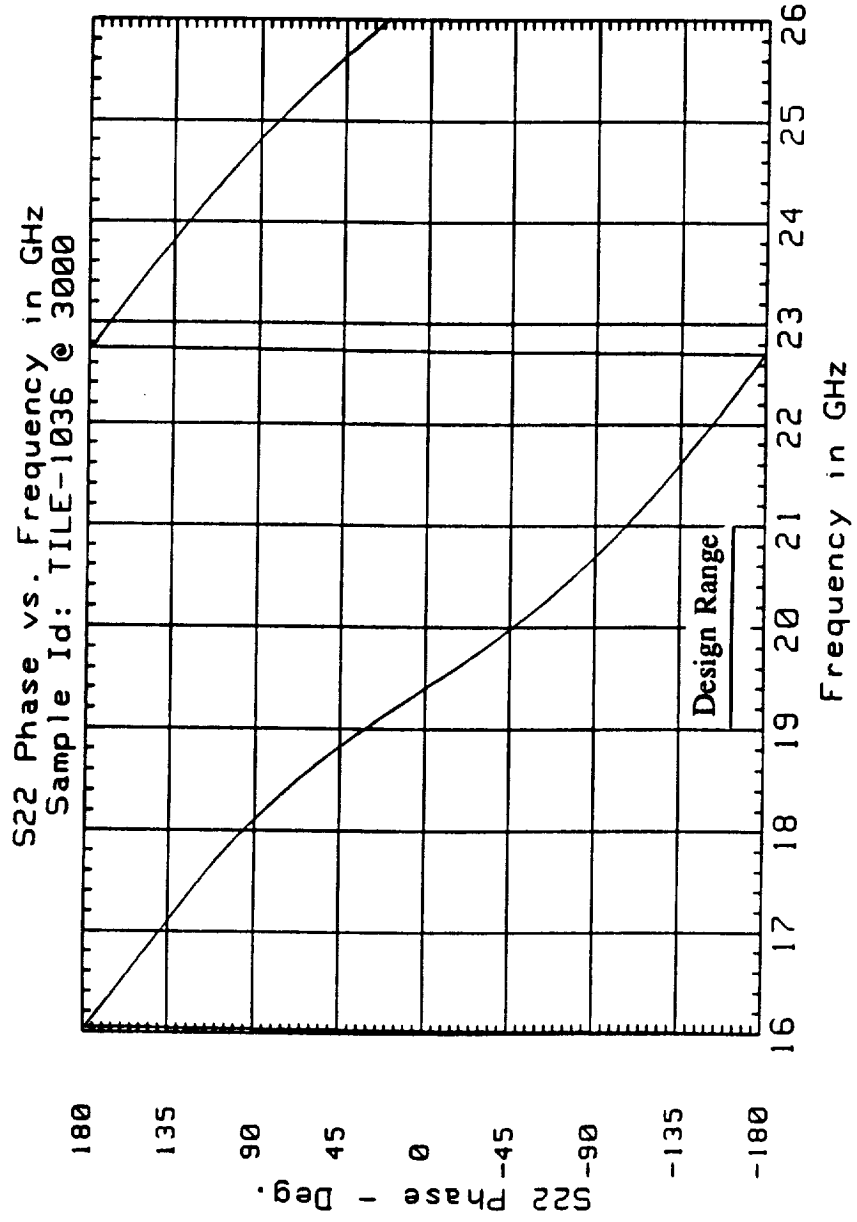

FIGURE 71 - S22 PHASE MEASURED FOR LI-2200
TITLE NUMBER 159849-003-1036 AT 3000°F

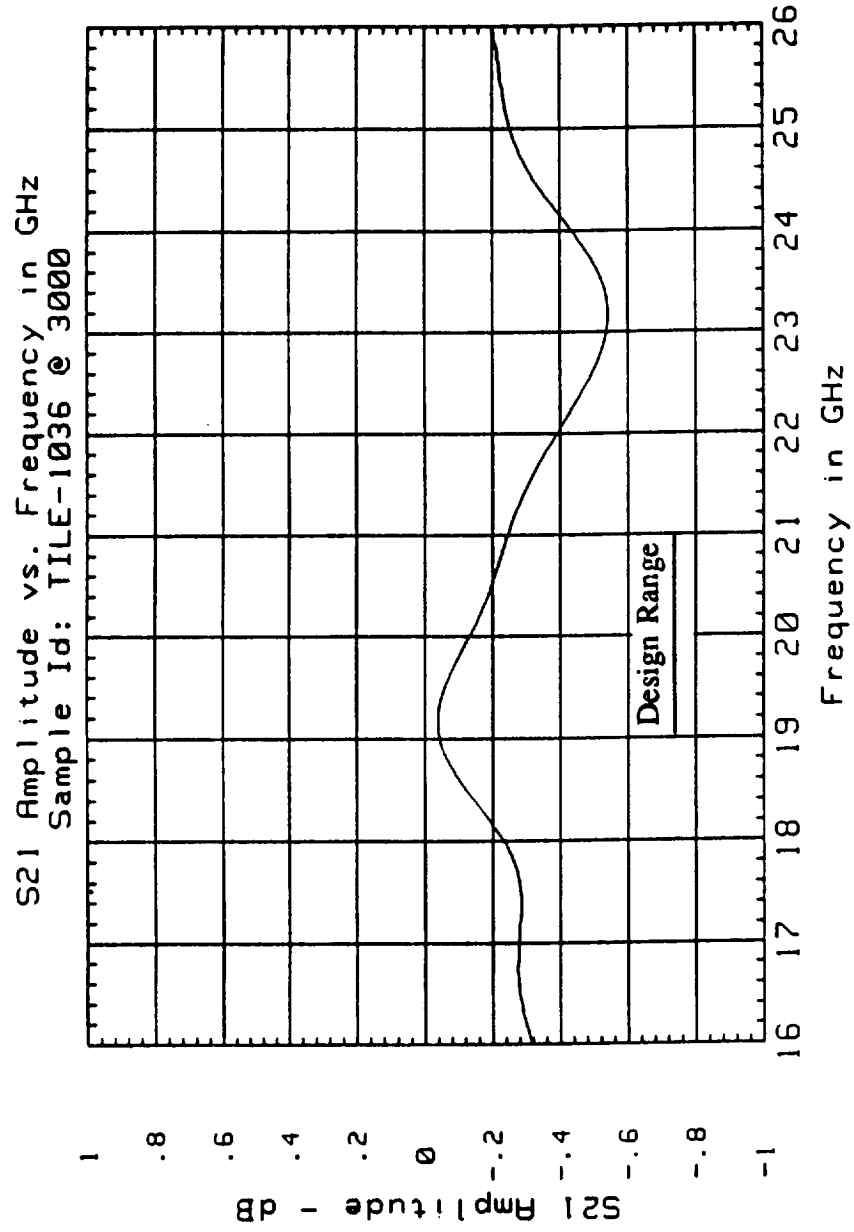

FIGURE 72 - S21 AMPLITUDE MEASURED FOR LI-2200
TITLE NUMBER 159849-003-1036 AT 3000°F

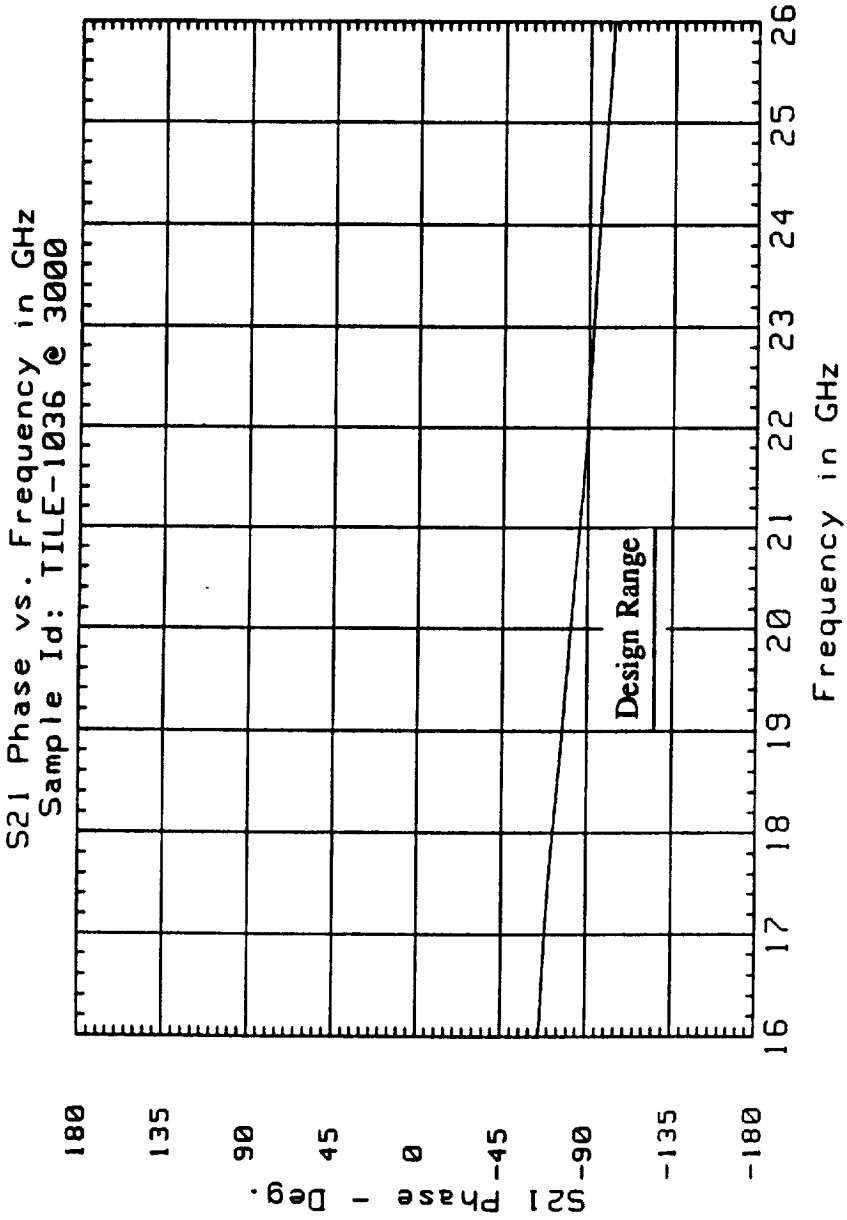

FIGURE 73 - S21 PHASE MEASURED FOR LI-2200
TITLE NUMBER 159849-003-1036 AT 3000°F

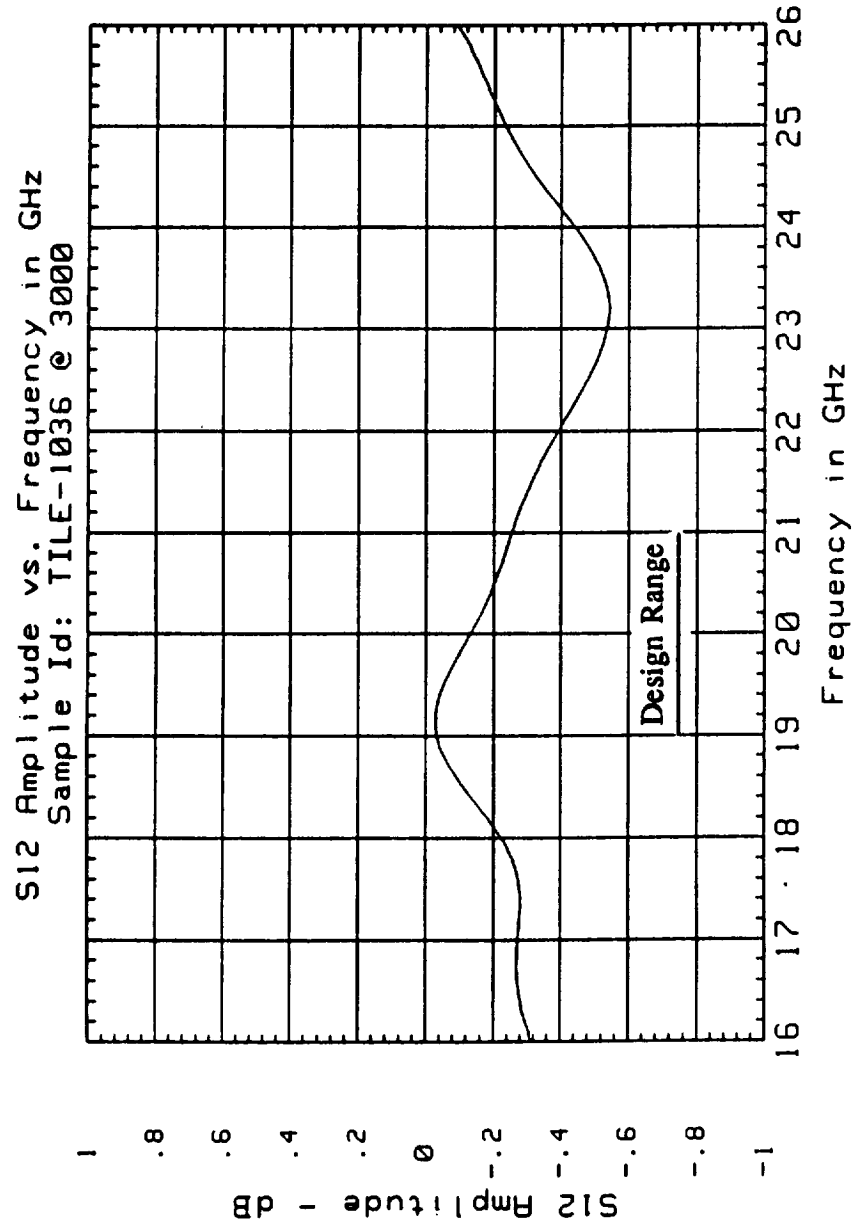

FIGURE 74 - S12 AMPLITUDE MEASURED FOR LI-2200
TILE NUMBER 159849-003-1036 AT 3000°F

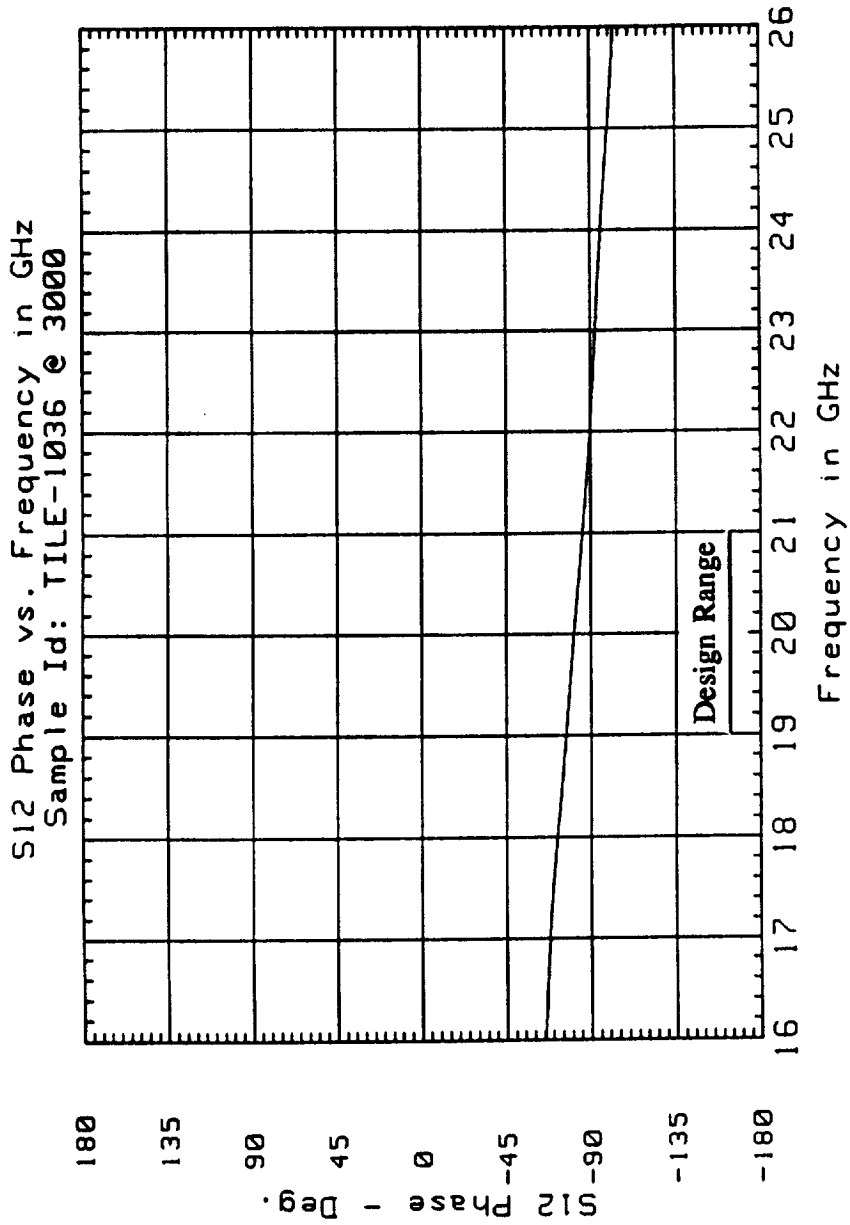

FIGURE 75 - S12 PHASE MEASURED FOR LI-2200
TITLE NUMBER 159849-003-1036 AT 3000°F

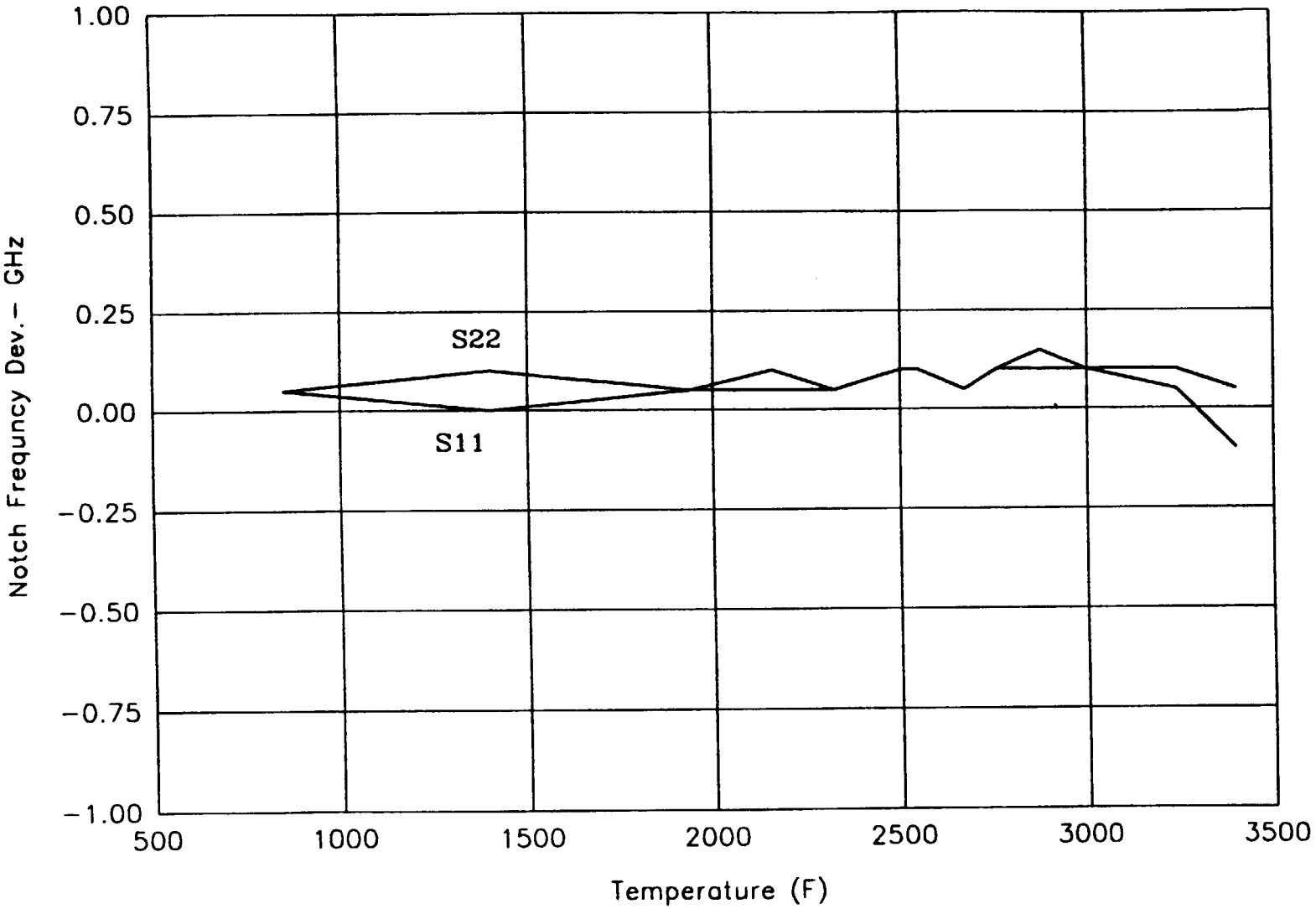

FIGURE 76 - SHIFT IN S11 AND S22 RESONANT NOTCH FREQUENCY VERSUS TEMPERATURE FOR THE LI-2200 SYSTEM

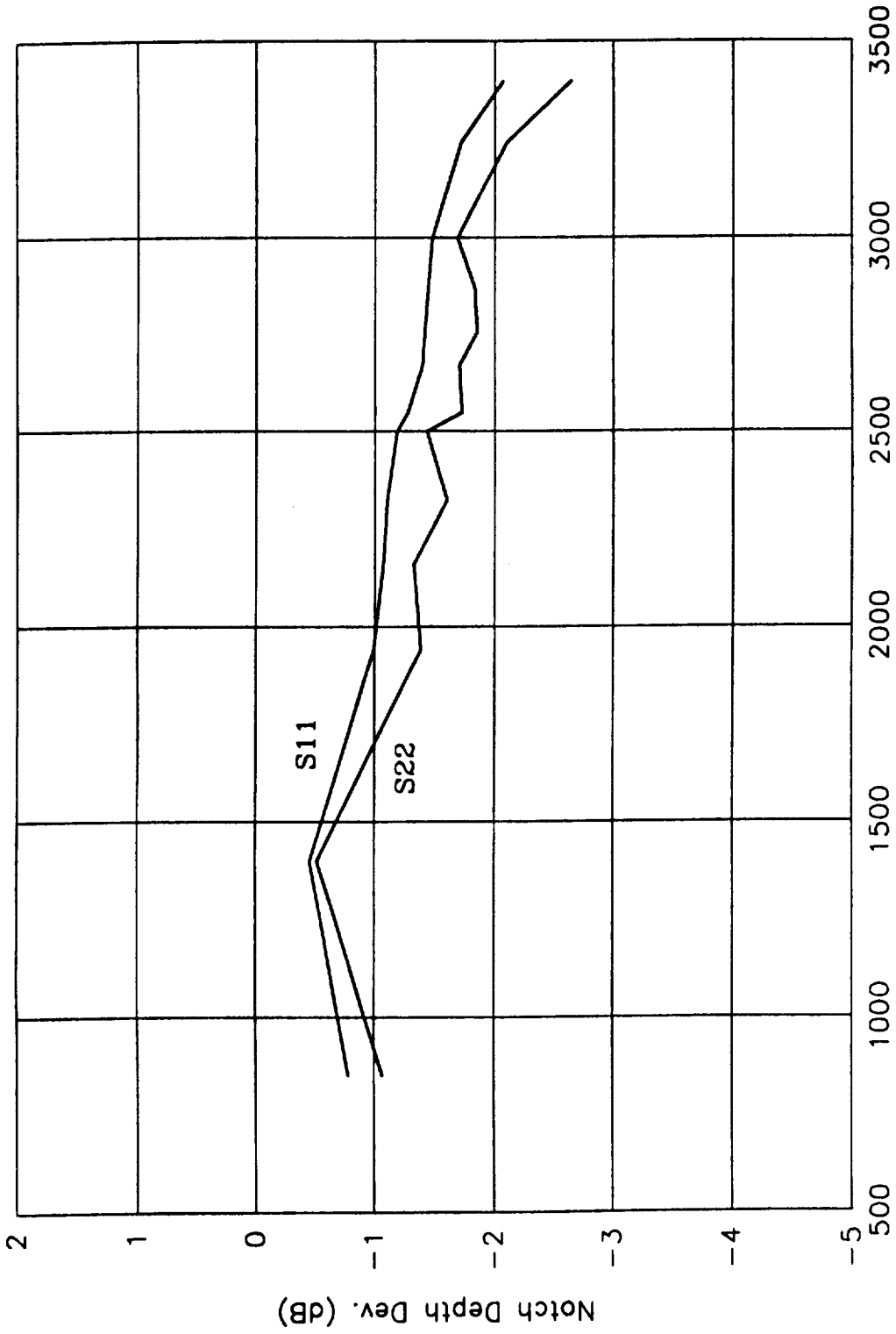

FIGURE 77 - SHIFT IN S11 AND S22 RESONANT NOTCH DEPTH VERSUS TEMPERATURE FOR THE LI-2200 SYSTEM

TABLE 1 - MATERIAL PROPERTIES USED DURING THERMAL MODELING

	RCG Coating @ 2800 °F	Tile Substrate @ 2800 °F	Rexolite 1422
Density lb/in^3	.0602	.0127	.0361
Specific Heat Btu/lb_m-°F	.390	.303	.335
Conductivity Btu/ft-hr-°F	1.08	.193	.0847
Emissivity	.85	-	.89/.38
Total Thickness in	.02	1.00	1.00

TABLE 2 - ELEVATED TEMPERATURE ELECTROMAGNETIC CHARACTERIZATION SYSTEM COMPONENT ORIGIN

	Component Description	Component Origin
2	Feed Horn Mounts	MCAIR
2	Antenna Feed Horns	NASA MANUFACTURED
2	.5 inch Linear Stages	MCAIR
2	Rod Holders and Rods	MCAIR
2	Rear Lens Mounts	PURCHASED
2	Forward Lens Mounts	NASA MANUFACTURED
2	Antenna Mounting Plates	MCAIR MANUFACTURED
1	Base Plate	MCAIR
1	2 inch Linear Stage	MCAIR
1	Specimen Holder	MCAIR MANUFACTURED
2	r=20 inch Quartz Lenses	NASA SUBCONTRACT
2	r=6 inch Quartz Lenses	NASA SUBCONTRACT
2	Feed Antenna Collars	MCAIR MANUFACTURED
4	Positioning Rail Carriages	MCAIR
2	2 meter Positioning Rails	MCAIR

TABLE 3 - MAXIMUM TEMPERATURES RECORDED DURING THE LASER HEATING QUALIFICATION

	Exposure #1	Exposure #2
Front Lens Surface (°F)	135.2	180.1
Rear Lens Surface (°F)	84.9	88.8
Lens Mount (°F)	141.6	174.5
Tile Rear Center (°F)	155.9	256.8
Tile Rear Edge (°F)	108.5	171.4
RCG Camera #1 (°F)	-	2890.2
RCG Camera #2 (°F)	-	2933.3

TABLE 4 - POWER LEVELS AND DURATIONS FOR EACH TEST
DURING ELEVATED TEMPERATURE ELECTROMAGNETIC CHARACTERIZATION

Target Temperature (F)	Sample ID	Maximum Laser Power (W)	Time at Temperature (S)
1,000	1044	104	46
1,500	1043	776	54
2,000	1038	2,194	44
2,200	1046	2,800	45
2,400	1048	3,129	43
2,500	1047	4,030	46
2,600	1042	4,627	42
2,700	1037	4,627	42
2,800	1040	5,895	43
2,900	1039	7,611	38
3,000	1036	8,283	26
3,400	1041	10,373	24
3,800	1041	13,432	22

TABLE 5 - SUMMARY OF THE DEFECTS NOTED AFTER ELEVATED TEMPERATURE ELECTROMAGNETIC CHARACTERIZATION

Target Temperature (F)	Sample ID	Type of Defect Noted		
		Cracking	Glazing	Compression
1,000	1044	No	No	No
1,500	1043	No	No	No
2,000	1038	No	No	No
2,200	1046	No	No	No
2,400	1048	Yes	No	No
2,500	1047	Yes	No	No
2,600	1042	Yes	No	No
2,700	1037	Yes	No	No
2,800	1040	No	Yes	No
2,900	1039	Yes	Yes	No
3,000	1036	Yes	Yes	No
3,400	1041	No	Yes	Yes
3,800	1041	No	Yes	Yes

APPENDIX A

DETAILED DESCRIPTION OF EQUIPMENT AND INSTRUMENTS

Inclusive pages: A-1 - A-3

DETAILED DESCRIPTION OF EQUIPMENT

15 kW CO2 CW Laser. The 15kW laser is an electric discharge convection (EDC) laser operating at 10.6 μm. It is a fast axial flow design with time profiled output capability. The laser output is a beam that has near uniform multimode intensity profile and a divergence of 16 milliradians when used in the normal stable resonator cavity mode. Laser power output is monitored using a beamspitter to direct 6.6% of the output beam into a laser power meter. Timed exposures from 20 milliseconds to 999 seconds are possible using a double bladed pneumatic shutter. The output energy of this laser is limited to 500,000 joules by the output coupling optics.

Non-Contact Thermometers. E^2T Technology Corporation, Pulsar II model 7000FF-HR. This unit is an electro-optic non-contact thermometer with sight-thru aiming and capable of measuring temperatures from 500-3000°F. It's spectral sensitivity is narrowband at 2.2 ±.05 μm. This instrument is traceable to NIST and has an accuracy of ±2%.

IRCON 7000 series, model Modline Plus. This unit is an electro-optic non-contact thermometer capable of measuring temperatures in the range 500-4000°F. It's spectral sensitivity is wideband at 4.8-5.2μm with peak sensitivity at midband. This unit is traceable to NIST.

Data Acquisition. Fluke 2280 Datalogger. This unit was used to read and record the type K thermocouples and to record the analog outputs from the non-contact thermometers.

Hewlett-Packard 7132A strip recorder. This unit was used to record the analog outputs from the non-contact thermometers.

Hewlett-Packard 8510B vector network analyzer. This instrument consists of the HP-8510B display and IF processor, a HP-8515A full S-parameter test set and a HP-8340A synthesized frequency source. This combination of equipment is capable of measuring the scattering parameters from a two port device over the frequency range .045-26.5 GHz and has full time domain processing capabilities. The HP-8510B was used to measure and process the four scattering matrix elements for the LI-2200 system.

Hewlett-Packard 360 workstation. This workstation consisted of a series 360 computer, a 20MB hard drive with 3.5 inch internal floppy drive, a 650MB magneto-optic disk drive, a monochrome monitor and a laser printer. This system was used to read and store all electromagnetic data from the HP-8510B as well as to process the electromagnetic data and present it in the form of plots.

APPENDIX B

ELEVATED TEMPERATURE ELECTROMAGNETIC CHARACTERIZATION PROCEDURE

Inclusive pages: B-1 - B-4

ELEVATED TEMPERATURE ELECTROMAGNETIC CHARACTERIZATION PROCEDURE

1. Calibrate the ETEC system using the TRL procedure developed and tested as described in section 2.6.1 of this document. Note the calibration status on the test documentation sheet.
2. Measure the S11 and S22 for the reflection calibration standard. Store this data to magnetic media with the file name convention TXX_METAL, where XX represents the first two digits of the test temperature. Eg. T10_METAL for the 1000°F test. Note this file name on the test documentation sheet.
3. Measure the S12 and S21 for the empty ETEC sample holder. Store this data to magnetic media using the file naming convention TXX_THRU, where XX represents the first two digits of the test temperature. Note this file name on the test documentation sheet.
4. Place the specimen to be tested in the specimen holder so that the RCG coated surface is in position to be exposed to the laser. Record the specimen ID number and any unusual physical characteristics on the test documentation sheet.
5. Measure S11, S22, S12 and S21 for the specimen and store the data on magnetic media using the naming convention RXX_SP, where XX represents the first two digits of the test temperature. Note this file name on the test documentation sheet.
6. Inform the laser operator team that the electromagnetic data acquisition system is ready.
7. Set the 15kW laser to the required operating parameters. A list of the power levels and exposure times can be found in Table 4.
8. Verify datalogger programming and capacity of datalogger tape drive.

9. Determine abort criteria and inform test personnel.

10. Initiate 15kW laser start-up sequence.

11. When air ejection system comes on-line, begin scanning on the Fluke 2280 datalogger.

12. Begin video recorder.

13. Begin timed laser exposure.

14. Monitor temperature output of the non-contact thermometer and advise the laser operator to increase or decrease the power level.

15. Upon stabilization at the required temperature, inform electromagnetic data acquisition operator to begin the electromagnetic measurements. Record the laser output power and current settings.

16. Upon completion of electromagnetic data acquisition, shut down power to the 15kW laser and place a insulating blanket over the forward lens of the DLSF antenna. Store the electromagnetic data on magnetic media using the naming convention TXX_SP, where XX represents the first two digits of the test temperature.

17. Examine the specimen for damage and record all pertinent observations on the test documentation sheet.

18. Allow the specimen to cool until the temperature is below the minimum threshold of the non-contact thermometer.

19. End scanning of the Fluke 2280 datalogger.

20. Remove specimen from specimen holder and set aside for cooling.

21. Remove the insulating blanket from the forward lens of the DLSF antenna and examine the lens for signs of thermal stress. Record and pertinent observations.

22. Upon completion of the laser exposures, photograph the samples and select the specimens that will undergo further failure analysis. Reduce thermal and electromagnetic data.

APPENDIX C

MAGNETIC MEDIA STORAGE FORMAT

Inclusive pages: C-1 - C-5

MAGNETIC MEDIA STORAGE FORMAT

All electromagnetic data collected during this test program has been stored on magnetic media. Data acquisition and storage were performed on Hewlett-Packard workstations running HP-BASIC and all data has been stored on low density 3.5 inch diskettes using the logical interchange format.

Included on each diskette is a set of subprograms that can be used to read the data files generated by the data acquisition software. This software was written in HP-BASIC and can be included in any HP-BASIC program using version 5.0 or later. The software has been included as both PROGRAM and ASCII files for convenience.

There are two COM blocks required by the software included on the diskettes. They are given below with an explanation of each variable.

1. COM/Raw/Freq(800),S11(800,1),S22(800,1)S21(800,1),S12(800,1)

Freq - a one dimensional array containing the frequency points

S11 - a two dimensional array containing the port 1 reflection data

S22 - a two dimensional array containing the port 2 reflection data

S21 - a two dimensional array containing the transmission from port 1 to port 2

S12 - a two dimensional array containing the transmission from port 2 to port 1

Each of the two dimensional arrays contains magnitude and phase pairs. Some examples of the format are given below.

S21(0,0) - the magnitude of S_{21} at the 1st point

S21(0,1) - the phase of S_{21} at the 1st point

S11(200,0) - the magnitude of S_{11} at the 201st point

S11(200,1) - the phase of S_{11} at the 201st point

2. COM/Stuff/Header$(9)[124],Thick,Num

Header$ - a one dimensional string array that contains information about the file

Thick - a variable equal to the thickness of the part

Num - a variable equal to the number of data points

The nine items included in the Header$ are explained below.

Header$(0) - the date the file was created

Header$(1) - the data arrays included in this file

Header$(2) - the identification of the test part

Header$(3) - the program used to generate the file

Header$(4) - N/A

Header$(5) - the number of points in each data array

Header$(6) - N/A

Header$(7) - N/A

Header$(8) - the dimensions of the test part (thickness x length x width)

Header$(9) - any relevant comments about the test

All elevated temperature data has been stored using a simple file naming convention. This convention is described below.

CXX_SPEC

where:

C ➡ "R" for room temperature measurements

"T" for elevated temperature measurements

XX ➡ Temperature of the test divided by 1000. (ie: for the 1500 tests XX="15")

Room temperature was denoted by XX="00"

SPEC ➡ Indication of the data stored in the file.

"SP" ➡ S-Parameters of the test specimen.

"METAL" ➡ S11 and S22 of the reflection standard after calibration.

"THRU" ➡ S12 and S21 of the transmission standard after calibration.

"PROC" ➡ S-Parameters of the test specimen after data processing has been applied.

examples:

R22_SP ➡ Room temperature S-Parameters for the 2200 °F test specimen.

T22_SP ➡ Elevated temperature S-Parameters for the 2200 °F test specimen.

There were a number of data files generated during the initial phases of this testing which may be of some use when the elevated temperature measurements are reduced for the dielectric properties of the LI-2000 system's constitutive materials. These files have been included for completeness. They are:

CAL_A	S-Parameters of the reflection standard after TRL calibration.
CAL_B	S-Parameters of the transmission standard after TRL calibration.
TEFLON	S-Parameters of a .125 inch thick piece of TEFLON (ϵ'=2.05).
STANDARD	S-Parameters of the two layer verification standard.
STNDRD_DG	Data from file STANDARD after the de-glitching routine had been applied.
STNDRD_DGG	Data from file STANDARD after the de-glitching routine and time domain gating had been applied.
TILE	S-Parameters of a representative LI-2200 specimen.
TILE_G	Data from file TILE after time domain gating had been applied.
TILE_DG	Data from file TILE after the de-glitching routine had been applied.
TILE_DGG	Data from file TILE after the de-glitching routine and time domain gating had been applied.

REPORT DOCUMENTATION PAGE

Form Approved
OMB No. 0704-0188

Public reporting burden for this collection of information is estimated to average 1 hour per response, including the time for reviewing instructions, searching existing data sources, gathering and maintaining the data needed, and completing and reviewing the collection of information. Send comments regarding this burden estimate or any other aspect of this collection of information, including suggestions for reducing this burden to Washington Headquarters Services, Directorate for Information Operations and Reports, 1215 Jefferson Davis Highway, Suite 1204, Arlington, VA 22202-4302, and to the Office of Management and Budget, Paperwork Reduction Project (0704-0188), Washington, DC 20503.

1. AGENCY USE ONLY *(Leave blank)*	2. REPORT DATE	3. REPORT TYPE AND DATES COVERED
	September 1993	Contractor Report

4. TITLE AND SUBTITLE
High Temperature Electromagnetic Characterization of Thermal Protection System Tile Materials

5. FUNDING NUMBERS
C NAS1-18763

WU 592-01-11-12

6. AUTHOR(S)
Garrett G. Heil

7. PERFORMING ORGANIZATION NAME(S) AND ADDRESS(ES)
McDonnell Douglas Aerospace
Box 516
St. Louis, MO 63166

8. PERFORMING ORGANIZATION REPORT NUMBER
MDC 92B0034

9. SPONSORING/MONITORING AGENCY NAME(S) AND ADDRESS(ES)
National Aeronautics and Space Administration
Langley Research Center
Hampton, VA 23681-0001

10. SPONSORING/MONITORING AGENCY REPORT NUMBER
NASA CR-189687

11. SUPPLEMENTARY NOTES
Langley Technical Monitor: Robert T. Neece
Final Report - Task 15

12a. DISTRIBUTION/AVAILABILITY STATEMENT
Unclassified - Unlimited

Subject category 27

12b. DISTRIBUTION CODE

13. ABSTRACT *(Maximum 200 words)*

This study investigated the impact of elevated temperatures on the electromagnetic performance of the LI-2200 thermal protection system. A 15-kilowatt CO_2 laser was used to heat an LI-2200 specimen to 3000°F while electromagnetic measurements were performed over the frequency range of 19 to 21 GHz. The electromagnetic measurement system consisted of two Dual-Lens Spot-Focusing (DLSF) antennas, a sample support structure, and an HP-8510B vector network analyzer. Calibration of the electromagnetic system was accomplished with a Transmission-Reflection-Line (TRL) procedure and was verified with measurements on a two-layer specimen of known properties. The results of testing indicated that the LI-2200 system's electromagnetic performance is slightly temperature dependent at temperatures up to 3000°F.

14. SUBJECT TERMS
LI-2200, Thermal Protection System, electromagnetic characterization, dielectric properties, transmission loss, Transmission-Reflection-Line, heat shield tiles

15. NUMBER OF PAGES
138

16. PRICE CODE
A07

17. SECURITY CLASSIFICATION OF REPORT	18. SECURITY CLASSIFICATION OF THIS PAGE	19. SECURITY CLASSIFICATION OF ABSTRACT	20. LIMITATION OF ABSTRACT
Unclassified	Unclassified		